CRANFIELD UNIVERSITY

HAIDONG HUANG

OPTIMAL DESIGN OF A FLYING-WING AIRCRAFT INNER WING STRUCTURE CONFIGURATION

SCHOOL OF ENGINEERING
MSc THESIS

MSc BY RESEARCH
Academic Year: 2011 - 2012

Supervisor: Dr. Shijun Guo
January 2012

CRANFIELD UNIVERSITY

SCHOOL OF ENGINEERING

MSc BY RESEARCH

Academic Year 2011 - 2012

HAIDONG HUANG

OPTIMAL DESIGN OF A FLYING-WING AIRCRAFT INNER WING STRUCTURE CONFIGURATION

Supervisor: Dr. Shijun Guo
January 2012

This thesis is submitted in partial fulfilment of the requirements for the degree of Master of Science

ABSTRACT

Flying-wing aircraft are considered to have great advantages and potentials in aerodynamic performance and weight saving. However, they also have many challenges in design. One of the biggest challenges is the structural design of the inner wing (fuselage). Unlike the conventional fuselage of a tube configuration, the flying-wing aircraft inner wing cross section is limited to a noncircular shape, which is not structurally efficient to resist the internal pressure load. In order to solve this problem, a number of configurations have been proposed by other designers such as Multi Bubble Fuselage (MBF), Vaulted Ribbed Shell (VLRS), Flat Ribbed Shell (FRS), Vaulted Shell Honeycomb Core (VLHC), Flat Sandwich Shell Honeycomb Core (FLHC), Y Braced Box Fuselage and the modified fuselage designed with Y brace replaced by vaulted shell configurations. However all these configurations still inevitably have structural weight penalty compared with optimal tube fuselage layout. This current study intends to focus on finding an optimal configuration with minimum structural weight penalty for a flying-wing concept in a preliminary design stage.

A new possible inner wing configuration, in terms of aerodynamic shape and structural layout, was proposed by the author, and it might be referred as ‘Wave-Section Configuration’. The methodologies of how to obtain a structurally efficient curvature of the shape, as well as how to conduct the initial sizing were incorporated.

A theoretical analysis of load transmission indicated that the Wave-Section Configuration is feasible, and this was further proved as being practical by FE analysis. Moreover, initial FE analysis and comparison of the Wave-Section Configuration with two other typical configurations, Multi Bubble Fuselage and Conventional Wing, suggested that the Wave-Section Configuration is an optimal design in terms of weight saving. However, due to limitations of the author’s research area, influences on aerodynamic performances have not yet been taken into account.

Keywords:

Flying-wing aircraft, inner wing configuration, Wave-Section Configuration, optimal, FE analysis

ACKNOWLEDGEMENTS

I would like to express great appreciation to my supervisor Dr. Shijun Guo for his excellent support throughout the whole year. I benefited significantly from his constructive suggestions, inspiring talks and invaluable subject knowledge.

Acknowledgements also should be shown to the Aviation Industry Corporation of China (AVIC) and China Scholarship Council (CSC). Their sponsor made it possible for me to have such an incredible opportunity to study abroad.

Special thanks also go to Warren, who helped me a lot and made my life easy and enjoyable in UK. Besides, he looked through my thesis and gave me a lot of useful advices.

Last but not least, I also give my sincere thanks to my whole family, especially my wife, Xi Wang. She provides me with tremendous support and encouragement, and has made me feel very proud.

TABLE OF CONTENTS

LIST OF FIGURES

LIST OF TABLES

LIST OF ABBREVIATIONS

AC	Aerodynamic Centre
FAR	Federal Aviation Regulations
IRP	Individual Research Program
GDP	Group Design Project
MAC	Mean Aerodynamic Chord
CWBC	Conventional Wing-Box Configuration
MBC	Multi-Bubble Configuration
WSC	Wave-Section Configuration
WSCA	Wave-Section Configuration Aircraft

A	Aspect ratio
b	Span
C_{root}	Root chord
C_{tip}	Tip chord
$\bar{c}$	The length of Mean Aerodynamic Chord
h_s	Stringer height
$\overline{Y}$	The distance between Mean Aerodynamic Chord and the centreline
M	Bending moment
S	Wing area
t_b	Skin thickness
t_e	Equivalent thickness of the cover
t_s	Stringer thickness
T	Torque
W	Maximum taking-off weight
W/S	Wing loading
λ	Taper ratio
$\Lambda_{c/4}$	Quarter sweep angle

Λ_{LE}	Leading-edge sweep angle
Δp	The pressure differential
σ_s	Allowable shear stress
σ_p	Allowable tensile working stress
σ_b	Allowable stress

1 INTRODUCTION

1.1 The Aircraft Initial Design

The research project was started with the conceptual design of a long rang 200-seats flying-wing aircraft in a Group Design Project (GDP) from April 2011 to September 2011. This GDP is targeted on the phase-1 Conceptual Design, for which the phase-2 Preliminary Design and phase-3 Detailed Design are going to be finished in the next two years.

The flying-wing aircraft is named as Blue Bird. The concept of Blue Bird was preceded by a conventional approach sharing exactly the same requirements. Figure 1-1 shows the three-view drawing of the flying-wing concept design. Figure 1-2 shows the three-view drawing of a conventional concept taken as the reference design for comparison purpose in the GDP.

The author was involved in the GDP as a configuration and structure designer to take the responsibility of the overall configuration and geometric sizing in cooperation with other fellow students working as a team. The specific contributions will be presented in Chapter 1.

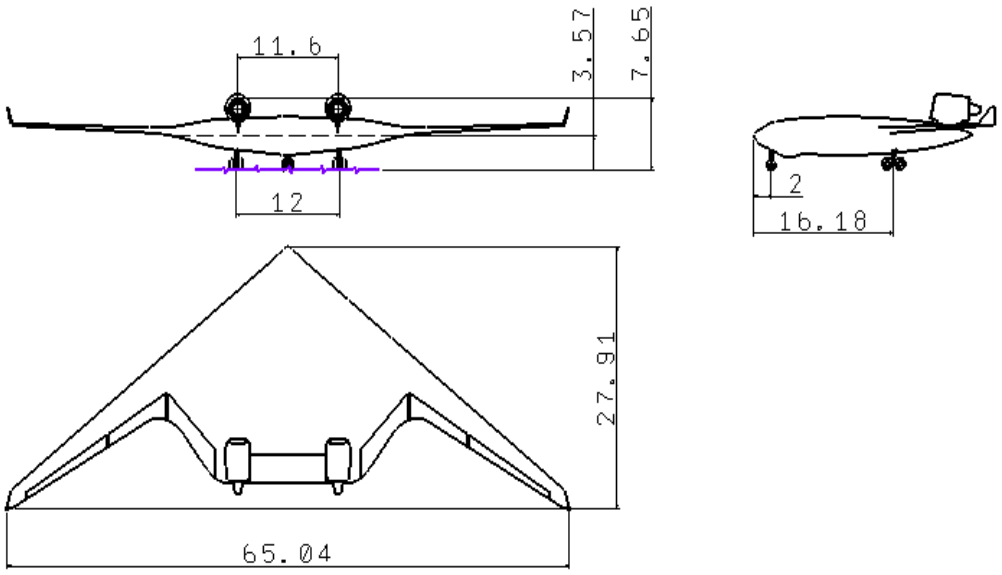

Figure 1-1 The flying wing concept aircraft

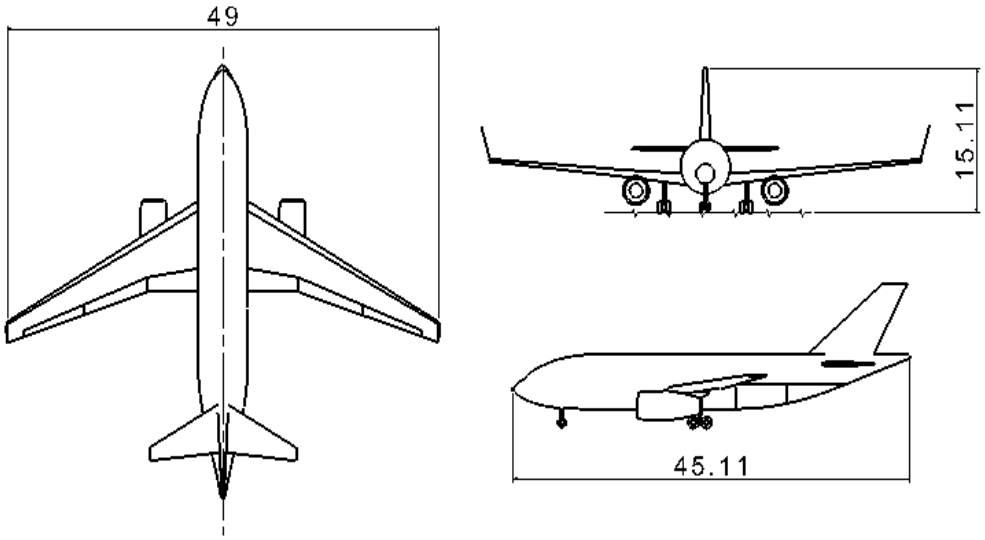

Figure 1-2 The conventional concept aircraft

1.2 Individual Research Project (IRP)

1.2.1 Backgrounds

Following the GDP, the author continued and focused the study on the inner wing structure design as an IRP.

Aircraft designers never stopped looking for new concepts that could introduce higher efficiency to the air transportation. Flying-wing aircraft have been considered as one of the most potential configurations, hence attracting tremendous research interests and efforts among the aircraft engineers. It has been proved very successful by the appearance of the B2 bomber, the first actual flying-wing aircraft in the world, coming into usage as a military aircraft. In the commercial market, probably more attempts are under way, for instance, the industry giant Boeing is proceeding with the X48 project.

Flying-wing aircraft are more difficult to use in commercial transportation, because more design problems would have to be overcome. One of them is the structural configuration of the inner wing section (fuselage) due to pressurisation. Conventional aircraft all have a cylindrical tube fuselage that is a most efficient way to react the internal pressure in membrane stress. While for the flying-wing aircraft of a noncircular shape fuselage (inner wing), the internal

pressure differential will result in bending stress in the skin covers, and brings weight penalty to the airframe. Consequently, flying-wing aircraft come out heavier than the conventional tube design. This is a critical problem because keeping weight low is always the most important design driver in aircraft design. In order to resolve this obstacle, several configurations have been proposed, of which examples are Vaulted Ribbed Shell (VLRS), Flat Ribbed Shell (FRS), Vaulted Shell Honeycomb Core (VLHC), Flat Sandwich Shell Honeycomb Core (FLHC), Multi Bubble Fuselage (MBF), and Y Braced Box Fuselage. However, it remains a subject worthy of more research, as there is always room for improvement.

1.2.2 Aim and Objective

This thesis aims to find an optional design of the pressurised inner wing structural configuration of the flying-wing aircraft, in terms of weight. Three configurations will be constructed, analysed and compared. The two typical types of configurations, the FRS concept and MBF concept are included. The third configuration is proposed by the author, Wave-Section Configuration, which will be specified in Chapter 4.3. The following objectives are covered in the scope of this thesis:

1. Deriving the optimal curvature of the inner wing covers in terms of weight saving;
2. Proposing a new inner wing (fuselage) structural configuration and verifying its feasibility;
3. Finding an optimal inner wing structural configuration;
4. Summarizing the advantages and disadvantages/challenges with regard to the new configuration proposed by the author.

1.2.3 Methodology and Approaches

The methodology in the following approaches is employed in the research. Firstly, a literature review is carried out to gain knowledge of the development of flying-wing aircraft and the existing inner wing structural configurations.

Secondly, the commercial software Matlab is used to find the optimal curvature of the shell subject to bending and pressure differential. Thirdly, the CATIA software package is utilized to create the geometrical models where needed. Fourthly, theoretical methods and empirical equations are used to achieve the initial sizing of the structure members. Finally, Patran/Nastran is employed to conduct the FE analysis and verify the design.

2 LITERATURE REVIEW

Aircraft concept designers have been constantly looking for new concepts that can bring high efficiency to aviation industry. Flying-wing concept is one of the most attractive configurations. This chapter is intended to have a review of Flying Wing aircraft development.

2.1 Flying-Wing Aircraft Concept

2.1.1 A definition of Flying Wing

Flying wing is categorised as one of all-lifting vehicles (ALV), for which one definition is provided in Reference [1]:

> A vehicle that has all horizontal orientated elements (i.e., wing, fuselage, tail, etc..) are continuous and aerodynamically shaped to contribute proportionally equivalent amounts of lift throughout the flight envelope.

This broad definition above allows for various aviation vehicles, including wings , fuselages, tails, etc. As to the Flying Wing, a provision of definition is also provided in Reference [1]：

> A tailless airplane accommodating all of its parts within the outline of a single airfoil.
>
> All-Wing
>
> > Aircraft consisting of nothing but wing.(Northrop's definition)
>
> Tailless
>
> > An aircraft consisting of a single wing, without conventional fuselage or tail.

Figure 2-1 below shows an example of a conventional configuration aircraft and flying-wing aircraft.

Figure 2-1 Conventional aircraft (B787) and Flying Wing (YB-49)

(http://en.wikipedia.org)

2.1.2 Categories of flying wing

Generally, flying-wing aircraft may be categorized in three types, flying wing (FW), blended wing body (BWB) and delta wing (DW). A flying wing is a tailless fixed-wing aircraft which has no definite fuselage, with most of the crew, payload and equipment being housed inside the main wing structure. [2] Blended Wing Body (BWB) aircraft have a flattened and airfoil shaped body, which produces most of the lift with the wings contributing the balance. The body form is composed of distinct and separate wing structures, though the wings are smoothly blended into the body. [2] The delta wing is a wing planform in the form of a triangle. It is named for its similarity in shape to the Greek uppercase letter delta (Δ). (http://en.wikipedia.org/wiki/Delta_wing) Figure 2-2 shows one example of each type of the flying wing aircraft.

(a) Flying wing (b) NASA's prototype of a Blended Wing aircraft (c) The delta wing Avro Vulcan bomber

Figure 2-2 Three types of flying wing (http://en.wikipedia.org)

2.1.3 Advantages and challenges of Flying Wing

The reason why flying-wing aircraft have been attracting so many engineering efforts is that they are believed to possess substantial potentials, aerodynamically, economically and environmentally. Yet there is an enormous amount of challenges that need to be confronted. Table 2-1 below shows some of the advantages and challenges/disadvantages.

Table 2-1 Advantages and disadvantages of flying-wing aircraft

Flying-wing aircraft	
Advantages	Aerodynamic advantages are achieved through • Reduced Wetted Area • Structurally efficiently use of wing span • Relaxed static stability • Optimum span loading Noise Reduction • Tailless • Smooth lifting surfaces • Minimizes exposed edges and cavities Relaxed stability, quite low or no trim loss; More cabin layout flexibility; Facilitating system integrating.
Challenges/ Disadvantages	Inboard wing design • Thick, large chord, transonic airfoils ,t/c~18% • Shock strength on the center body • Pillowing of the pressurized outer skin results in modified aerodynamic shapes. Usually longitudinal & lateral statically unstable or neutral stable; Low pitch & yaw damping, bad dynamic stability. Emergency escape

2.1.4 History of Flying Wing

Although the aviation market is dominated by conventional aircraft, typically with wings to generate lift, tube fuselages to carry payloads and cargoes, tails/canards for control, and nacelles to accommodate propulsion systems, Flying Wings can be traced back to the very first aircraft, the Wright Brothers' airplane.

Due to challenges listed in the preceding chapter and technical limitations, flying-wing aircraft had always been limited to merely concepts, until the American B2 came into practice in 1989. An image of the B2 is shown in Figure 2-3. (http://en.wikipedia.org/wiki/B-2_Spirit).

Figure 2-3 B2 (Northrop Grumman B-2 Spirit)

However, before the emergence of B2, a number of concepts were proposed.

The inspiration for Flying Wing aircraft initially arose from observing plant seeds and birds. However, the concept quickly evolved into the type of planforms we see today. By 1905, untapered swept planforms for a Flying Wing was utilized by John Dunne (1875-1949, British) to improve the stability characteristics. In 1910, tapered swept wing planforms had already appeared. The most aggressive use of arrow planforms could be attributed to the German Horten brothers, and it allowed for improved stability and control with high levels of aerodynamic performance. Alexander Lippish (1894-1976, German) is regarded as the first person who contributed to use the delta planforms for a Flying Wing in 1930. The Blended Wing Body (BWB) commercial transporter, Boeing/NASA

X-43, is also a remarkable development as it set a new path for Flying Wing.[1] Figure 2-4 shows some early remarkable FW concepts.

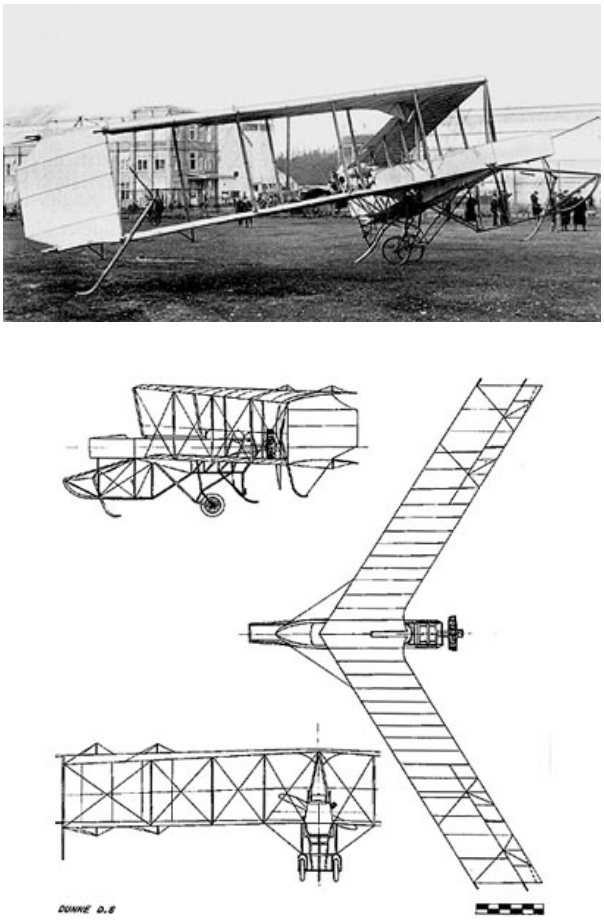

(a) Dunn D8 (http://www.ctie.monash.edu.au/hargrave/dunne.html)

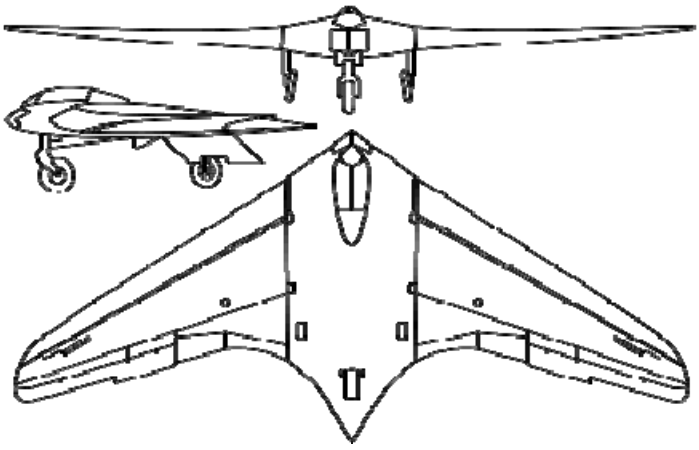

(b) Horten Ho 229 (http://en.wikipedia.org/wiki/Horten_brothers)

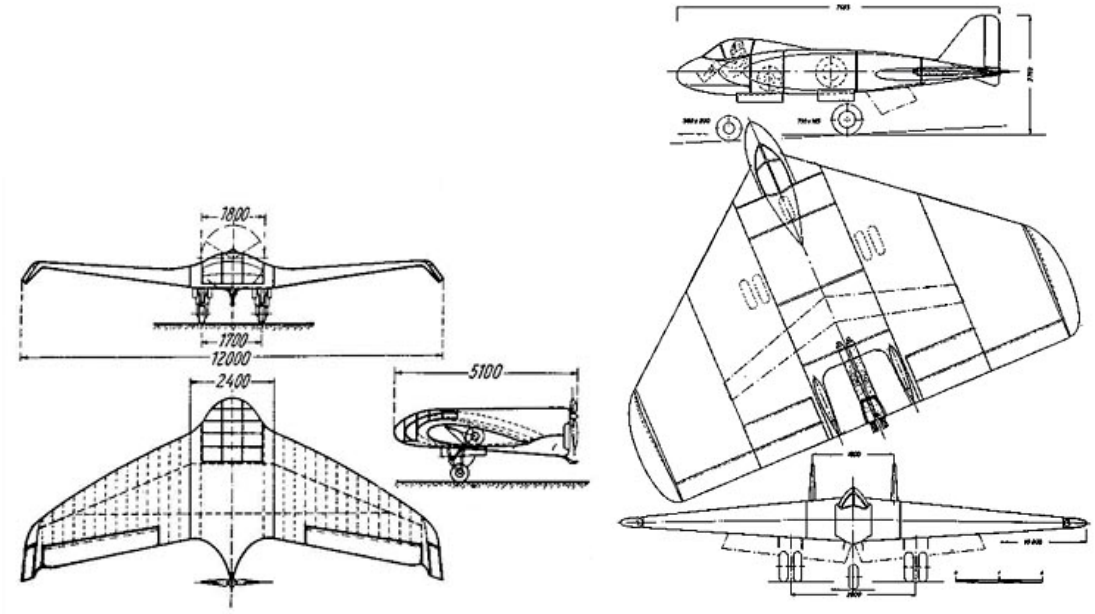

(c) Delta Wing- Alexander Lippish
(http://www.ctie.monash.edu.au/hargrave/lippisch.html)

(d) NASA-X43 (http://en.wikipedia.org/wiki/NASA_X-43)

Figure 2-4 Early typical Flying Wing

After B2 became widely known, massive interest and effort has been invested in Flying Wing aircraft design, which has consequently significantly stimulated new techniques. These include laminar flow control (LFC), vectored thrust, and active stability. These relevant emerging technologies promote designers' interests greatly as a result. To date, there has been more than 100 flying-wing

aircraft developed and flown across the world, not to mention the huge number that have remained as concepts or just as drawings.

One of the most important concepts arising from the above development is the Blended Wing Body X-48, shown in Figure 2-5. It was initially developed by McDonnell Douglas in the late 1990s, but it was not favoured by Boeing after their merger. The most difficult problem arises in ensuring a safe and fast escape in case of an accident, since the locations of emergency doors are totally different from those of conventional aircraft. However, Boeing is now renewing development of the BWB in collaboration with NASA, and a BWB model was successfully flown in 1997.

Figure 2-5 BWB X-48

(http://en.wikipedia.org/wiki/Boeing_X-48)

2.2 Inner Wing Structural Configurations for Flying-Wing Aircraft

As already stated in Chapter 2.1.3, the pressurised inner wing (or fuselage) design remains a significant challenge for Flying Wing aircraft. With conventional aircraft, the fuselage has a circular cylindrical shape ideal for pressurisation, and the pressure results in skin-membrane stress. While for flying-wing aircraft, since the inner wing is somewhat rectangular, it is relatively inefficient to resist pressure loads by bending that consequently brings weight penalty. Figure 2-6 illustrates stress associated with cylindrical shell and rectangular box under pressure p. As to the former, which has a radius of R and

thickness of t, the membrane stress is equal to p(R/t). For the latter one, it can be modelled as a simply supported beam or plate in a length of l and thickness of t, then the maximum bending stress is $0.75p(l/t)^2$, assuming R is with the same magnitude as l. The problem is magnified by the non-linear effect of the compressive load acting on the deflected beam or plate. (The compressive load on the top as well as the equivalent tensile load on the bottom is generated by the bending moment.) In order to resolve this problem, several inner-wing structural configurations have been proposed by other authors. The remaining contents of this chapter will review each of these proposals.

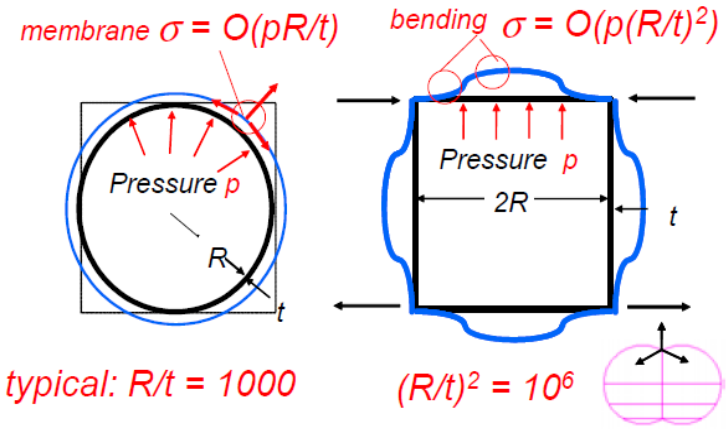

Figure 2-6 High bending pressure associated with un-cylindrical pressure vessel [3]

2.2.1 The FRS/VRS/FLHC/VLHC Concepts

In Reference [4] an isolated cabin bay-3 of an early 800-passenger BWB was analysed. As can be seen in Figure 2-7, the planform and two fuselage concepts of a 800-passenger BWB are shown. Besides the two concepts shown, Flat Ribbed Shell (FRS) and Vaulted Ribbed Shell (VRS), two additional concepts, Flat sandwich shell with Light and Heavy Honeycomb Core (FLHC) and vaulted shell with Light and heavy Honeycomb Core (VLHC), were also analysed. Analysis of the results revealed that the FRS and VRS concepts appeared to be better than the others. The VLHC concept was considered less potential due to its manufacturing complexity, even though it offers the

advantage of a cylindrical pressure vessel. And the FLHC concept was not favoured because of weight penalty and maintenance concerns.

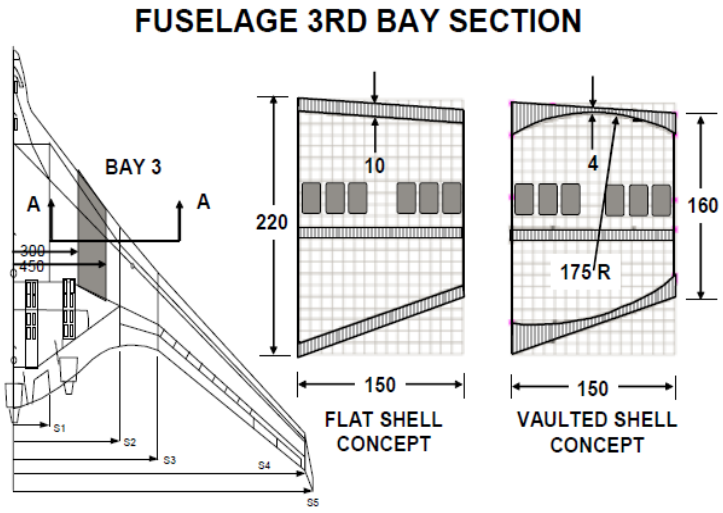

Figure 2-7 800-passenger BWB bay-3 section, Flat Ribbed Shell and Vaulted Ribbed Shell Configurations [4]

2.2.2 Multi-Bubble Fuselage (MBF)

NASA is the pioneer of a concept called Multi-Bubble Fuselage, which comprises inner skins and outer covers together, seen in Figure 2-8. The inner vessels react the pressure ideally in membrane stress, while the outer covers only balance the bending by compression in the top surface and by tension in the bottom surface. This arrangement manages to preserve the advantages of conventional circular fuselages.

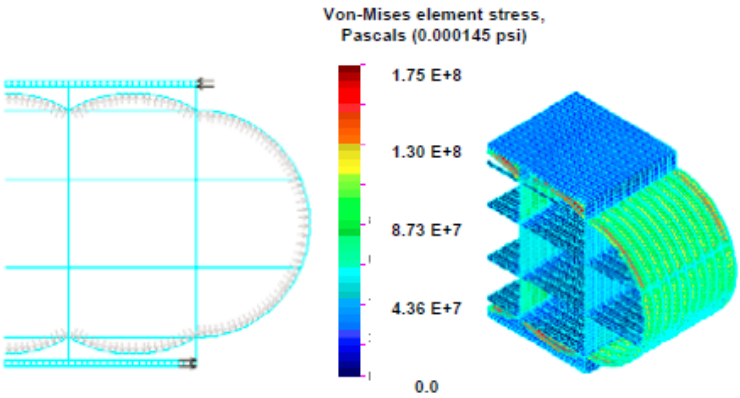

Figure 2-8 Multi-Bubble Concept [3]

2.2.3 Y-Braced Box Fuselage (YBBF)

Due to manufacturing considerations for Multi-Bubble Fuselage, NASA altered it giving rise to a new concept, Y-Braced Box Fuselage, as shown in Figure 2-9. The bending at the intersection of the roof and the walls is reduced by introducing Y braces, and it does not add significant weight penalties.

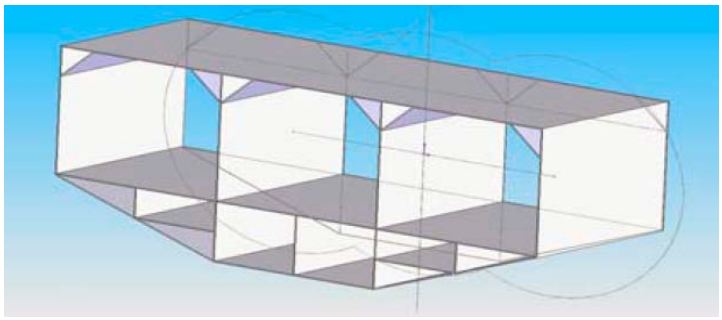

Figure 2-9 Y-Braced Box Fuselage Concept [5]

2.2.4 Columned Multi Bubble Fuselage (CMBF)

As shown in Figure 2-10, a Columned Multi Bubble Fuselage is a modification of Multi-Bubble Fuselage. The walls are replaced by a series of columns. This unfortunately results in weakening the structure's ability to resist chordwise bending because of the absence of walls (or ribs). This problem was solved by reconfiguring the panels such that it has curvature both spanwise and chordwise preserving hoop tension working way. This idea was initially inspired by a pool air mattress holding pressure in a flat and wide volume. Figure 2-10 shows the pool air mattress and Y Braced Multi Bubble Fuselage configuration.

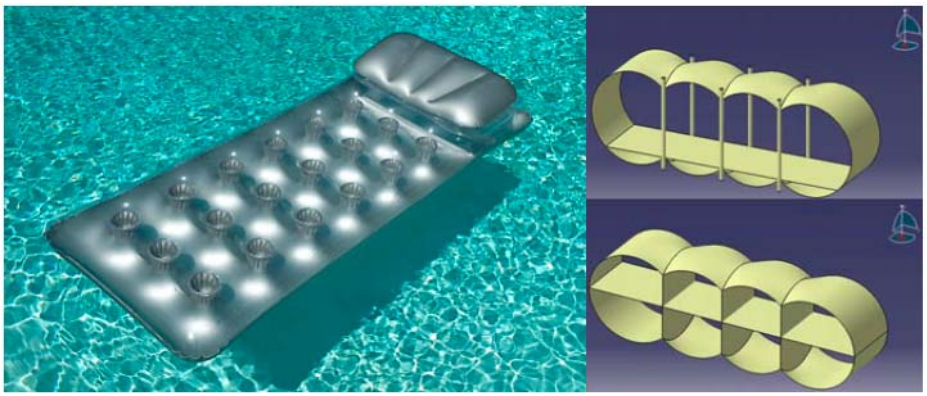

Figure 2-10 Pool air mattress and Columned Multi Bubble Fuselage [6]

3 INITIAL DESIGN OF THE FLYING-WING AIRCRAFT

3.1 Introduction

As has been introduced in Chapter 1.1, the author was engaged in a group design project, taking part in two aircraft concept designs based on the same requirements. In the conventional concept design, the author was responsible for the wing configuration and geometrical sizing. In the flying-wing concept design, the author took charge of the overall configuration and geometry sizing. This chapter is going to specify the author's contributions to the wing configuration and geometry of the GDP. Apart from these, a database regarding certain basic items of the 150-250-seat existing aircraft as well as the Blue Bird is collected by the author, and it is attached in Appendix A.

It is necessary to state the following key requirements for the flying-wing aircraft:

- Seating capacity: 250 seats
- Range: 7500 nm
- Cruise speed: M0.80-0.85
- Cruise altitude: 35,000 ft
- Cruise L/D: 22

3.2 Conventional Concept

1. Wing Area

For long range aircraft, the wing loading is most likely within 620-700 kg/m^2. (Reference [7]) The wing area can be initially given as:

$$S = W/(W/S) \quad \textbf{(3-1)}$$

where

S is the wing area

W is the maximum taking-off weight

W/S is the wing loading

2. Geometry Selection

In Reference [9], a guide as to selecting wing initial geometry parameters is provided, as shown in Table 3-1.

Table 3-1 Wing geometry parameters

Parameter	$M_N \le 0.65$	$0.65 \le M_N \le 0.95$	$M_N \ge 0.95$ subsonic LE	$M_N \ge 0.95$ Supersonic LE
Sweep, $\Lambda_{c/4}$	0	$\cos^{-1}\left(\frac{0.95-0.1C_L-t/c}{M_N}\right)^2$ $\Lambda_{1/4} \le 35°$	$\cos^{-1}\left(\frac{1}{M_N}\right)+6°$	$\le\left[\cos^{-1}\left(\frac{1}{M_N}\right)-6°\right]$
Aspect ratio, A	Short rang 5-7 Long rang 10-12	7-10	1.5-3	2-4
Taper ratio, λ	0.5-0.6	0.2-0.3	0.1	0.2-0.4
Thickness/chord ratio(Root), $(t/c)_R$	0.15-0.20	0.10-0.15	>0.06	0.02-0.03
Thickness/chord ratio(Tip), $(t/c)_T$	65% root value	65% root value	root value	root value

Reference [9] also suggests that it is desirable to set certain parameters as follows in an initial design stage.

Twist angle: $-3°$

Incidence angle: $1°$

Dihedral angle: $5°$

After W/S, A, λ, and $\Lambda_{c/4}$ have been obtained, the value of span b, root chord c_{root}, tip chord c_{tip}, leading edge sweep angle Λ_{LE}, mean aerodynamic chord $\bar{c}$ and its position relative to centreline, $\bar{Y}$, can be calculated by the following equations:

$$b = \sqrt{A \cdot S} \tag{3-2}$$

$$c_{\text{root}} = 2 \cdot S / \left[b(1+\lambda) \right] \tag{3-3}$$

$$c_{tip} = \lambda \cdot c_{root} \tag{3-4}$$

$$\tan \Lambda_{LE} = \tan \Lambda_{C/4} + \left[(1-\lambda) / A(1+\lambda) \right] \tag{3-5}$$

$$\bar{c} = (2/3) c_{root} \left(1+\lambda+\lambda^2\right) / (1+\lambda) \tag{3-6}$$

$$\bar{Y} = (b/6) \left[(1+2\lambda) / (1+\lambda) \right] \tag{3-7}$$

These parameters appeared above are demonstrated in the following Figure 3-1.

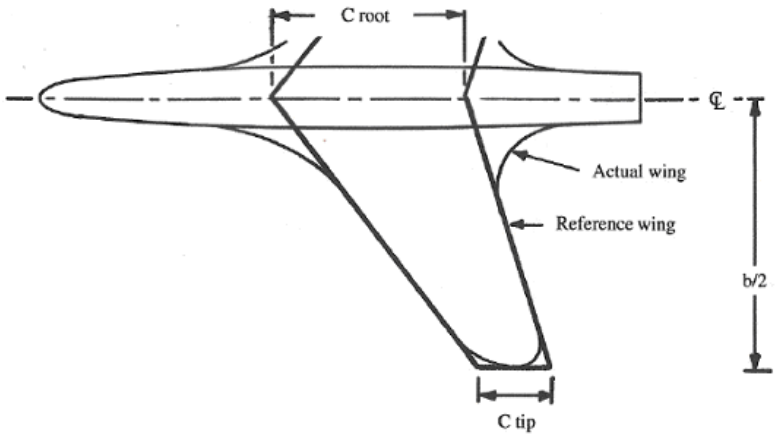

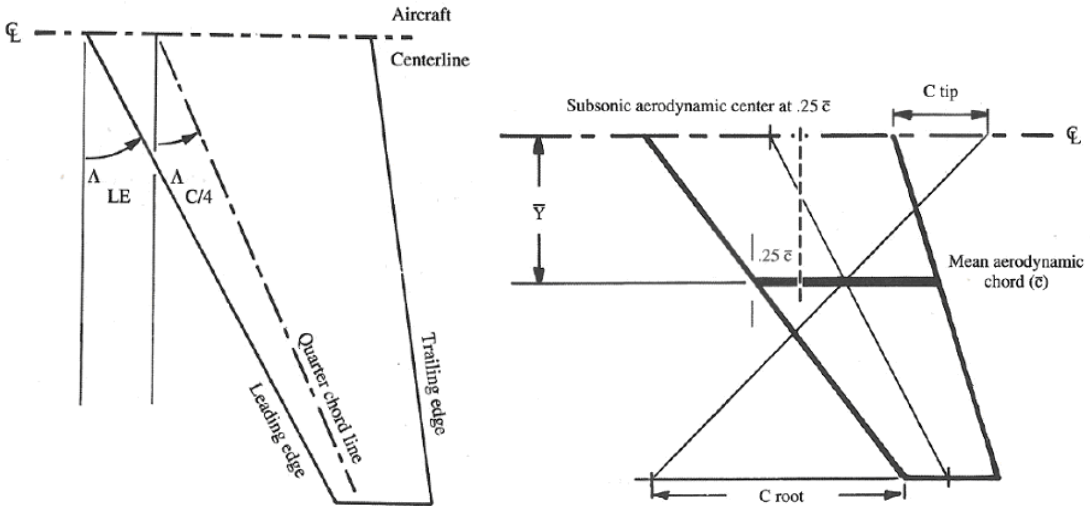

Figure 3-1 Wing geometry [9]

3. Wing Sub-panels Initial Sizing

According to historical statistics (Reference [7], [9]), initial size of wing sub-panels could be given as illustrated in Table 3-2.

Table 3-2 Wing sub-panels initial sizing

Component	Spanwise	Chordwise
Leading-edge high lift devices	Whole span	10-20% of the wing chord, typically 16%
Aileron	Outer 25% to 30% of the wing span	Rear 20-30% of the wing chord
Flap	From the side of the fuselage to aileron	Rear 20-30% of the wing chord
Spoiler	The same as the flap	

4. Wing Longitudinal Position

For the initial design it is sufficient to assume that the quarter mean aerodynamic chord point is located at the centre of gravity of the whole aircraft, which is usually estimated according to historical statistics initially.

5. Wing Vertical Position

At the initial design stage it is difficult to determine the precise vertical position of the wing with respect to the fuselage, however, it is necessary to decide whether it is high-wing or mid-wing or low-wing. In general the three options have their own preferred applications, as can be seen in Table 3-3.

Table 3-3 Wing vertical location

Wing vertical position	Preferred applications
High wing	Freight aircraft Smaller propeller-powered transport aircraft Some light aircraft Some combat aircraft Unmanned aircraft
Mid wing	Some high performance combat types Weapons systems aircraft with a long internal weapons bay Possibly multi-deck transport aircraft
Low wing	Majority of passenger transport aircraft Some light single- and twin-engine trainers Some combat aircraft

Following Table 3-3, a decision of low wing position was made.

6. Summarize

To summarize, the main geometrical parameters of the conventional concept aircraft are shown in Table 3-4 below. A 3-view drawing is given in Figure 3-2. The wing planform is indicated in Figure 3-3, in which the dashed lines

represent the actual edges while the solid lines demonstrate the idealised shape.

Table 3-4 Wing geometry parameters

Items	Vaues
Reference wing area	270 ㎡
Span	49.2 m
Aspect ratio	9
Root chord	8.75 m
Tip chord	2.17 m
Taper ratio	0.25
Leading edge sweep angle	30 °
Quarter chord sweep angle	26.5 °
Mean aerodynamic chord	5.83 m
Twist angle	-3°
Dihedral angle	5 °
Incidence angle	1 °
Wing aerofoil thickness	14%
Kink span/wing span	35%

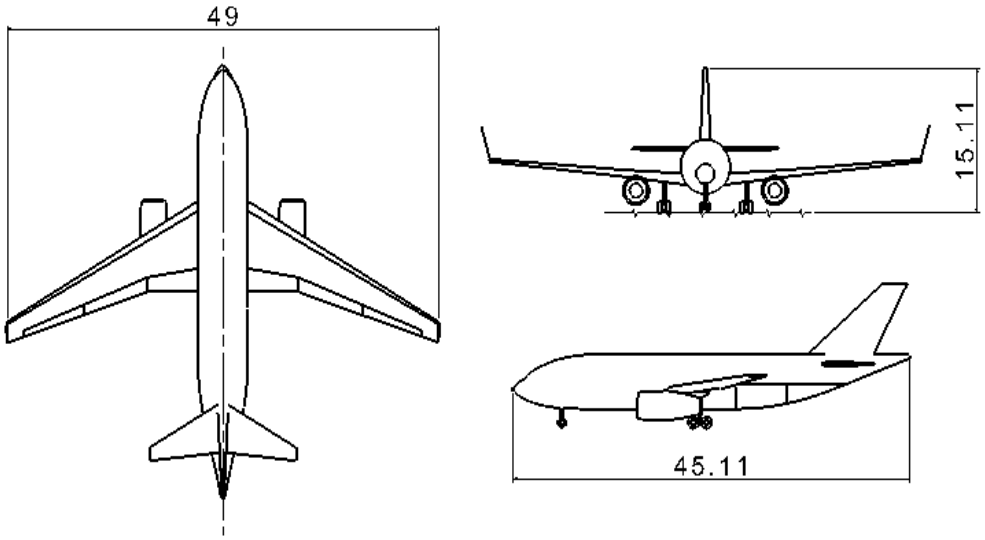

Figure 3-2 3-view drawing of the conventional concept aircraft

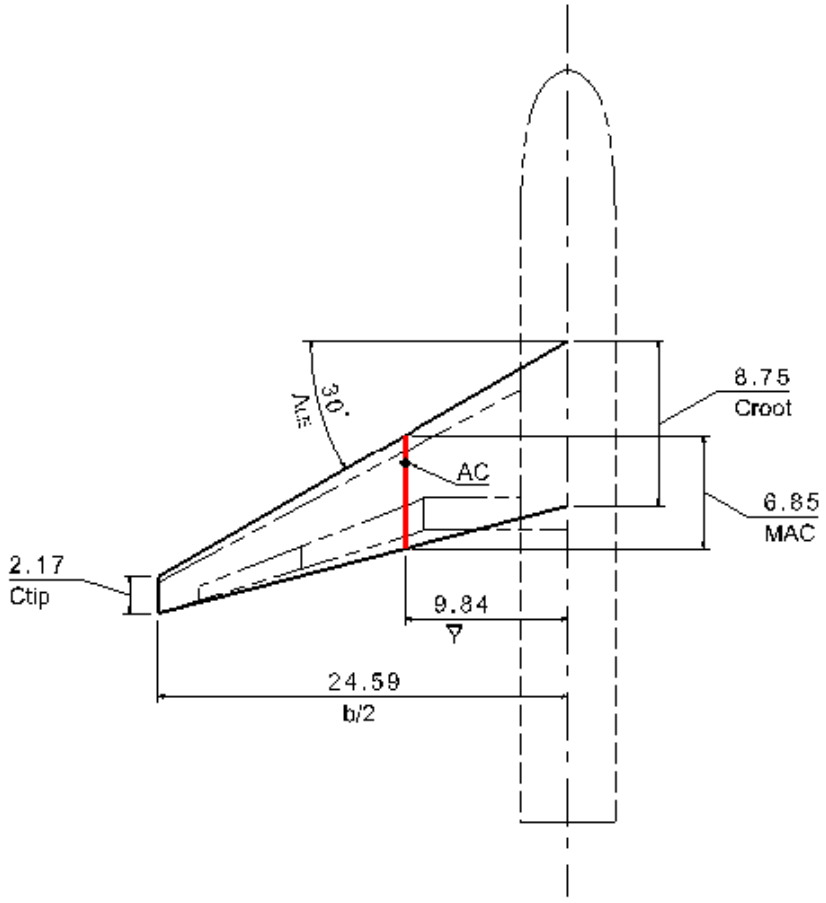

Figure 3-3 The conventional wing planform

3.3 Flying-Wing Concept

3.3.1 Concept Evolvement

Figure 3-4 shows the three flying-wing options considered in the beginning. Because DV configuration is more suitable for supersonic transport, it was excluded. Compared with BWB configuration, FW configuration is bound to have lower manufacturing cost, better load distribution, etc, so the pure flying-wing configuration was favoured initially.

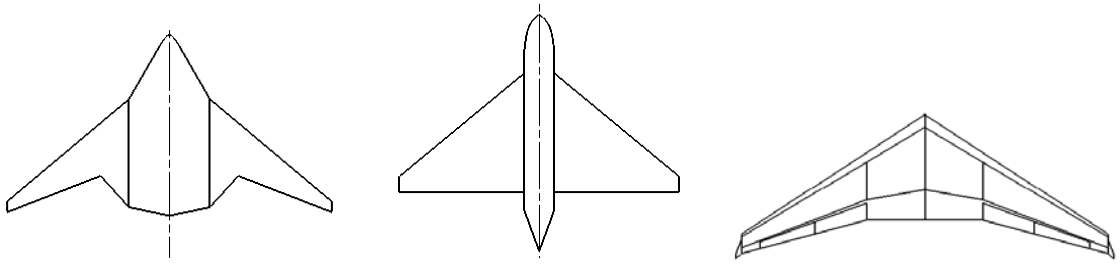

(a) BWB (b) DV (c) FW

Figure 3-4 Three flying-wing configurations

However, dozens of problems arose regarding the pure FW configuration, like the seating arrangement, cargo position, fuel tank location, etc, among which the most critical one was the conflict between the aerofoil thickness and the chord. If the chord was kept acceptable, as Figure 3-5 shows, in order to get the height required by cabin and cargo section, a far too thick aerofoil was needed, which would increase the drag tremendously. Alternatively, the height required could be met by extending the chord as shown in Figure 3-6. In that case, the whole wing ended up to be far too huge because a certain aspect ratio must be ensured. Eventually compromises were inevitably made to the pure and clean flying wing, by extending the chord of inner wing to get a certain height, and kinking the outer wing significantly to reduce the wetted area. Figure 3-7 shows the refined planform.

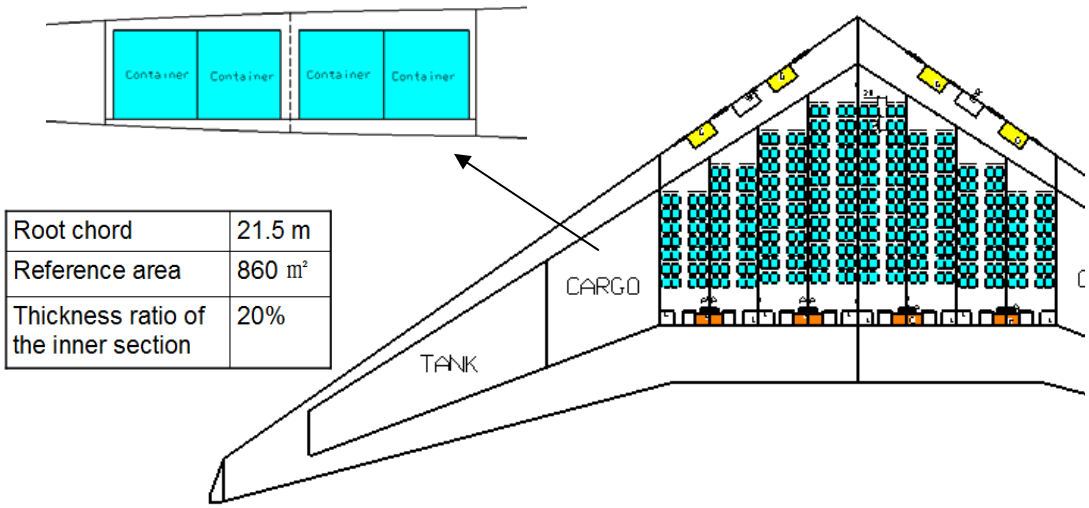

Root chord	21.5 m
Reference area	860 ㎡
Thickness ratio of the inner section	20%

Figure 3-5 Initial layout of the pure Flying Wing

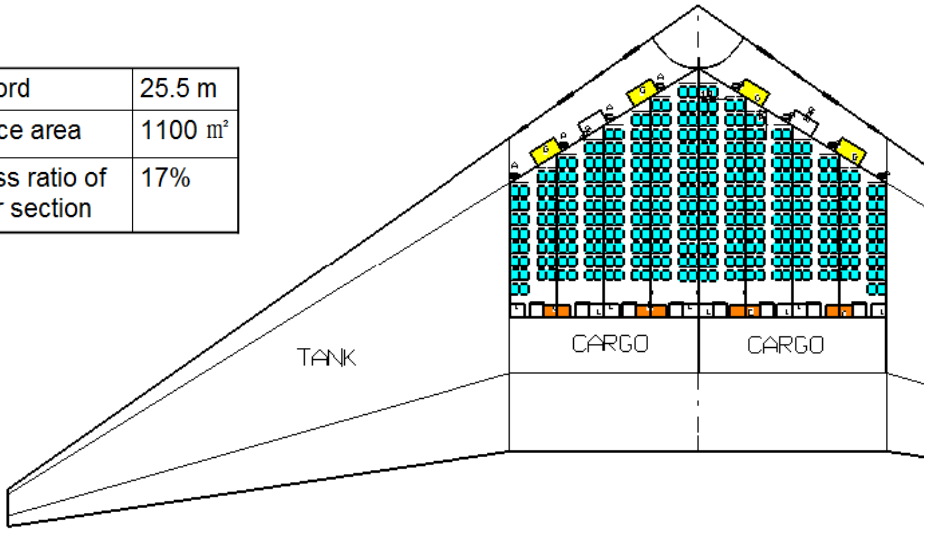

Root chord	25.5 m
Reference area	1100 ㎡
Thickness ratio of the inner section	17%

Figure 3-6 Modified initial layout of the pure Flying Wing

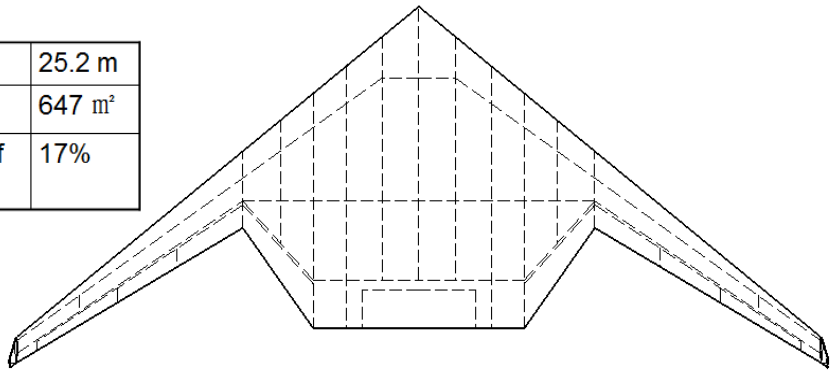

Root chord	25.2 m
Reference area	647 ㎡
Thickness ratio of the inner section	17%

Figure 3-7 Refined planform

3.3.2 Overall Configuration

The overall configuration layout is presented in Figure 3-8 below. The red coloured section shows the flight deck. The yellow colour represents the cabin. And the light green colour is for cargo. The dark green coloured sections represent outboard fuel tanks in the wing, and the shadowed area shows a tank section below the cargo, and the shadowed area in the middle shows another bit of tank below the cabin. Because an initial estimation of the centre of gravity (CG) indicated that the CG was a little bit backward, so it didn't take advantage of the volumes at the back for fuel tanks, and instead the fuel tanks were located forward keeping the volume at the back for system devices. Two bays coloured in dark were especially reserved for main landing gears, which were carefully designed so that it could be housed completely in the wing itself, without adding fairings. In the trailing edge, there are trim and control panels, split drag rudders, ailerons, flaps and elevators. With respect to the split drag rudder, it was employed and intended to make the wing clean, beautiful, and to reduce drag and weight as well. Two turbofan engines were installed over the wing at the rear. Eventually, the aircraft achieved the capability of carrying 250 passengers, 100 cubic metre of petrol, and 44 cubic metre cargo volumes.

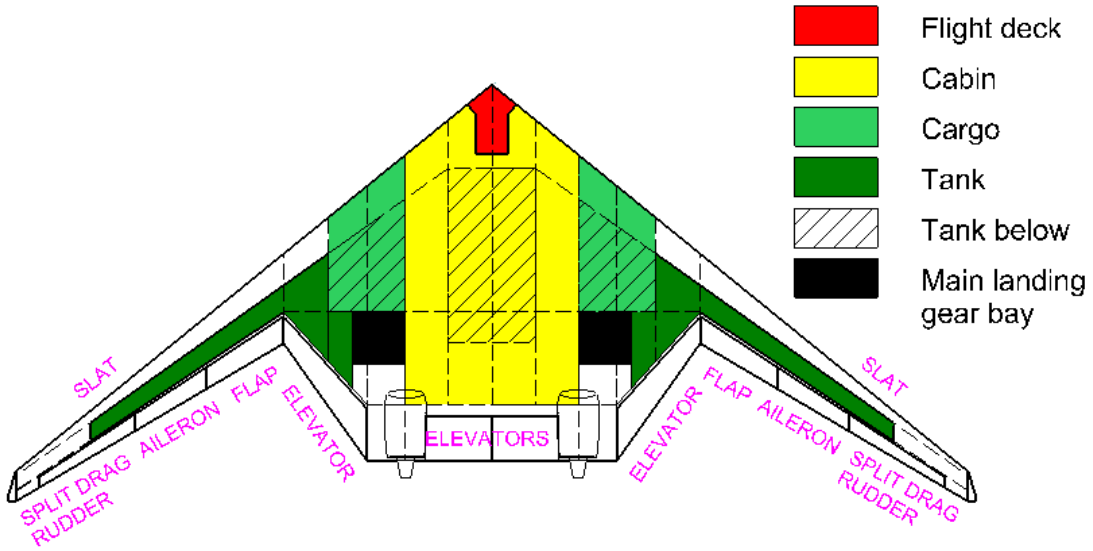

Figure 3-8 Overall configuration

Figure 3-9 shows the pressurized volume associated with the configuration in blue solid curves.

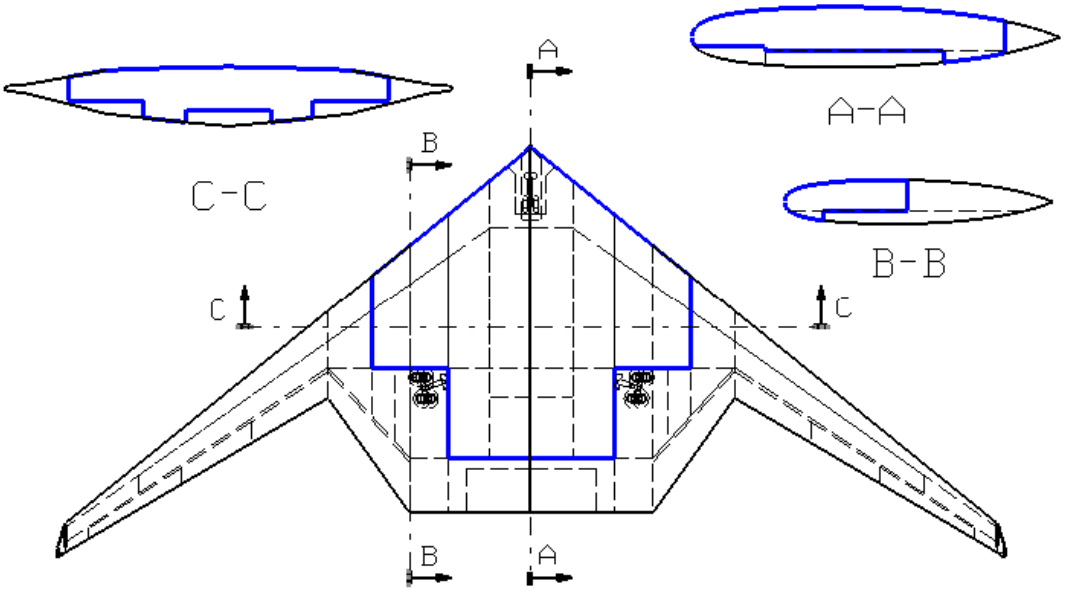

Figure 3-9 Pressurised volume

3.3.3 Geometry Sizing

A 3-view drawing of the Blue Bird is shown in Figure 3-11, from which it can be seen that the Blue Bird is about 65 metres in span, 28 metres in length and 7.7 metres in height. Figure 3-11 shows the main planform geometry parameters. Generally, the Blue Bird can be defined by inner wing, mid wing and outer wing. The inner wing is the section from the centreline to the first kink, and the mid wing is from the first kink to the second kink, and the outer wing is the outboard part of the second kink. Two airfoils are used for the wing. The first one is used for the inner wing, and the second one is used for the outer wing. The airfoil for the mid wing is to blend smoothly from the inner wing to the outer wing. In the inner wing, there are three spars. The front spar is located at 14% percent of the chord, and mid spar 50%, and rear spar 80%. While in the outer wing, there are two spars. The front spar is in the same line with the front spar of the inner wing, to say, 14% percent, and the rear spar is located at 65%. The kink position is primarily determined by the height of the local aerofoil thickness needed. Dimensions of 32 and 2 are set to get a sensible aspect ratio. The

leading edge angle is given at 39 degrees due to aerodynamic considerations. The other dimensions are kept to minimum while satisfy the volume requirement of the cabin, cargo and oil.

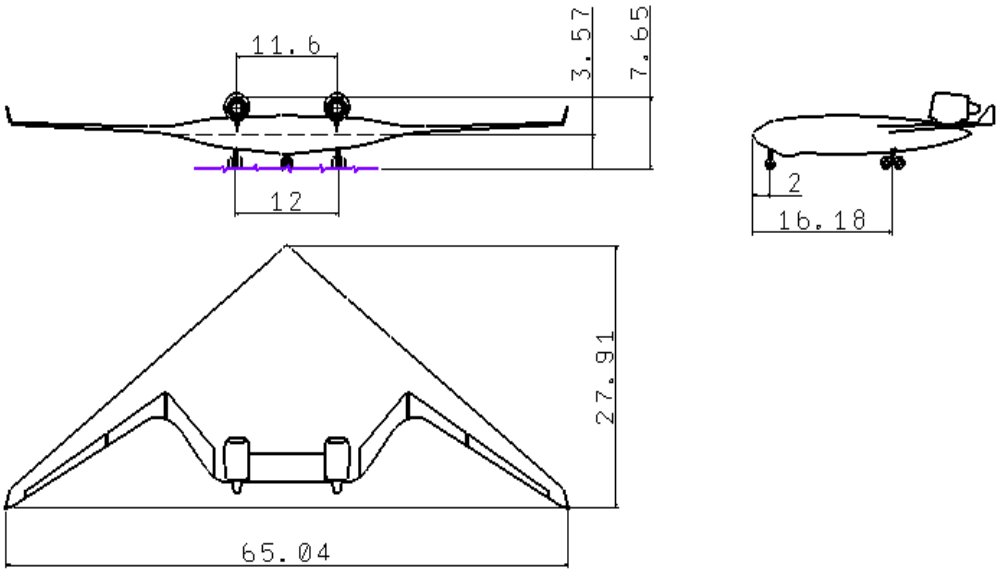

Figure 3-10 3-view drawing

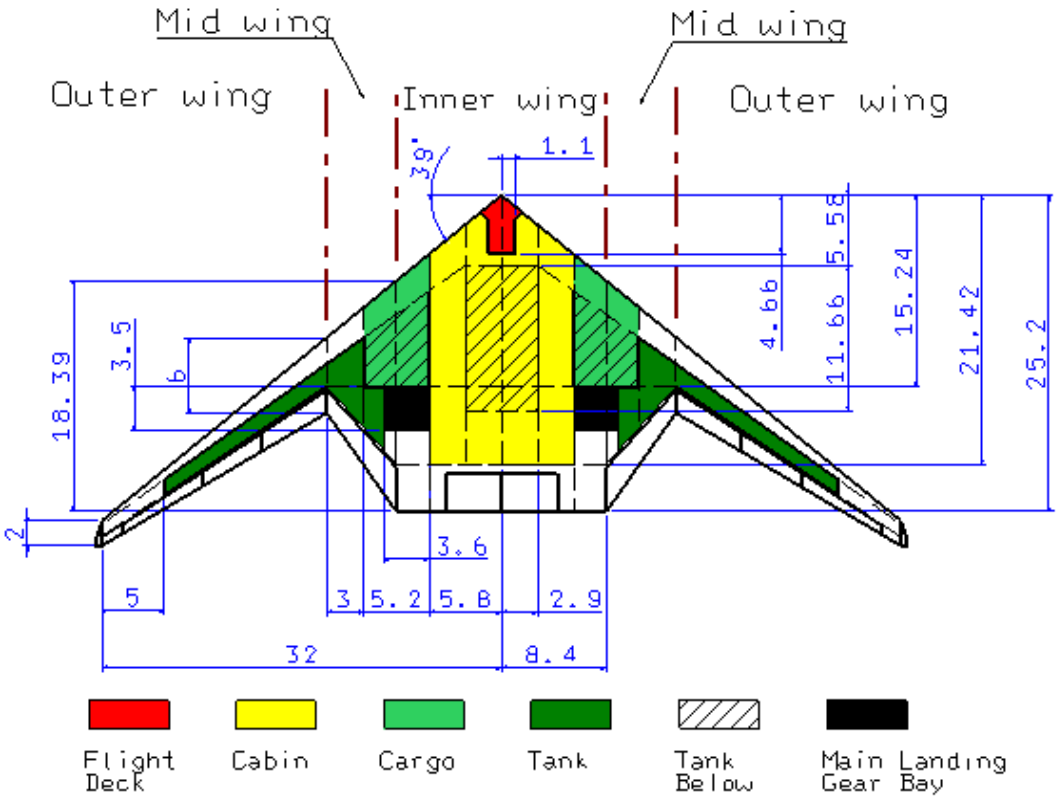

Figure 3-11 Wing planform dimensions

The dimensions of the leading edge devices and trailing edge devices are demonstrated in Figure 3-12 below. A fin is located at each wing tip, and the dimensions are shown in Figure 3-14.

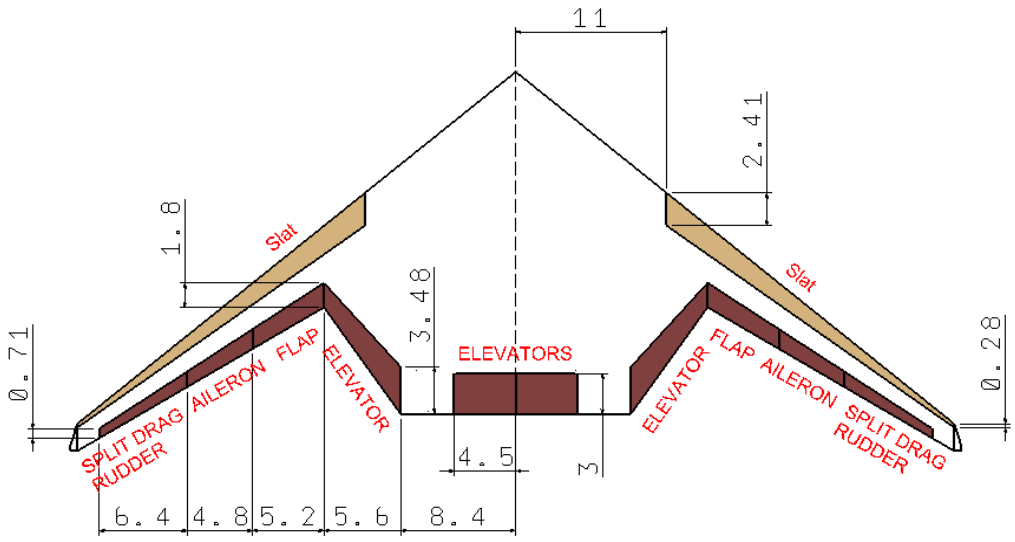

Figure 3-12 Leading edge and trailing edge devices

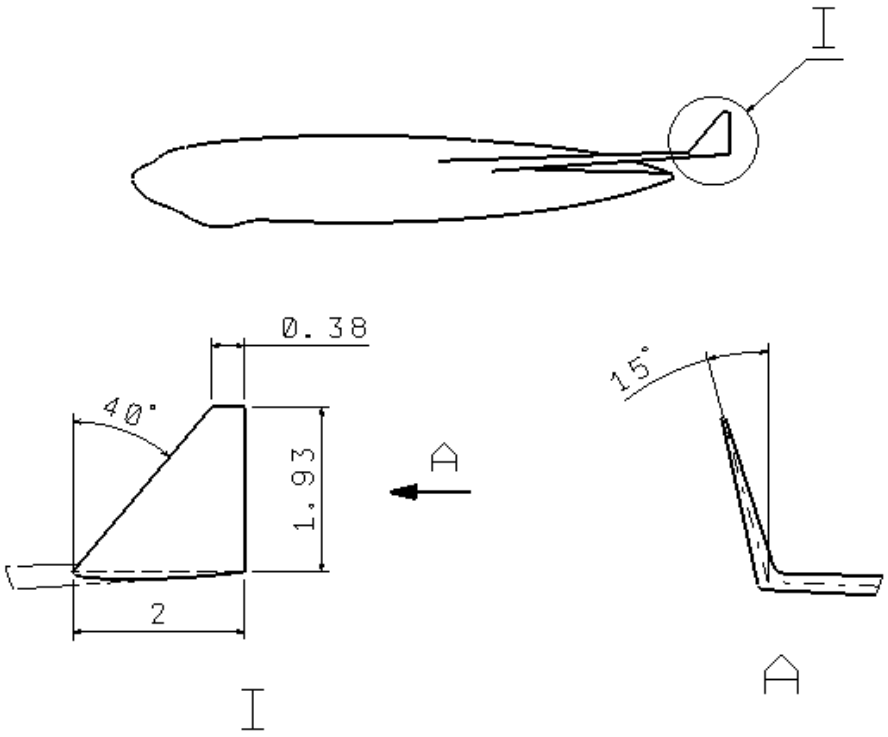

Figure 3-13 The dimensions of the fin

Due to the consideration of the stability, the wing is set to have a dihedral angle of 2 degrees, which is shown in Figure 3-14.

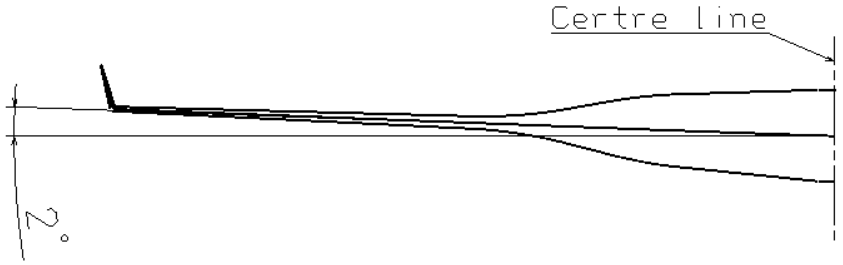

Figure 3-14 The dihedral angle

3.3.4 Summarize

To conclude, the main parameters of the Blue Bird are listed in Table 3-5 below. Figure 3-15 shows the idealised wing planform, in which the dashed lines represent the actual edges and the solid lines demonstrate the idealised shape.

Table 3-5 Main geometry parameters of the Blue Bird

Gross area	647 ㎡
Wing loading	272 kg/m^2
Aspect ratio	6.33
Root chord	25.2 m
Tip chord	2 m
Taper ratio	0.11
Leading edge sweep angle	39 °
Quarter chord sweep angle	34.3 °
Mean aerodynamic chord	12.28 m
Dihedral angle	2 °

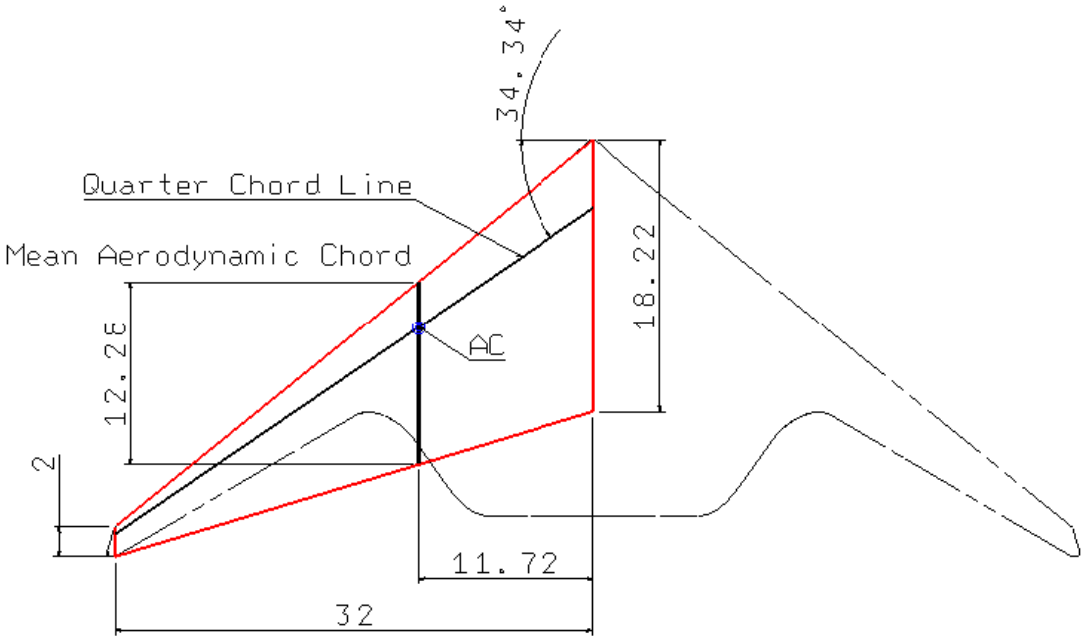

Figure 3-15 The idealised wing planform of the Blue Bird

4 INNER WING STRUCTRAL CONFIGURATION

In this chapter, three inner wing structure configurations will be proposed for the Blue Bird design. The first one is the Conventional Wing-Box Configuration (CWBC), simply a conventional wing box. The second one is the Multi-Bubble Configuration (MBC). The third one is a new concept proposed by the author, namely, Wave-Section Configuration (WSC). All of them are going to be introduced in this chapter, and will be initially sized by the methodologies in Chapter 1, and will be analysed and compared in Chapter 1.

4.1 Conventional Wing-Box Configuration

Figure 4-1 illustrates the Conventional Wing-Box Configuration of the fuselage section. The top and bottom covers are in skin-stringer construction. Besides taking the internal pressure differential load, the top cover also takes the compression load resulting from bending, and the bottom cover withstands the corresponding tensile load as well.

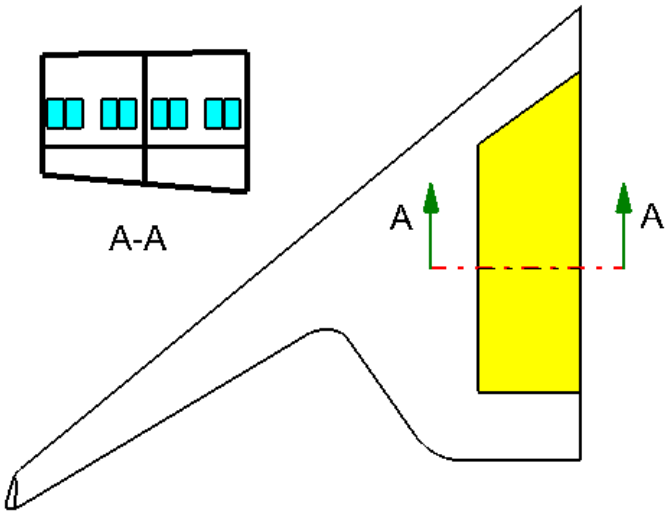

Figure 4-1 Conventional Wing-Box Configuration

4.2 Multi-Bubble Configuration

Figure 4-2 demonstrates an alternative concept for the fuselage section, Multi-Bubble Configuration. This arrangement utilizes the inner curved skin to resist internal pressure load, and allows the outer flat covers to react the bending

moment, resulting in compression at the top surface and tension at the bottom skin.

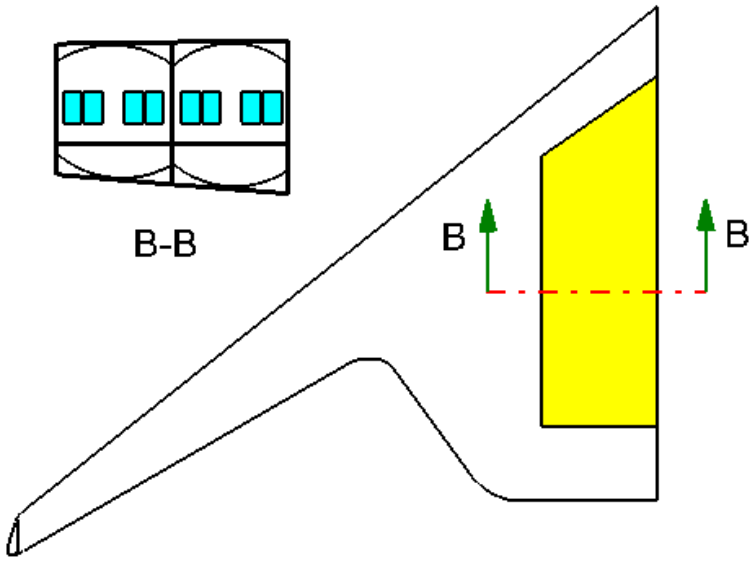

Figure 4-2 Multi-Bubble Configuration

4.3 Wave-Section Configuration

4.3.1 Refined Shape

The shape of the Blue Bird concept accomplished in the GDP program is shown in Figure 4-3. The author made attempts to refine the shape so that a new inner wing concept might be able to be employed. This chapter is going to illustrate how the shape is refined. And Chapter 4.3.2 is intended to discuss whether an optimal shape could be achieved. Lastly, the configuration will be specified in Chapter 4.3.3.

During the first stage, an initial version of the revised shape was completed based on the overall configuration of the Blue Bird, as shown in Figure 4-4. Since there are eight compartments needing pressurising in total, with the centre four compartments for cabin section and the rest four for cargo volume, eight tubes are required accordingly. This almost certainly would exert a tremendous influence on the aerodynamic performance. Therefore, it was modified again in a later stage as that shown in Figure 4-5. As can be seen, the amount of tubes was reduced from eight to four.

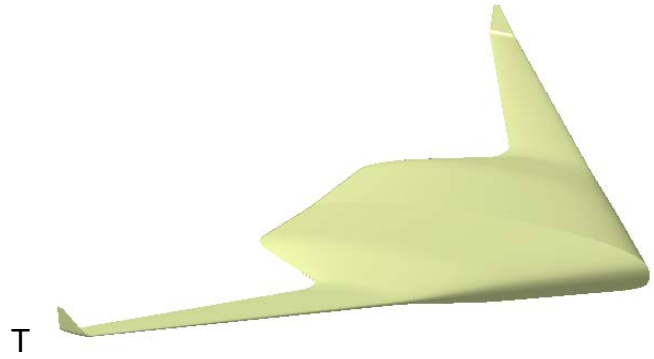

T

Figure 4-3 The Blue Bird

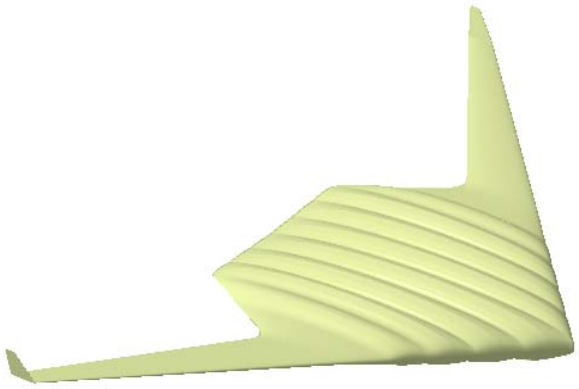

Figure 4-4 An initial version of the revised shape

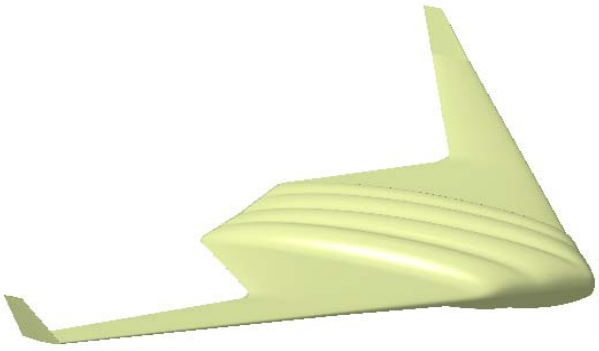

Figure 4-5 Final version of the revised shape

For the revised shapes shown in Figure 4-4 and Figure 4-5, the most significant feature lies in the shape of the inner wing (fuselage), which looks wrinkled spanwise and is still in standard airfoil shape in transverse section, so the concept of the inner wing configuration could be termed as the Wave-Section Configuration (WSC). In this thesis, the Wave-Section Configuration (WSC) will

particularly refer to the inner wing configuration of the final version of the revised shape, and the particular aircraft can be referred to the Wave-Section Configuration Aircraft (WSCA).

For the WSCA, some changes on the configuration arrangement were involved. Firstly, the cargo segment was relocated below the cabin in the centre, and the fuel tank previously located below the cabin was transferred to the outer wing. Secondly, the thickness of the wing airfoil in the middle two bays was increased slightly, but the thickness of the outer wing was reduced significantly. Figure 4-6 indicates the thickness changes between the Blue Bird and the WSCA. The dashed lines represent the Blue Bird and the dark lines represent the WSCA. Third, instead of carrying baggage plates like the Blue Bird, the most widely used standard LD3 container can be fitted in. The layout of cabin and tank

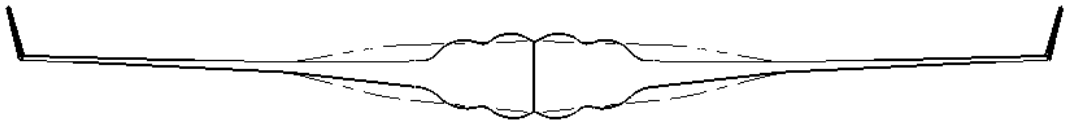

sections of the WSCA is shown in Figure 4-7.

Figure 4-6 Thickness changes

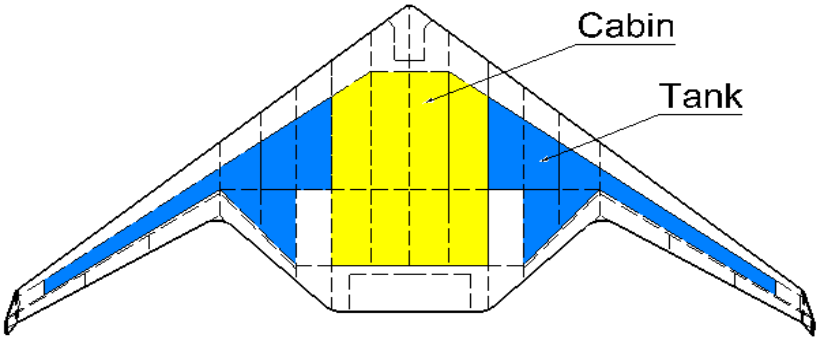

Figure 4-7 The layout of cabin and tank sections

The changes of the aerodynamic shape will impact on the drag of the aircraft. Due to limitations of time, this will not be incorporated in the scope of this thesis,

and the thesis is mainly intended to focus on the structural aspects. As to the Wave-Section Configuration, further work is needed to estimate its aerodynamic performance: on one side, the inner wing would introduce some drag penalties; on the other side, drag might be reduced because of the thickness reduction of the outer wing.

4.3.2 Optimal Radius of the WSC Wing Covers

For the inner wing covers of the WSC aircraft, two loads may be reacted by them. The first load is the pressure differential, which will result in membrane stress in the shell. The thickness of the shell required to resist the pressure load alone can be calculated by Equation (4-2).

$$t_p = \Delta pR / \sigma_p \qquad \textbf{(4-1)}$$

The second load is the compression (for the top shell) or tension (for the bottom shell) resulting from the bending moment, and this in return will cause bending moment in the shell as the compression/tension load is not in-plane. This case can be referred to as the Beam-Column theory, in which the curved beam is subjected to the compression load or tension load, with two ends simply supported. Because the results of compression load and tension load are basically the same theoretically, the compression load is going to be taken as an example. It is shown in Figure 4-8. The maximum bending moment, M, occurred in the middle of the beam. It is given in Equation (4-2), being equal to the compression load, P, multiplied by the force arm, δ, Where δ is able to obtained from the triangle relationship shown in the shadowed triangle in Figure 4-8, given by Equation (4-3). Therefore the resulting bending stress can be obtained by Equation (4-4), in which I is the moment of inertia of the beam transverse section, and y is the maximum distance to the axis of inertia. I is expressed in Equation (4-5), in which b is the width of the beam and t is the thickness of the shell. Substitute Equation (4-2) and (4-5) into Equation (4-4), the thickness t can be expressed by Equation (4-6).

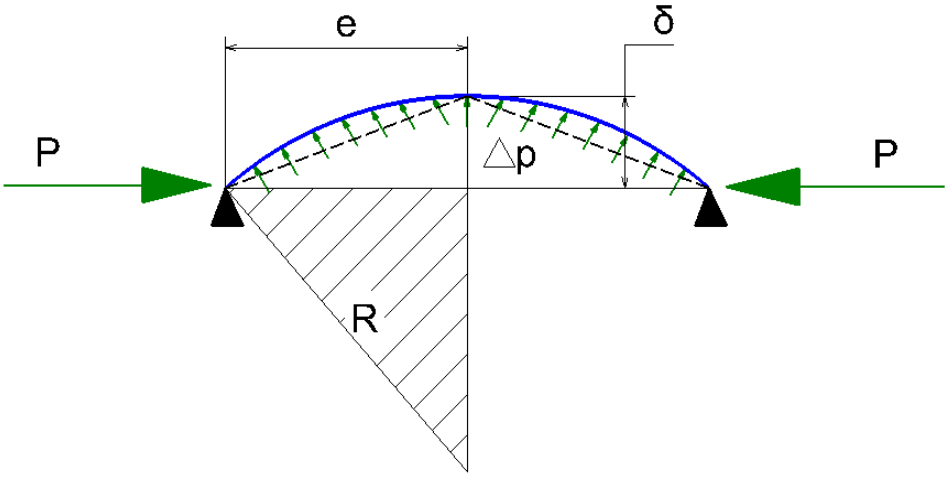

Figure 4-8 A Beam-Column model

$$M = P\delta \tag{4-2}$$

$$e^2 + (R-\delta)^2 = R^2 \tag{4-3}$$

$$\sigma_b = \frac{M \cdot y}{I} \tag{4-4}$$

$$I = \frac{1}{12} bt^3 \tag{4-5}$$

$$t = \sqrt[3]{\frac{12Myb}{\sigma_b}} \tag{4-6}$$

For a certain material, the allowable stress is given, so it can be known from Equation (5-19) and Equation (4-6) that the thickness required is connected with the radius of the beam.

By employing Equation (5-19) and Equation (4-2)-(4-6), two s-R curves can be figured out independently for the pressure load case and bending moment load case. As revealed in Figure 4-9, the weight is in direct proportion to the radius under pressure load case, while the weight is inversely proportional to the radius under the bending moment load case. Since the shell must have an adequate thickness to cater for both the pressure load case and the bending moment load case, the radius related to the intersection point of the two curved

is the optimal value in terms of lightest weight. The detailed calculation process can be found in Appendix A.

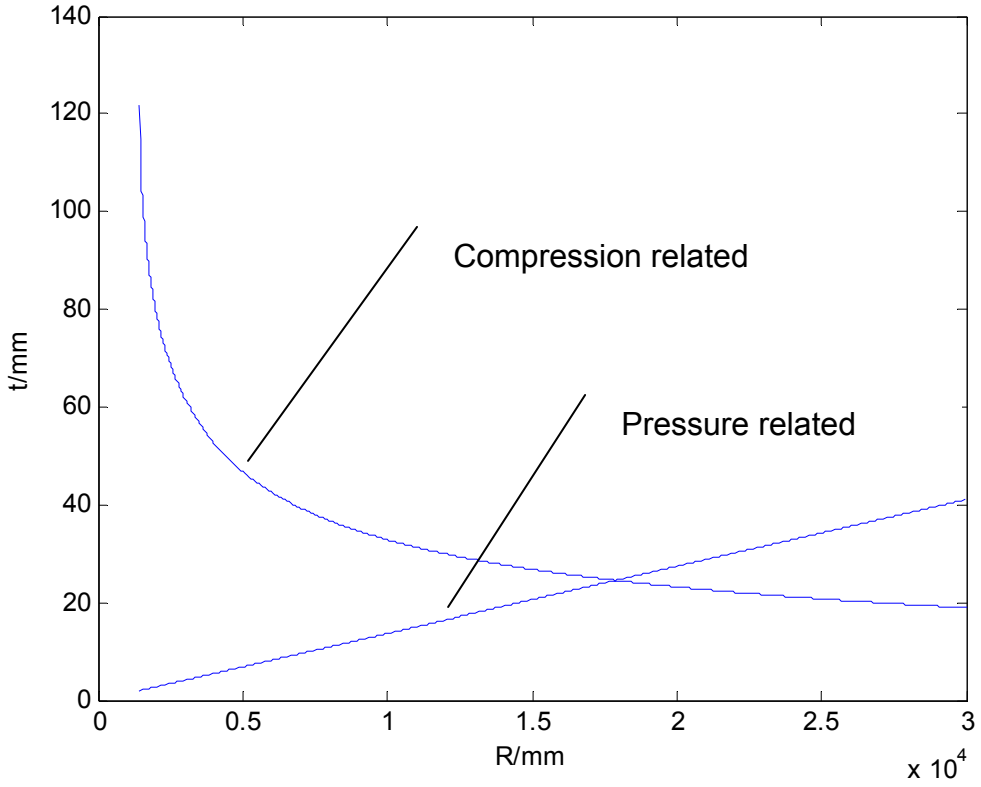

Figure 4-9 t-R curves

It can be seen from Figure 4-9 that the thickness required by pressure load increases as the radius goes up, while the thickness required by bending moment comes down, in inverse trend. The optimum design point is corresponding to the intersecting point of the two curves. It can be seen the optimum radius of the shell is about 18 metres when the thickness is approximately 25mm, in which the minimum thickness can be achieved under both pressure load and compression load (resulted from bending moment). This can be regarded as a somewhat flat cover. It also can be seen that the compression load case is more critical and the minimum thickness is pretty much determined by it. However, the thickness is still too large to be accepted because that would introduce substantial weight penalties. In conclusion, the

curved cover is not as efficient as the flat one in withstanding compression load, but it is better able to resist pressure load than the flat cover does.

4.3.3 Inner Wing Configuration

As indicated in Chapter 4.3.2, it is not wise to utilize the curved covers to resist compression/tension loads resulting from bending moment, and use the flat covers to react pressure differential load. On the other hand, it is preferable to take advantage of the curved surfaces to resist the pressure load and avoid taking the bending moment. One possible solution is to direct the majority of the bending loads onto the spars and restore the advantage of curved covers to resist pressure loads. Nevertheless, in the outer wing sections, where the surfaces are almost flat, it is still desirable to utilize the covers to react bending moment. Figure 4-10 below illustrates the load path of the bending load P and internal pressure Δp .

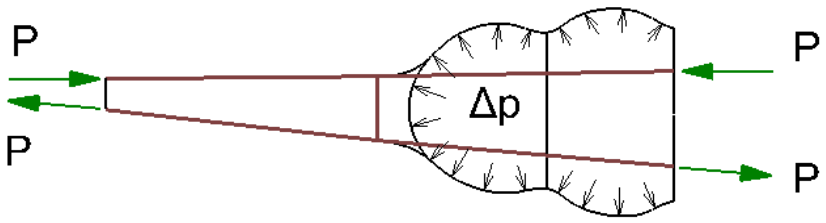

Figure 4-10 Load path

Figure 4-11 shows the Wave-Section Configuration of the inner wing (fuselage section). There are two tubes at each side of the wing, and the inboard tube is thicker than the outboard tube, so that the standard LD3 containers are able to be located below the cabin deck in the inboard tubes.

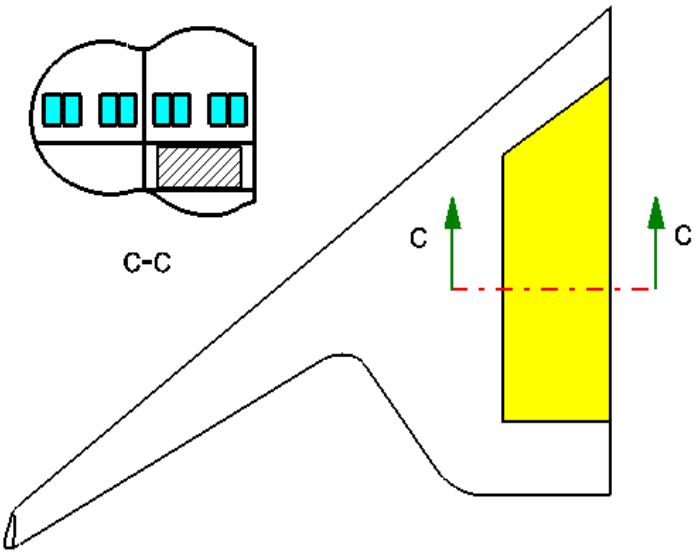

Figure 4-11 The Wave-Section Configuration

5 INITIAL SIZING PROCESS

This chapter is concerned about the methods employed to conduct the initial sizing for the three inner wing structural configurations discussed in the previous chapter, and the detailed process can be found in Appendix B.

5.1 Estimation of the Overall Shear Force, Bending Moments and Torsion

When the shear force diagram and bending moment diagram of the wing are not known precisely, it is generally desirable to make some rough assumptions for the purpose of initial sizing. As been shown in Figure 5-1, the total force, F, of a half wing can be assumed to be located at the point of the quarter of the mean aerodynamic chord, which has a distance of $\overline{Y}$ to the centreline. F could be assessed to equal the half maximum taking-off weight multiplied the maximum overload factor, 2.5, and the security factor, 1.5. That is expressed in Equation (5-1). Therefore, the maximum bending moment is given in Equation (5-2).

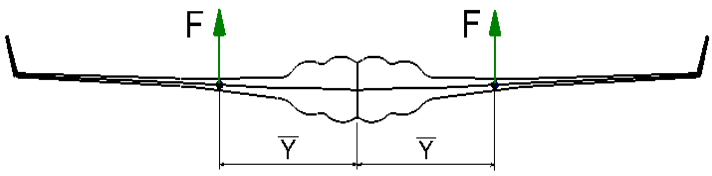

Figure 5-1 Total force

$$F = \frac{1}{2} Mg \times 2.5 \times 1.5 \tag{5-1}$$

$$M_y = F \cdot \overline{Y} \tag{5-2}$$

The flexural axis can be obtained by drawing a line going through two shear centres of the cross-sections. Based on the dimensions of the cross section shown in Figure 5-2, the shear centre is given by Equation (5-3). Figure 5-2 illustrates a wing cross section to define the shear centre, which is not limited to a specific spanwise position.

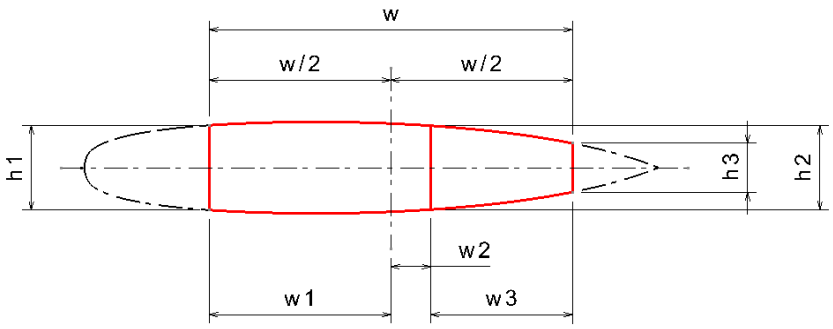

$$h_T = h_1 + h_2 + h_3 \qquad h = (h_1 + h_2 + h_3)/3$$

Figure 5-2 The cross section

where

h_T is the effective depth of all the spars

h is the idealised depth or the mean depth of the cross section

$$e_c = h_1^2 / (h_1^2 + h_3^2) \tag{5-3}$$

Two cross sections concerning the inner wing are used to define the shear centres. One is in the centreline position and the other is located at the outer side of the cabin section. After two shear centres have been located, the flexural Axis can be achieved by simply making a line going through them. Then the torque moment can be given approximately by Equation (5-4).

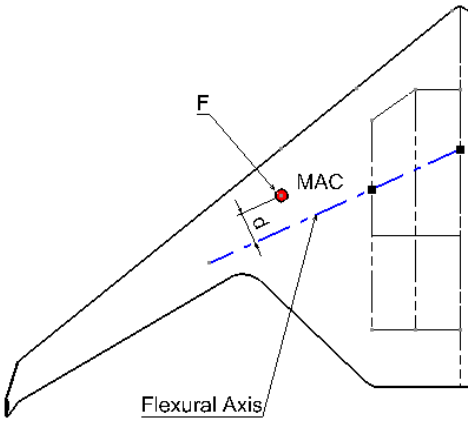

Figure 5-3The flexural axis

$$T = Fd \tag{5-4}$$

5.2 Overall bending moment

The following method (Reference [8]) is based on the assumption that the spar booms and the primary wing box covers are idealised as a single cover, having an uniform thickness.

a) Evaluate the idealized depth of the inner box section, h:

$$h = (h_1 + h_2 + h_3)/3 \tag{5-5}$$

b) Calculate the effective direct loads, P, in the upper and lower surfaces needed to resist the bending moment, M:

$$P = M / h \tag{5-6}$$

c) Evaluate the cross-section area required to react the bending moment at each side of the neutral axis of the wing box beam, A_b:

$$A_b = \frac{P}{\sigma_b} \tag{5-7}$$

d) Assume a uniform equivalent thickness of the cover, t_e, across the width of the box, w, is:

$$t_e = \frac{A_b}{w} = \frac{M}{hw\sigma_b} \tag{5-8}$$

where

σ_b is the allowable stress of the material used

e) The idealized value, t_e, is derived from the area of the skin and stringers. As an initial estimate, it is desirable to suggest that the skin contributes 65 percent of the effective area, so the thickness of the skin, t_b is:

$$t_b = 0.65t_e = \frac{0.65M}{hw\sigma_b} \quad \textbf{(5-9)}$$

f) Therefore, the stringers take up 35 percent of the effective area.

g) Stringer pitch is often 1.5 to 5 times the stringer height, determined by practical considerations. For initial work a value of 3.5 can be assumed.

h) In terms of separate Zed-section stringers, the width of each of the shorter flanges is often approximately 40 percent of the stringer height, providing a total cross-section area of '$1.8h_s t_s$' where h_s and t_s are respectively the stringer height and thickness. So the following equation can be derived based on the assumption that the total stringer area is 35 percent of the whole effective area:

$$0.35t_e \times 3.5h_s = 1.8h_s t_s \quad \textbf{(5-10)}$$

So that t_s is approximately:

$$t_s = 0.68t_e \quad \textbf{(5-11)}$$

This suggests that the stringer thickness should be roughly equal to the skin thickness.

i) The width to thickness ratio of the free flange is typically about 16, due to local and overall bucking considerations. Hence $0.4h_s$ equals $16t_s$, and therefore：

$$h_s = 40t_s$$

The stringer area = $72(t_s)^2 = 70(t_b)^2$

5.3 Overall Torque moment

The following method (Reference [8]) is used to derive the thickness of outer surfaces and spar webs required to react the torsion loading.

Equation (5-12) gives the approximate corresponding shear flow in the covers and webs:

$$Q_T = T / 2A \tag{5-12}$$

where

A is the enclosed area of the primary box cross-section at a given span wise, and T is the magnitude of the ultimate applied, distributed torsion.

For a selected material, the allowable shear stress is σ_s , so the average material thickness required to react the torque moment can be given as:

$$t_q = Q_T / \sigma_s = T / 2A\sigma_s \tag{5-13}$$

5.4 Spar Webs

While an adequate initial estimate of the shear thickness needed in the upper and lower covers is given in the previous chapter, it is necessary to take account of the additional vertical shear loads to obtain the required thickness of the spar webs. [8]

a) Evaluate the total effective depth of all the spars, h_T :

$$h_T = h_1 + h_2 + h_3 \tag{5-14}$$

b) The shear flow in the webs due to the ultimate vertical shear force, V, is:

$$Q_V = V / h_T \tag{5-15}$$

c) The net shear flow in the webs is then approximately given by:

$$Q_w = Q_V + 2xQ_T / w \tag{5-16}$$

where

x is the chord-wise location of a particular web relative to the mid-point of the box.

d) The web thickness can be got then:

$$t_w = Q_w / \sigma_s \tag{5-17}$$

5.5 Fuselage pressurization

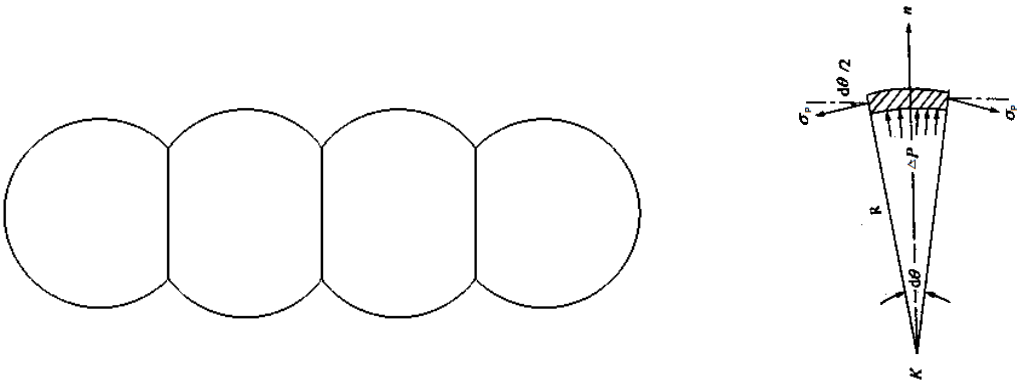

(a) The cross section (b) A part-of-cylinder shell

Figure 5-4 The pressurised vessel of the MBC and WSC

The pressurized vessel of the MBC and WSC is roughly shown in Figure 5-4(a). Because the vertical webs have equal pressure on both sides, they do not affect the loads applied on the part-of-cylinder shell (as shown in Figure 5-4(b)), in which no bending moment is generated and only tension stress exists. With respect to Figure 5-4(b), Projecting the forces to the n axis, the balance equation is achieved:

$$2\sigma_p t_p \sin\frac{d\theta}{2} = \Delta p 2R \sin\frac{d\theta}{2} \tag{5-18}$$

so

$$t_p = \Delta p R / \sigma_p \tag{5-19}$$

Where

t_p is the thickness of the shell required

Δp is the maximum working differential pressure

R is the lacal radius of the shell

σ_p is the allowable tensile working stress.

5.6 Flat pressure panels

According to the method provided by ESDU Data Sheet 71013, for a flat rectangular panel having isotropic material properties and simply supported edges under pressure load, the required thickness is approximately:

$$t = [0.71 \Delta p a^2 \{n^3 / (n^3 + 1.5)\} / \sigma_a]^{1/2} \quad \textbf{(5-20)}$$

If there are two rows of fasteners at each panel edge, the thickness is approximately:

$$t = [0.5 \Delta p a^2 \{n^4 / (n^4 + 0.6)\} / \sigma_a]^{1/2} \quad \textbf{(5-21)}$$

where

σ_a is the allowable stress

Δp is the pressure differential

a is the length of the shortest side

n is the ration of the longer to shorter side

5.7 Initial Sizing

By using the methods presented above, an initial sizing is obtained as shown in Table 5-1. Note that the largest one is selected when more than one value is obtained. The calculation process can be found in Appendix B.

Table 5-1 Initial Sizing Results

Configuration	Skin		Spar	
	Thickness/mm	Critical condition	Thickness/mm	Critical condition
CWBC	5.3	Pressure	Front: 2.6 Mid: 1.8 Rear: 2.4	Shear
MBC	Outer cover: 1.3	Pressure	Front: 2.6 Mid: 1.8 Rear: 2.4	Shear
	Inner skin: 2.6	Shear		
WSC	Curved skin: 2.6	Pressure	Curved spar flange: 200×42	Bending
	Flat skin: 3.0	Bending	Front spar web: 9.9 Middle spar web: 4.8 Rear spar web: 8.5	Shear

6 FE ANALYSIS

6.1 Introduction

This chapter is primarily concerned with the FE analysis of the three configurations of the inner wing presented in Chapter 1. The FE analysis is aimed at verifying and adjusting the initial design to ensure that the stress level is close, but not exceeding the allowable limit in the components of the three configurations. In the design, aluminium alloy is used as the material, for which the allowable (ultimate) tension/compression stress is 340 MPa and the allowable shear stress is 170 MPa. Based on the results, the optimal configuration can be determined in terms of weight.

6.2 Nastran/Patran

Nastran/Patran are employed as the FEA tool in this thesis. They have historically been proved to be sophisticated and reliable, and they are widely used across the aerospace industry. Nastran is a powerful solver, capable of dealing with many types of analysis, including linear cases and non-linear cases. Patran is a friendly pre/post processor, which caters for purposes ranging from geometry modelling and results visualization.

6.3 FEA Process

Generally, a FEA process goes through the steps of importing geometry, meshing geometry, defining material properties, defining element properties, applying boundary constraints, applying loads, submitting for analysis and analysing results. This is shown in Figure 6-1 below.

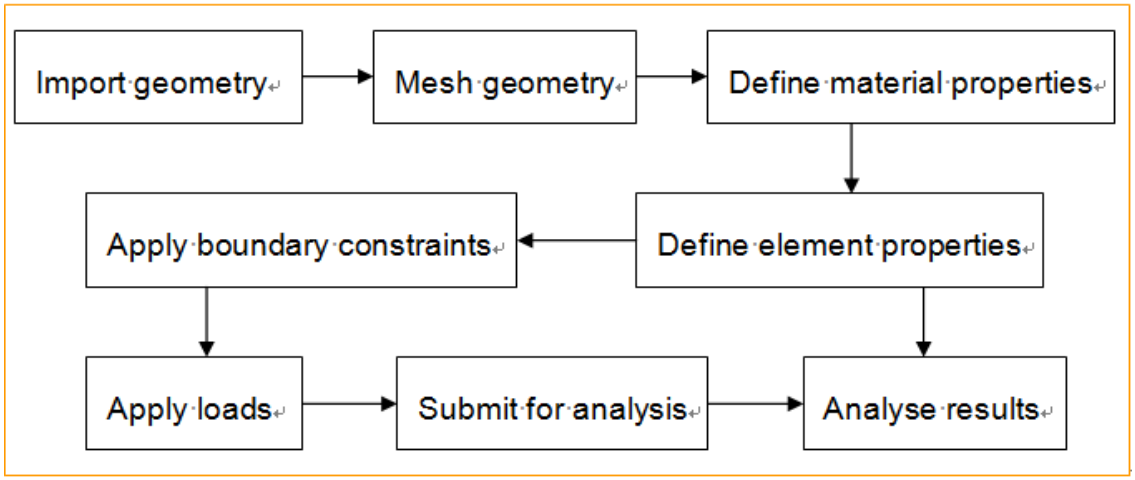

Figure 6-1 FEA process

6.4 FE Model

6.4.1 Introduction

For simplification, it is sensible to model only part of the inner wing to conduct the FE analysis instead of the whole inner wing section, because the entire inner wing has somewhat similar features. The models are in between the front spar and the middle spar, and are 11 metres spanwise, inclusive of the cabin and cargo volumes. And finally, the analysis results will be extended to the whole inner wing box, which is in between the front spar and the rear span, also 11 meters in span.

6.4.2 Geometry

1. Conventional Wing-Box Configuration

The shadowed area in the left drawing of Figure 6-2 shows the location of the model, and the right diagram is the geometry of the CWBC model. As can be seen, the CWBC geometry mainly comprises top covers, bottoms covers, front spar, aft spar and five ribs.

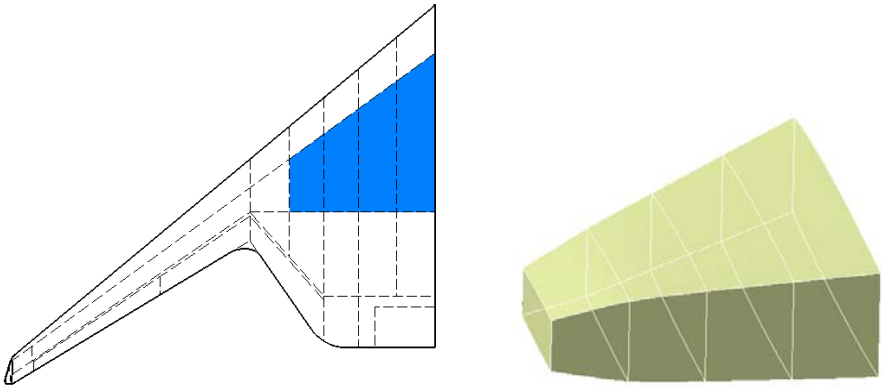

Figure 6-2 CWBC geometry

2. Multi-Bubble Configuration (MBC)

The MBC has similar geometry to the CWBC as shown in Figure 6-2, because they have the same shape and planform arrangement. The only difference is that the MBC has outer covers and inner pressure vessels. In the FE analysis, only the outer wing box will be modelled. The stress and mass of the pressurized inner vessels will be calculated separately by hand for simplicity without compromising the accuracy. The inner vessels are only connected to the vertical ribs, which have equal pressure on both sides and would not be affected significantly.

3. Wave-Section Configuration

The WSC geometry is shown in Figure 6-3 of the right part, and the left part shows where the model locates in the aircraft planform. The model consists of curved skin, flat skin, spars and ribs.

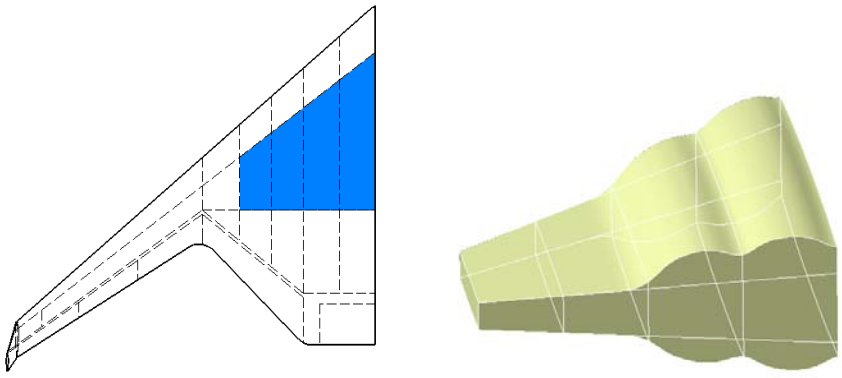

Figure 6-3 WSC geometry

6.4.3 Meshing

The meshing process generates the nodes on which the elements are based. The first step is to create mesh seeds, which determine the element size and controls the node locations at certain places (i.e. at the intersections). It is very important to make sure that the intersecting structural sections share the same nodes. After this, meshing can be generated. Two element types are utilized for the models. One is the QUAD4 shell element, which is typically used for representing skins, spar webs and rib webs. The other one is BAR2, which is used to represent beam elements, modelling stringers, spar caps and rib caps. The meshing process should be followed by the equivalence function that will delete the overlapped nodes, or problems will be caused when the analysis is activated.

The meshing model of the CWBC and MBC is shown in Figure 6-4, and that of the WSC is shown in Figure 6-5.

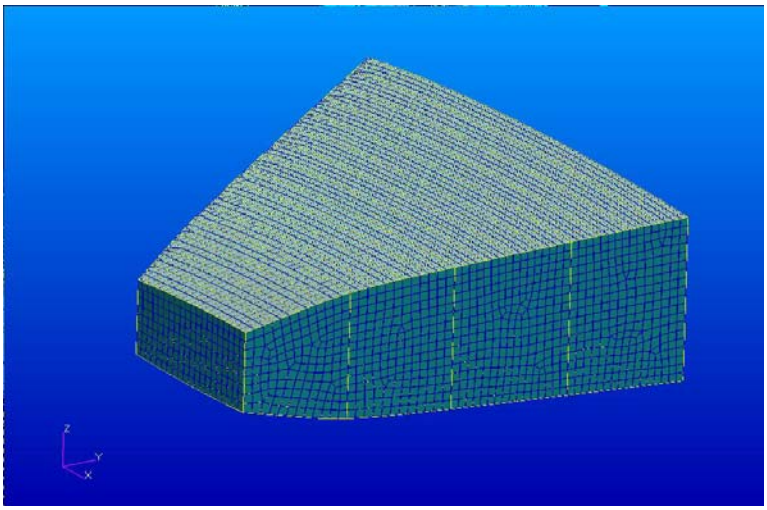

Figure 6-4 Meshing of the CWBC and MBC model

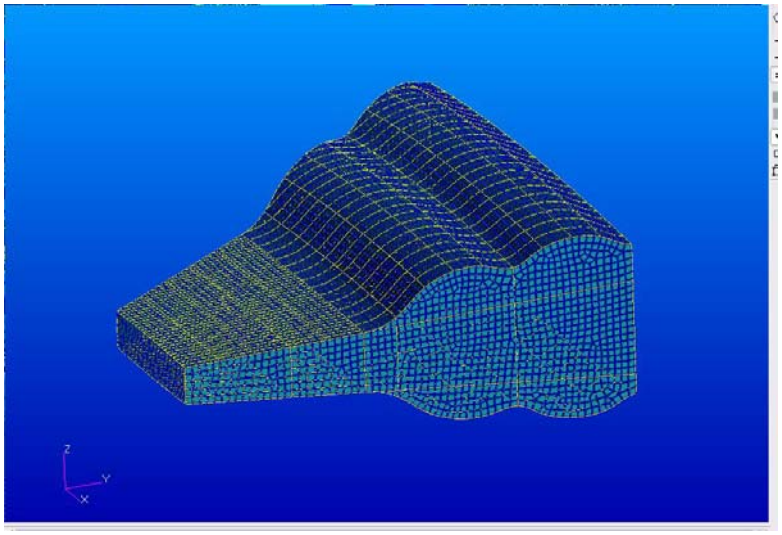

Figure 6-5 Meshing of the WSC model

6.4.4 Defining Material Properties

In the scope of this thesis, structural materials are limited to aluminium alloy. In particular, 2024 aluminium is used for skins, stingers; and 7050 aluminium is used for spars and reinforced ribs. The main material properties of these two alloys are listed in Table 6-1 below. Generally, the allowable tension and compression stress is no more than 340 MPa, and the hoop tensile stress of the skin is around 100 MPa. These are going to be constraints of the FE analysis in the later stages.

Table 6-1 Material properties

Material	Yong's modular, E	Poison ratio	Density	σ_b /MPa
2024	71000 MPa	0.33	2700 kg/m^3	340 (100 for hoop stress)
7050	71000 MPa	0.33	2700 kg/m^3	340

6.4.5 Defining the Element Properties

The Shell Element property is applied to the skin, requiring knowledge of material and skin thickness.

The Beam Element property is applied for the stringers, spar caps and rib caps. This requires the input of the material, the transverse section, and the position (node offsets). In the inner wing models, the typical Z cross section is utilized for stringers, and rectangular section is used for spar caps and rib caps.

6.4.6 Applying Boundary Constraints and Loads

The three models, CWBC model, MBC model and WSC model, are analysed under the same boundary constraints and loads. With the boundary constraints, the centre rib is fixed and all other components have six degrees of freedom. With respect to the loads, there are four separate loads applied to the FE models. The first load is the shear force that is applied onto the nodes of the tip-rib caps. The second load is the compression load on the top cover, which is produced by the bending moment. The third load, tension load on the bottom cover, is also resulted from the bending moment, and it is equal to the compression load. Lastly, the internal pressure differential load is applied to the pressurization vessels.

The shear force and bending moment can be obtained from Mr Chao Tong' s work in Reference [10]. The shear force is 350,000 N, and the bending moment is 3,710,000 N • m at the spanwise station of 11 metres, which is the size of the models in span. Those loads are multiplied by an overload factor of 2.5, and a ultimate load factor of 1.5. Then the bending moment is converted into the compression force and tension force. The pressure load is calculated to be 0.137 MPa, which is 1.5 (security factor) times the maximum pressure differential when the aircraft approaches the designed flight ceiling.

Figure 6-6 shows the constraints and loads of the CWBC model and MBC model. Figure 6-7 shows the constraints and loads of the WSC model. The detail of how the loads are calculated can be found in Appendix C.

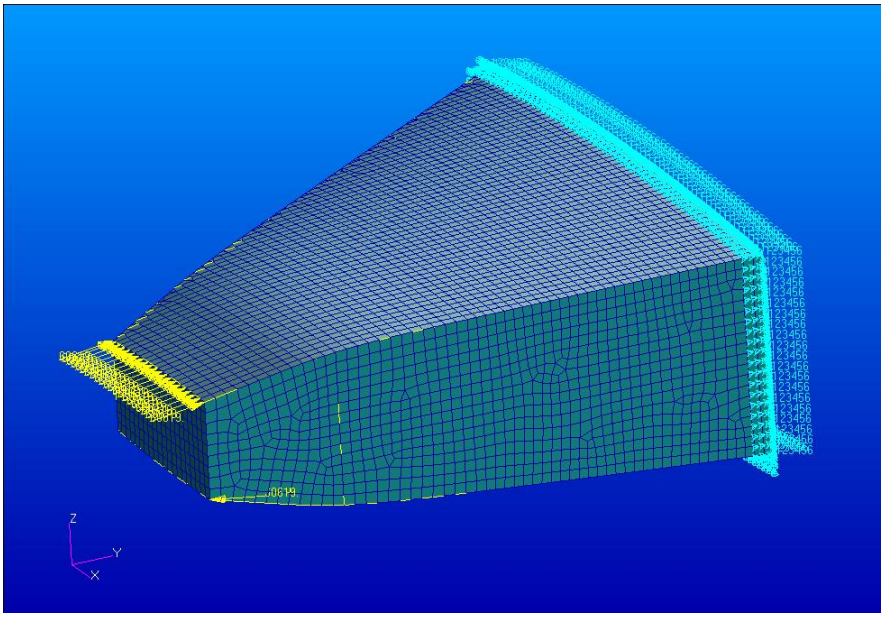

Figure 6-6 The constraints and loads of the CWBC and MBC model

(Compression/tension: 6.08×10^{6} N, shear force: 7.88×10^{5} N, pressure differential: 0.137MPa)

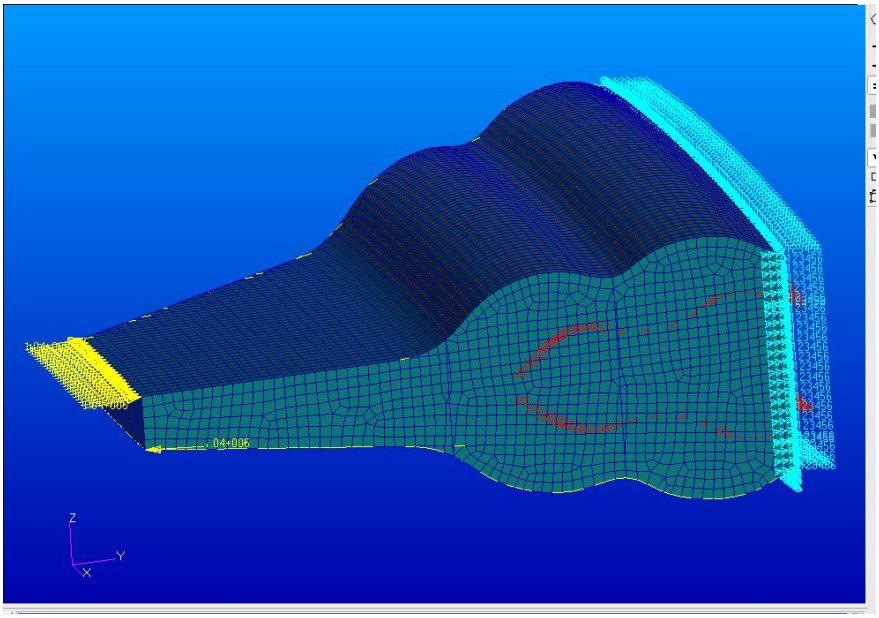

Figure 6-7 The constraints and loads of the WSC model

(Compression/tension: 1.07×10^{7} N, shear force: 7.88×10^{5} N, pressure differential: 0.137MPa)

6.5 Submitting for Analysis

The models are input to Nastran for analysis, in the form of linear static solution.

6.6 Results Analysis

The results are checked and recalculated by modifying the element properties in Patran or in bdf document until they become reasonable, and the results are also validated by means of hand calculations and actual aircraft comparison. Eventually, the FEA results for the three types of inner wing configuration are illustrated as follows.

1. CWBC

The stress of the CWBC model is shown in Figure 6-8, and the maximum stress is 360 MPa.

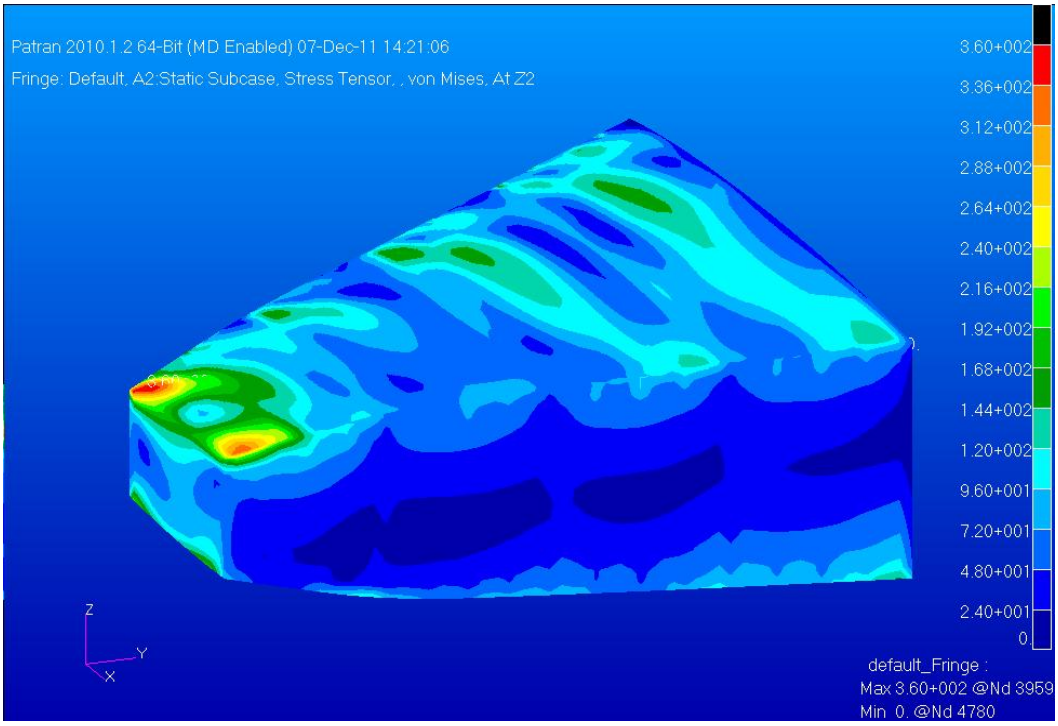

Figure 6-8 Stress of the CWBC model

2. MBC

It can be seen from Figure 6-9 that the maximum stress in the MBC model is 320 MPa.

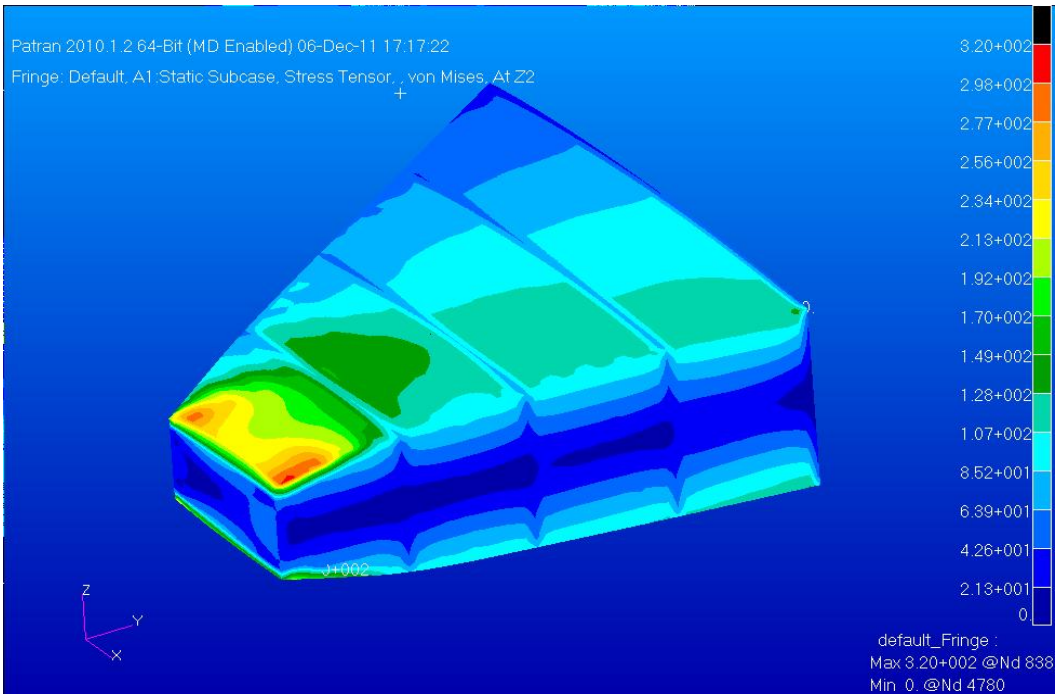

Figure 6-9 Stress of the MBC model

3. WSC

For the WSC model, the FEA process can be broken into two phases. In the fist phase, the thickness of each structural item is continually adjusted according to the analysis results but kept constant across the whole dimension. The results of displacement and stress are shown in Figure 6-10 and Figure 6-11. As can be seen, the maximum displacement is about 270 mm, and the maximum stress reaches about 1000 MPa, much higher than the allowable stress (340 MPa). It can be seen from Figure 6-11 that the problem is the stress concentration, which occurs at the shape transition places of the skins and spars.

Hence in the next phase, certain places of the skins and spars where the stress concentrates are strengthened. Finally the design is improved significantly and the FEA results indicate that it becomes acceptable. The displacement is shown in Figure 6-12, reducing from 270 mm to about 180 mm. The stress distribution is shown in Figure 6-13, and this is reduced from 1000 MPa to the acceptable level around 340 MPa.

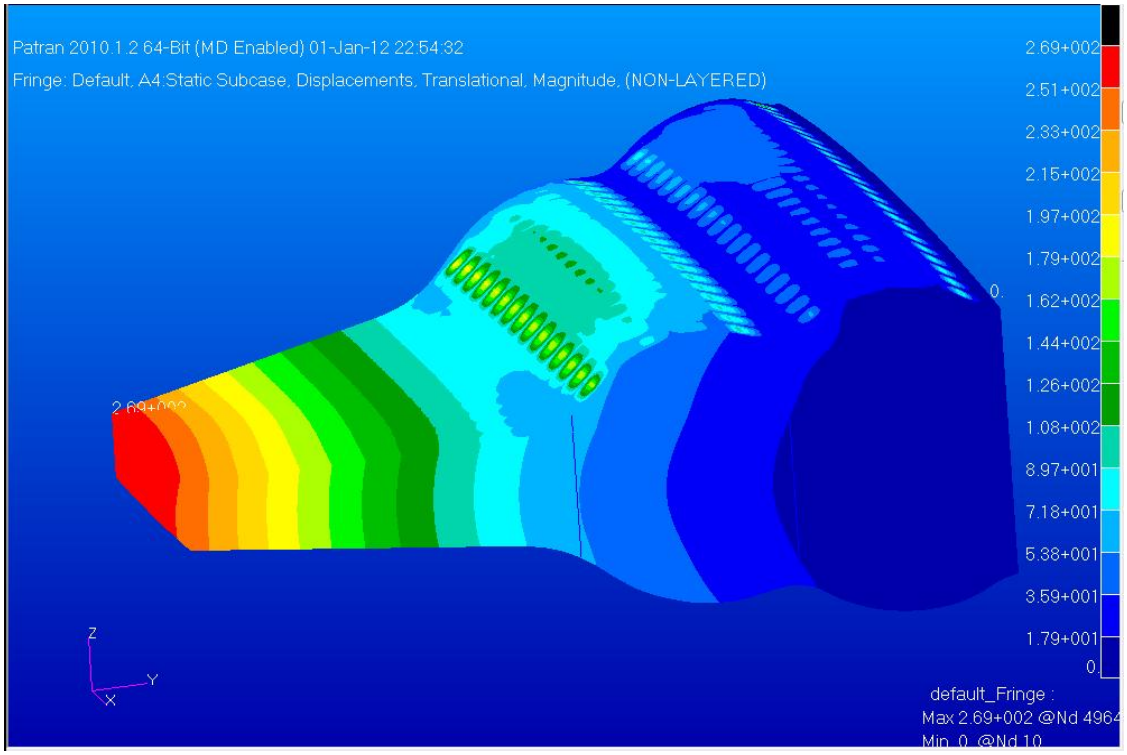

Figure 6-10 Displacement of the WSC model

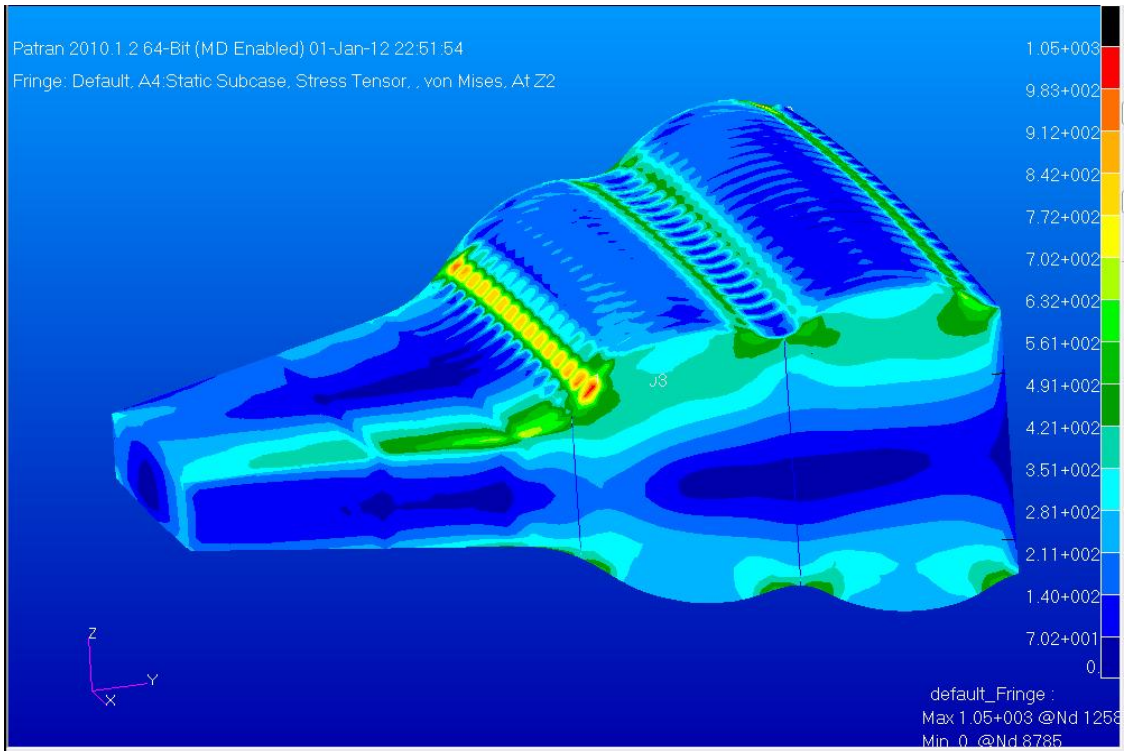

Figure 6-11 Stress of the WSC model

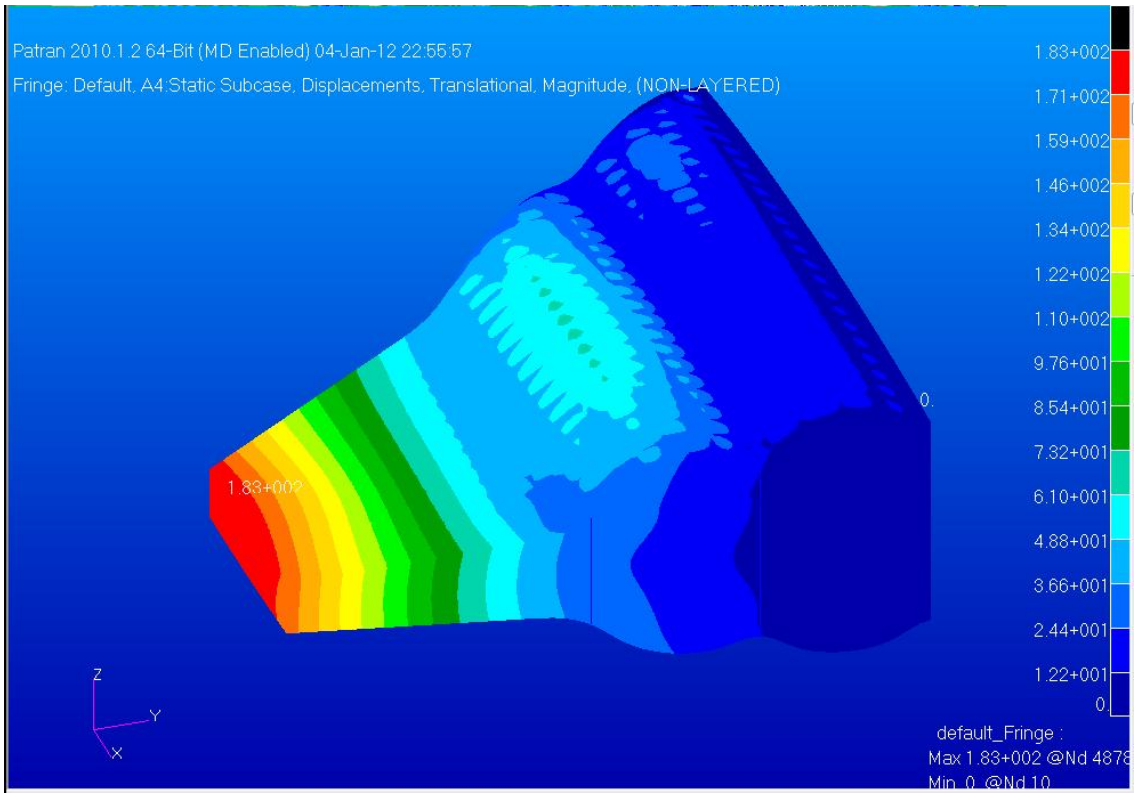

Figure 6-12 Displacement of the WSC model: after being strengthened

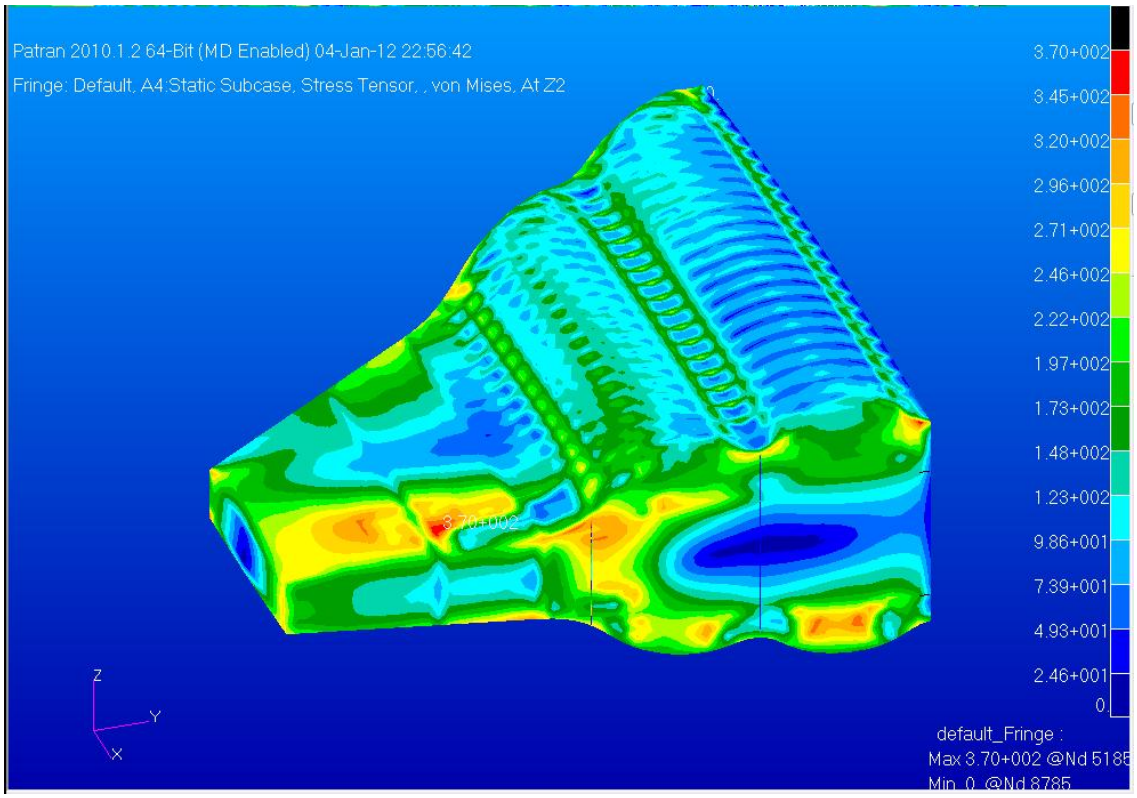

Figure 6-13 Stress of the WSC model: after being strengthened

4. Geometrical Parameters

The primary geometrical parameters of the three models are summarized in Table 6-2 below.

Table 6-2 Primary geometrical parameters of the models

	CWBC/mm	MBC/mm	WSC/mm
Skin thickness	6	Outer cover: 2 Inner shell: 2.6	Flat section: 3 Curved section:2
Spar cap	200×5	200×5	200×50
Spar web thickness	3	3	3
Rib cap	200×5	200×5	200×10
Rib web thickness	3	3	5
Skin stringers/mm	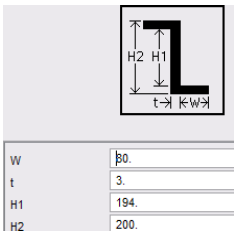	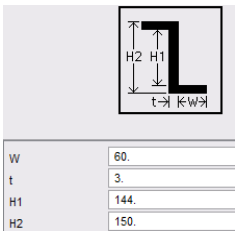	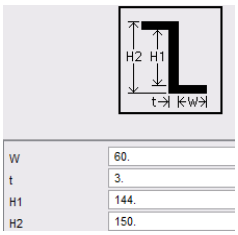

6.7 Discussion

6.7.1 Refinement of the WSC

1. Skin section

For the WSC configuration, it can be seen from the previous chapter that stress concentration occurred at the valley of the skin, and it is mainly caused by the pressure load, because almost no stress concentration exists any more at the valleys when the internal pressure load is removed. That result is shown in Figure 6-14.

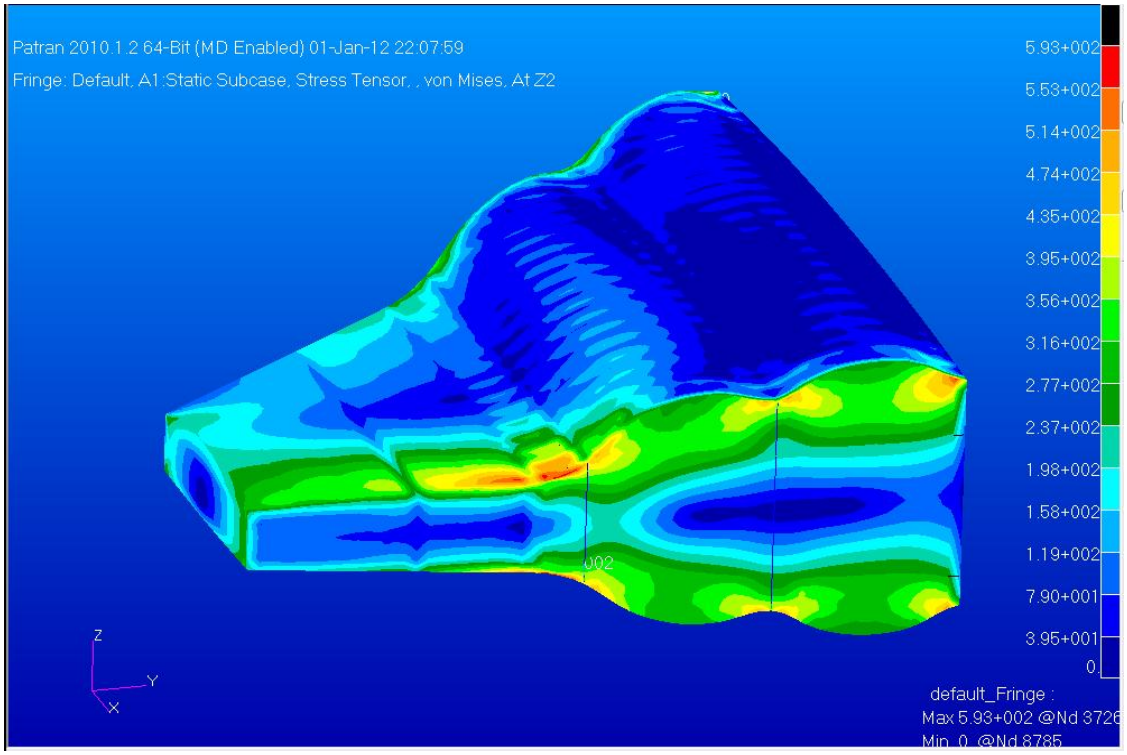

Figure 6-14 Stress of the WSC model

(Compression/tension: 1.07×10^{7} N, shear force: 7.88×10^{5} N)

In order to solve this problem, two different detailed configurations concerning the pressured skin are modelled. They are of the same thickness, the same boundary constraints, and subject to the same pressure load. The thickness is set as 2.6 mm, which is determined by the stress of 100 MPa under the pressure load of 0.137 MPa. They are all simply supported at the two short edges. The first model has the same section with that in the initial WSC configuration, for which the curve is not in a constant radius. Figure 6-15 shows the results of the displacement and stress. It can be seen that the stress concentration occurs around the radius changing places, and the displacement is also very big.

In the second model, the radius of the skin is kept constant, and the situation is improved resultantly. That is indicated in Figure 6-16, in which the highest stress is reduced to be no more than 100 MPa, and the displacement is also reduced significantly.

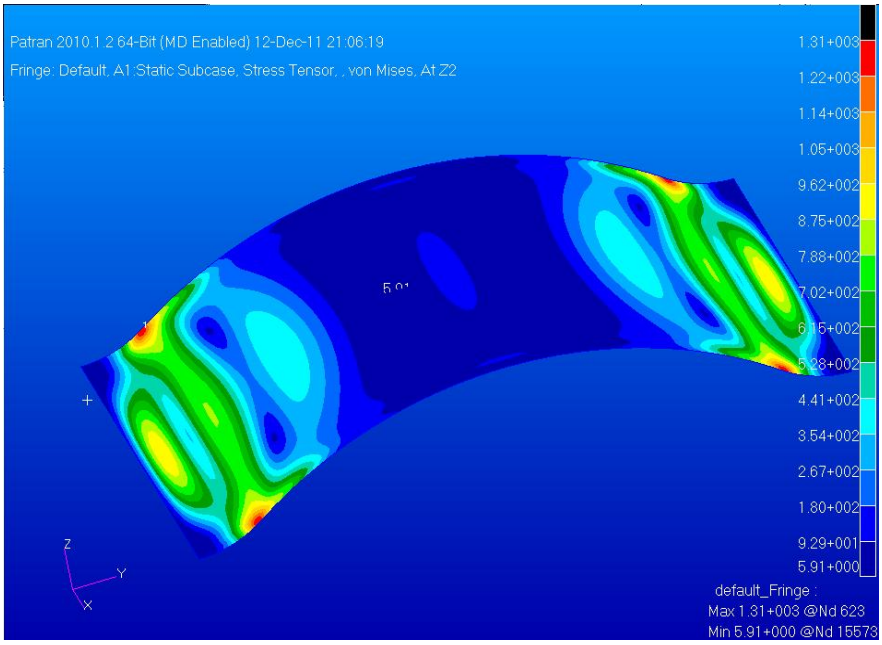

(a) Stress

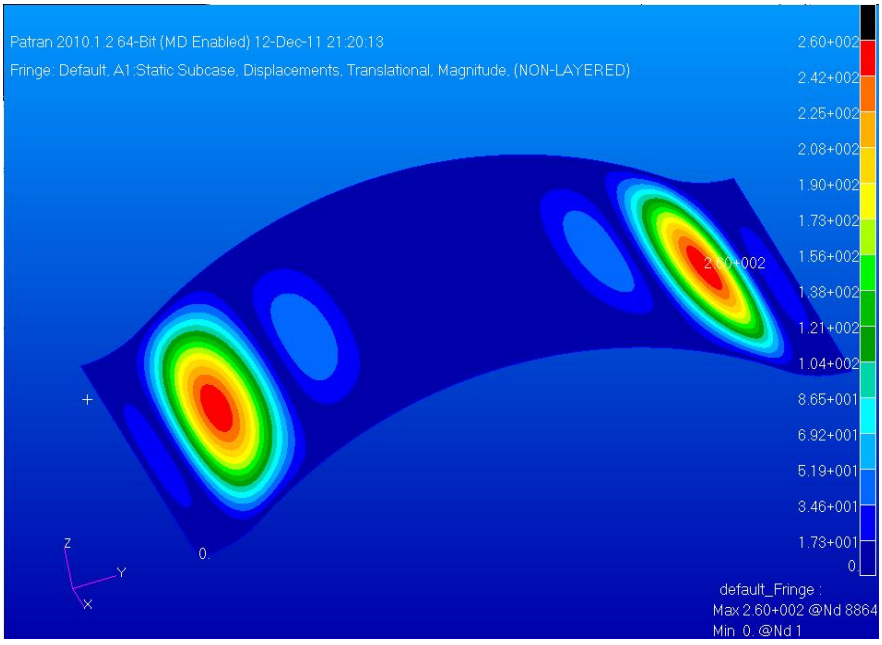

(b) Displacement

Figure 6-15 Skin with variable radius

(thickness: 2.6 mm; pressure load: 0.137 MPa)

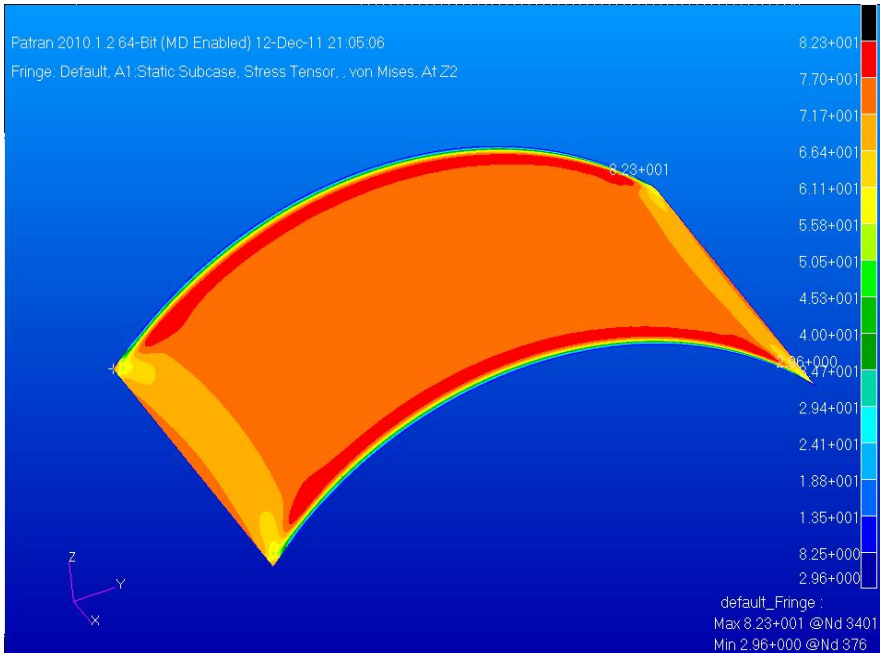

(a) Stress

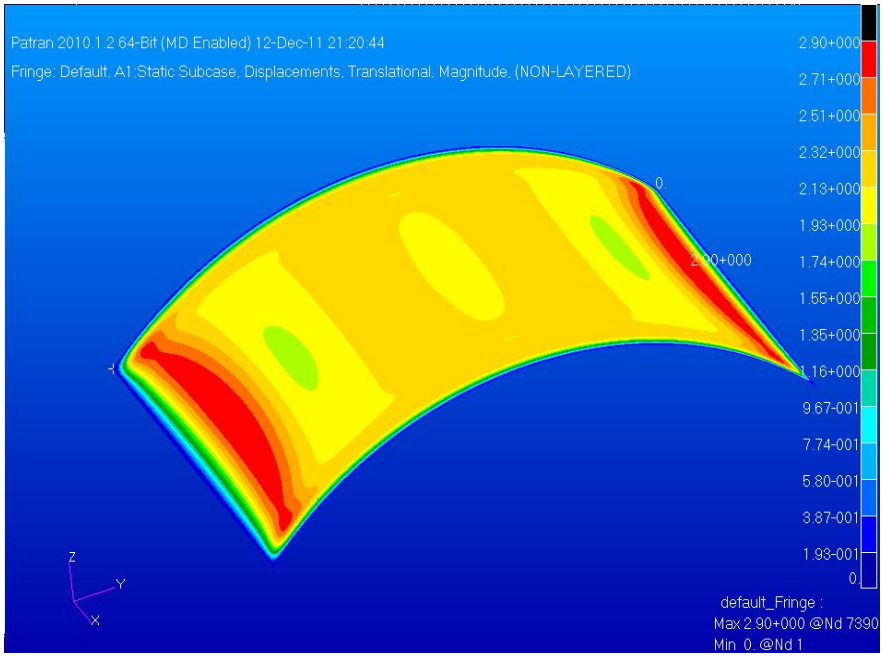

(b) Displacement

Figure 6-16 Skin with constant radius

(thickness: 2.6 mm; pressure load: 0.137 MPa)

The analysis results suggest that it is preferable to maintain the pressure surface cylindrical, and this will result in a sharp intersection in between the

bubbles, which may introduce negative influence to the aerodynamic performance. So the author proposed a configuration that will restore the advantage of cylindrical pressure surface and have a smooth surface as well, as shown in Figure 6-17. The rib is in a Y-section shape. The flanges are not perpendicular to the web plane as typical, instead a curved spar with approximately the same radius as the skin is connected to it. Therefore, the curved flanges can be utilised in reacting the pressure, and the valley skin will only function as the fairing.

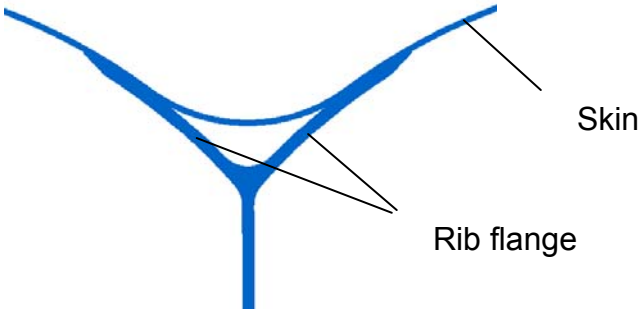

Figure 6-17 Y rib and the skin

2. Spar

From the results analysis in 6.6, it has already been known that severe stress concentration occurred at the neck sections. That is demonstrated in Figure 6-18, in which spar flanges are curved. The stress concentration is caused by the load path which is not in a straight line so that additional bending moment is produced, resulting in the rise of the stress. Therefore it might be ideal to maintain the primary flanges of the spar straight such that the additional bending moment can be avoided. It is important to keep the straight caps much stronger than the curved flanges so that the majority of the loads can be distributed to them instead of the curved flanges. This is verified by a FE analysis, and the geometry and the stress result are shown in Figure 6-19. It can be seen that the stress concentration is substantially reduced when two straight caps are added aligned with those in the straight section.

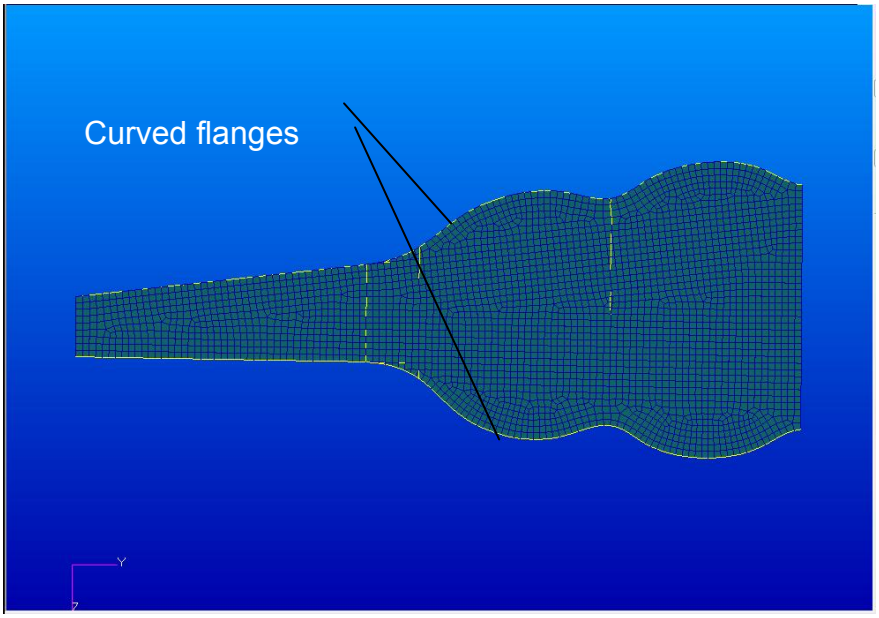

(a) Geometry

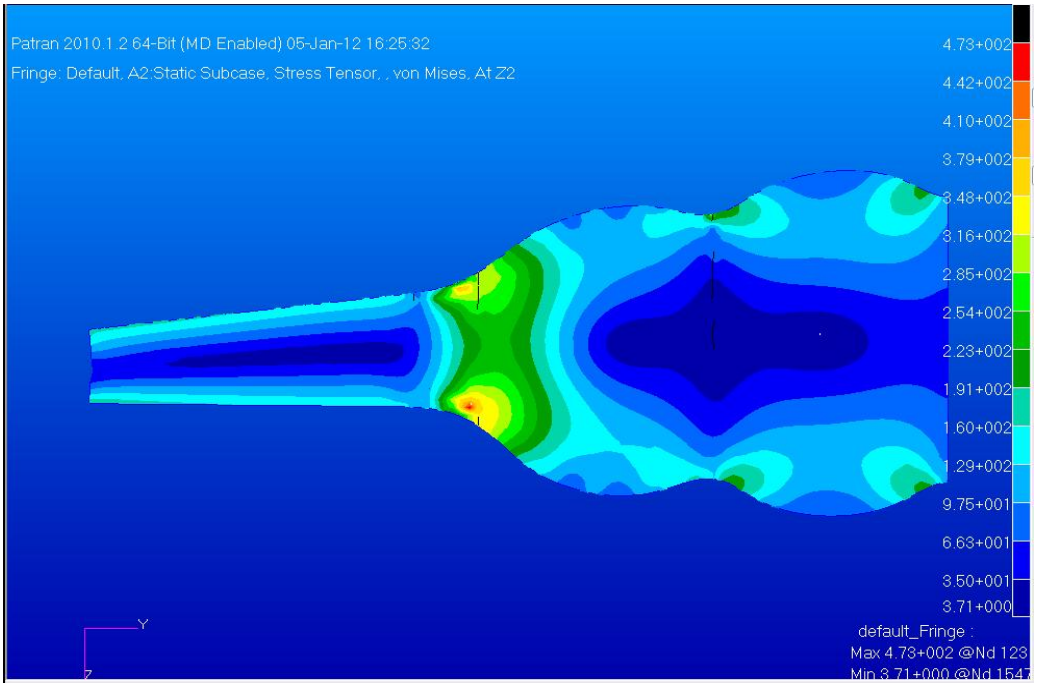

(b) FE model

Figure 6-18 Initial spar

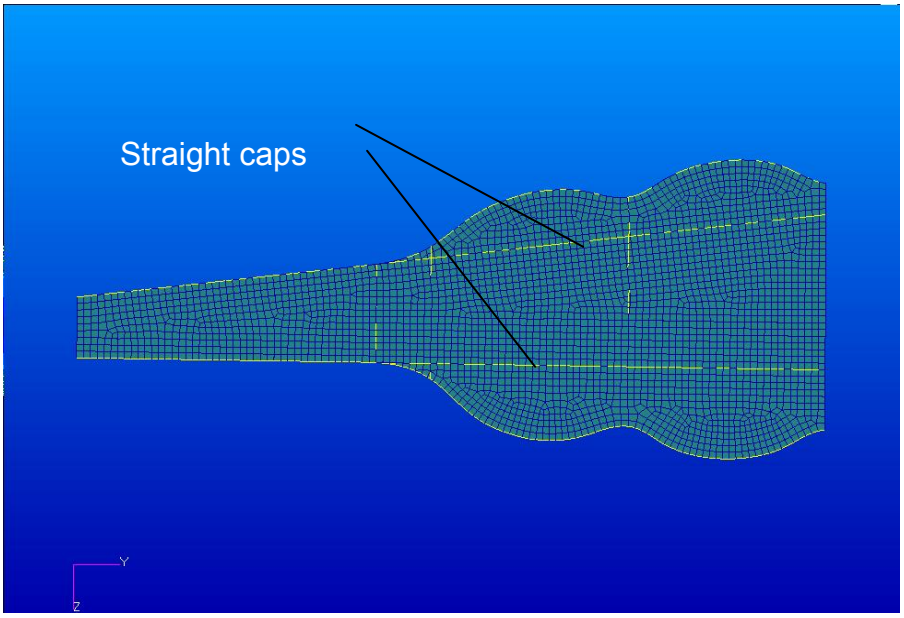

(a) Geometry

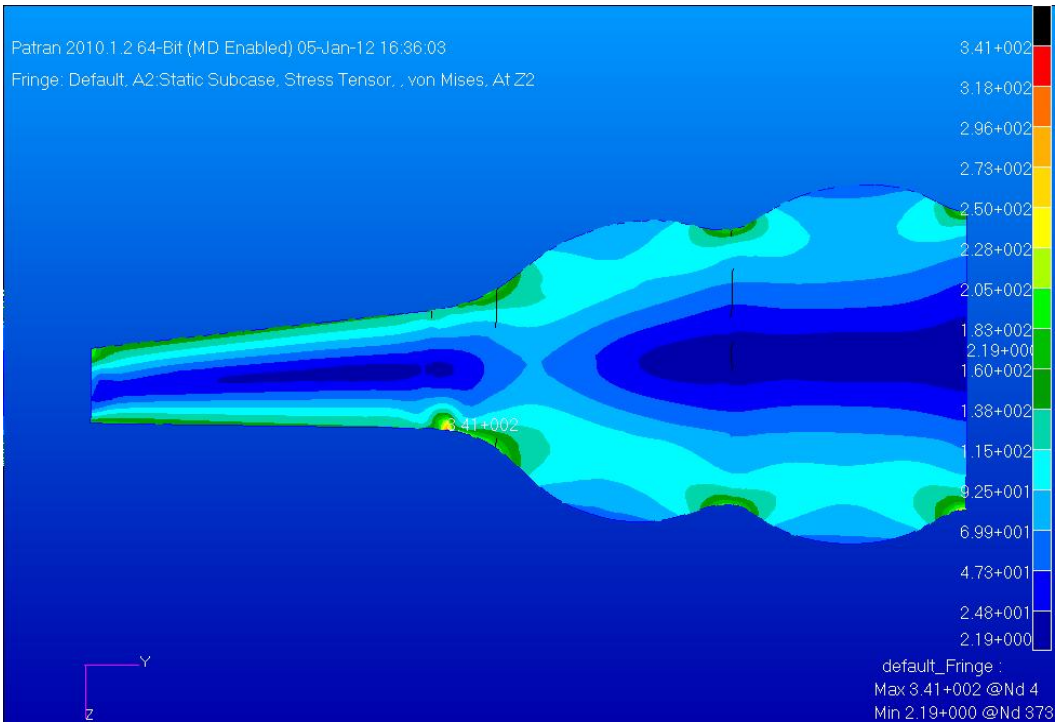

(b) FE model

Figure 6-19 Redesigned spar

The following Figure 6-20 further illustrates that the height of the cabin allows for the flanges of the spar being straight, as the flanges do not affect the arrangement of the cabin floor and cabin ceiling.

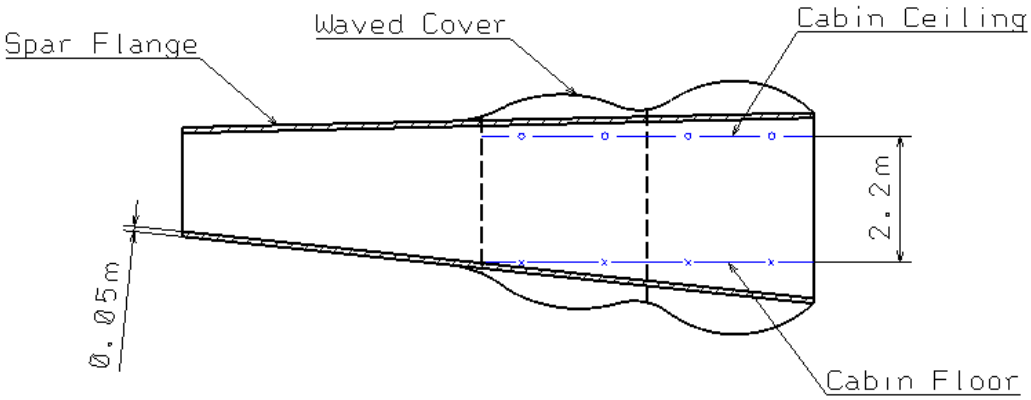

Figure 6-20 Straight flanges of the spar

6.7.2 Weight Comparison

The FE models for the CWBC, MBC and WSC all comprises skins (including horizontal and transverse stiffeners), spars, and ribs. The area and weight of each item can be obtained from the FE models. They are presented in Table 6-3.

Table 6-3 Area and weight of the FE models

	Area/ m^2			Weight/kg		
Items	CWBC	MBC	WSC	CWBC	MBC	WSC
Skin	173	173	182	3483	2612	1813
Spar	73	73	78	722	722	2120
Ribs	130	130	113	1337	1337	1221
Total	376	376	373	5542	4671	5154

With the MBC model, the weight of the skin doesn't include that of the internal pressure vessel, for it is not included in the FE model. The area of the pressure vessel can be estimated from the CATIA geometry model, and the thickness of it can be calculated from Equation (5-19), then the weight of the pressure vessel

is estimated as 440 kg. Adding this to the skin weight from the FE model (2172 kg), it totals at 2612 kg.

As the three models are just part of the inner wing box section, it is necessary to extend the values achieved in Table 6-3 to the whole inner wing box sections, assuming that the mass of each item is averagely distributed across the area. The area and weight for the whole inner wing box of the three configurations are given in Table 6-4.

Table 6-4 Area and weight expanded to the whole inner wing

	Area/ m^2			Weight/kg		
Items	CWBC	MBC	WSC	CWBC	MBC	WSC
Skin	310	310	322	6241	4680	3249
Spar	94	94	74	930	930	2730
Ribs	208	208	181	2139	2139	1953
Total	612	612	607	9310	7749	7932

It can be seen from Table 6-4 that the Multi-Bubble Configuration is the lightest one, followed by the Wave-Section Configuration, and the Conventional Wing-Box Configuration is the heaviest one. To make it clearer, the particular comparison between the WSC and the MBC is also illustrated in Figure 6-21.

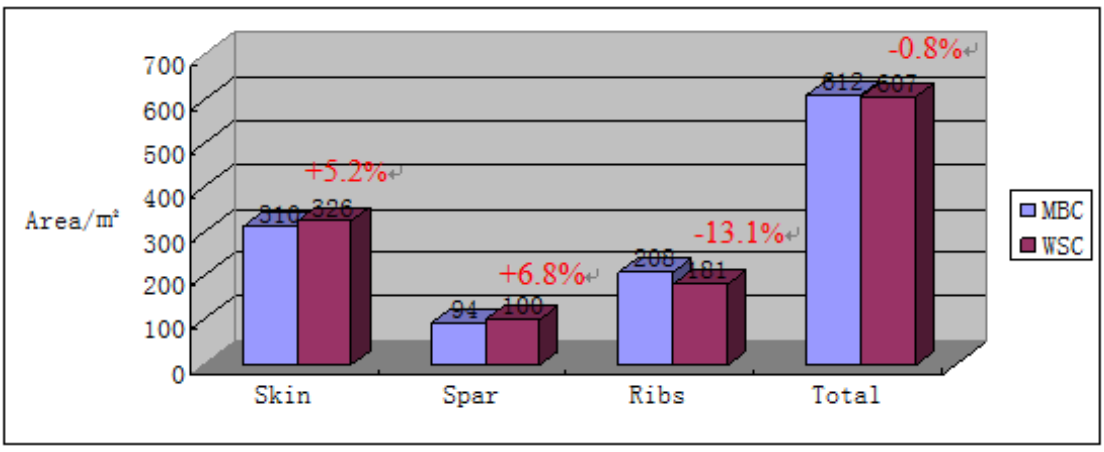

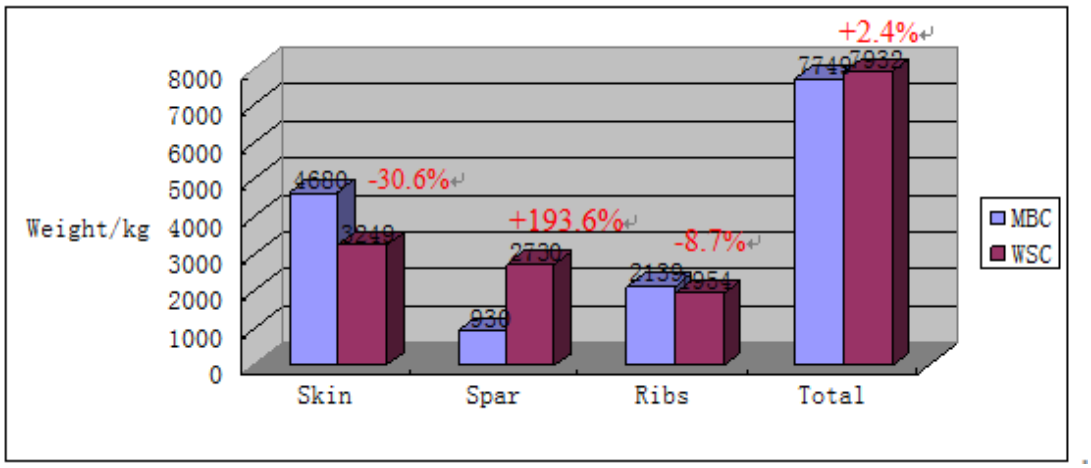

Figure 6-21 Area and weight comparison

It can be seen from Figure 6-21 that the total area of the main structure components for the MBC and WSC configuration is quite close. However It can also be seen that the weight of the skin of the WSC model is reduced by 30.6 percent than that of the MBC model, while the weight of the spar is approximately double increased, 193.6 percent, which is much bigger than the reduction of the skin weight. In result, the total weight of the WSC configuration is 2.4 percent heavier than that of the MBC configuration.

6.8 Summary

To summarize, some key conclusions could be made as follows:

- For the inner wing structural configuration, the lightest configuration might be the Multi-Bubble Configuration (7749 kg), followed by the Wave-Section Configuration (7932 kg) and finally the Rectangular Box Configuration (9310 kg).
- The Wave-Section Configuration inner wing demands careful designing, especially the skins and spars, because it seems likely that the stress concentration will easily occur.

7 CONCLUSION AND FUTURE WORK

A new inner wing structural configuration based on the Blue Bird (a flying-wing concept of a Group Design Project) was proposed by the author. It was named the Wave-Section Configuration (WSC), as it has wave like transverse sections, which remain in standard airfoil in cross sections for the inner wing section (fuselage) configuration of flying-wing aircraft. (Chapter 4.3.1) The WSC was compared with two other typical configurations, Conventional Wing-Box Configuration and Multi-Bubble Configuration. The commercial design and analysis tools of Matlab, CATIA, Patran/Nastran and Excel are all employed in the research of this thesis. The results suggested that the Multi-Bubble Configuration is the optimal configuration regarding the pressurised inner wing structural configuration for flying-wing aircraft, however, the Wave-Section Configuration still might be a possible approach, as it is only about 2.4 percent heavier than that of the Multi-Bubble Configuration. (Chapter 6.7.2) Although stress concentration may occur in the Wave-Section Configuration, it can be solved by alternative structural approaches and this has been verified by means of carrying out some detailed analysis (Chapter 6.7.1).

The Wave-Section Configuration has highlighted some advantages along with some disadvantages/challenges, which can be summarised as follows:

Advantages:

- Safer, because the fuel tanks are located in the outer wing instead of that below the cabin. (Chapter 4.3.1)
- Thinner in the outer wing (Chapter 4.3.1)
- Capable of carrying most widely used standard LD3 containers (Chapter 4.3.1)

Disadvantages/Challenges:

- Aerodynamic influence of the wave-section shape (Chapter 4.3.1)

- Adding complexity to the design as well as the manufacturing (Chapter 6.8)

With respect to the Wave-Section Configuration, further work is still required.

Further work:

- Estimating the drag rise resulting from the curved surfaces, as well as the drag reduction attributed to the thickness decreasing of the airfoil of the outer wing, determine whether the configuration is practical.
- Optimisation work could be carried out to improve the design, especially regarding the curved skins and curved spars.

REFERENCES

[1] Richard M. Wood and Steven X. S. Bauer, “Flying Wings/Flying Fuselages”, AIAA 2001-0311, Aerospace Sciences Meeting and Exhibit, 39th, Reno, NV, Jan. 8-11 January 2001

[2] Dictionary of Aeronautical Terms, third edition, page 224. Aviation Supplies & Academics, 1997. ISBN 1-56027-287-2

[3] V.Mukhopadhyay, “Blended Wing Body (BWB) Fuselage Structural Design for Weight Reduction”, AIAA 2005-2349, 46th AIAA/ASME/ASCE/AHS/ASC Structures, Structural Dynamics and Materials Conference , Austin, Texas, Apr. 18-21, 2005

[4] Mukhopadhyay, V., “Structure Concepts Study of Non-circular Fuselage Configurations”, Paper No. AIAA SAE WAC-67, World Aviation Congress, Los Angeles, Calif. Oct. 22-24, 1996.

[5] Velicki, A., and Hansen, D.A., “Novel Blended Wing Body Structural Concepts”, NASA TCAT NRA Phase-Ⅰ Final Report, Boeing Co. CA, July 2004

[6] S. H. Cho, C. Bil and R. Adams, “Design and Analysis of BWB Military Cargo Certre Body Structure”, AIAA 2011-7026, AIAA Centennial of Naval Aviation Forum “100 years of Achievement and Progress”, 21-22 September 2011, Virginia Beach, VA

[7] Denis Howe, “Aircraft Conceptual Design Synthesis”, Professional Engineering Publishing Limited London and Bury St Edmunds, UK, 2000.

[8] Howe D., “Aircraft loading and structural layout”, Professional Engineering Publishing, 2004

[9] Daniel P. Raymer, “Aircraft Design: A conceptual Approach”, 4th edition, American Institute of Aeronautics and Astronautics, Inc., Reston, Virginia, 2006.

[10] Chao Tong, “Effect of Layout Options on Flying Wing Airliner Structural Loads”

[11] Federal Aviation Regulations, Part 25, available at: http://www.flightsimaviation.com/data/FARS/part_25.html

[12] Specification-for-AVIC4th-GDP, Cranfield University, 2011

BIBLIOGRAPHY

[1] Lloyd R. Jenkinson, Paul Simpkin, Darren Rhodes, “Civil Jet Aircraft Design”, London : Arnold, 1999.

[2] Michael Chun-Yung Niu, “Airframe structural design”, Hong Kong : Conmilit Press, 1999.

[3] Michael Chun-Yung Niu., “Airframe stress analysis and sizing”, Hong Kong : Conmilit Press, 1999

[4] Jan Roskam, “Airplane design, Part I, Preliminary sizing of airplanes”, Ottawa, Kansas : Roskam Aviation and Engineering Corporation, 1985

[5] John P. Fielding, “Introduction to aircraft design”, Cambridge [Cambridge University Press], 1999

[6] Denis Howe, “Blended Wing Body Airframe Mass Prediction”, Journal of Aerospace Engineering (Professional Engineering Publishing) [serial online]. December 21, 2001;215(6):319.

[7] V.Mukhopadhyay, J.Sobieszczanski-Sobieski, NASA Langley, Hampton, VA I. Kosaka, G. Quinn and C.Charpentier, Vanderplaats R&D Inc., Colorado Springs, CO, “Analysis Design and Optimisation of Non-cylindrical Fuselage for Blended-Wing-Body (BWB) Vehicle”, AIAA 2002-5664, 9th AIAA/ISSMO Symposium on Multidisciplinary Analysis and Optimization, Atlanta, Georgia, Sep. 4-6, 2002

[8] R. Liebeck, “Design of the Blended-Wing-Body subsonic transport”, AIAA 2002-0002, AIAA Aerospace Sciences Meeting and Exhibit, 40th, Reno, NV, Jan. 14-17, 2002

[9] Sung Hwan Cho, Cees Bill and Javid Bayandor, “Structural Design and Analysis of a BWB Military Cargo Transport Fuselage”, AIAA 2008-165, 46th AIAA Aerospace Sciences Meeting and Exhibit, Reno, Nevada, Jan. 7-10, 2008

[10] Richard Gilmore, Sean Wakayama, Dino Roman, “Optimisation of High-Subsonic Blended-Wing-Body Configurations”, AIAA 2002-5666, 9th AIAA/ISSMO Symposium on Multidisciplinary Analysis and Optimisation , 4-6 September 2002, Atlanta, Georgia

[11] Vladimir G. Dmitriev, Leonid M. Shkadov, Vladimir E. Denisov, Boris I. G urevich, Sergei V. Lvapunov, Oleg V. Sonin, “The Flying-Wing Concept-Chances and Risks”, AIAA 2003-2887, AIAA/ICAS International Air and Space Symposium and Exposition: The next 100 Y, 14-17 July 2003, Dayton, Ohio

[12] Alex Velicki, Patrick Thrash, Dawn Jegley, “Airframe Development for the Hybrid Wing Body Aircraft”, AIAA 2009-932, 47th AIAA Aerospace Sciences Meeting Including the New Horizons Forum and Aerospace Exposition, 5-8 January 2009, Orlando, Florida

[13] Nimeesha B. Kuntawala, Jason E. Hicken, and David W. Zingg, “Preliminary Aerodynamic Shap Optimisation of a Blended-Wing-Body Aircraft Configuration”, AIAA 2011-642, 49th AIAA Aerospace Sciences Meeting Including the New Horizons Forum and Aerospace Exposition, 4-7 January 2011, Orlando, Florida

[14] Daniel J. Thompson, Joshuo Feys, Michael D. Filewich, Sharif Abdel-Magid, Dennis Dalli, and Fumitaka Goto, “The Design and Construction of a

Blended Wing Body UAV", AIAA 2011-841, 49th AIAA Aerospace Sciences Meeting Including the New Horizons Forum and Aerospace Exposition, 4-7 January 2011, Orlando, Florida
[15] Liebeck, R. H., "Blended-wing-body subsonic commercial transport", AIAA-1998-438, Aerospace Sciences Meeting and Exhibit, 36th, Reno, NV, Jan. 12-15, 1998
[16] Bradley, K. R., "A Sizing Methodology for the Conceptual Design of Blended-Wing-Body Transports", MS Thesis, Joint Institute for Advancement of Flight Sciences, George Washington University, Sep. 2003
[17] Hitch, H. P. Y., "Pressure Cabins of Elliptic Cross Section", Aeronautical Journal, Vol. 92 No. 916 Jun-Jul. 1988, pp. 207-223
[18] Wakayama, S. and Kroo, I., "The Challenge and Promise of Blended – Wing-Body Optimisation", AIAA Paper 98-4736, Sept. 1998
[19] Nimeesha Kuntawala University of Toronto, Toronto, CANADA; Jason Hicken University of Toronto, Toronto, CANADA; David Zingg University of Toronto, Toronto, CANADA, "Preliminary Aerodynamic Shape Optimization of a Blended-Wing-Body Aircraft Configuration", AIAA-2011-642, 49th AIAA Aerospace Sciences Meeting including the New Horizons Forum and Aerospace Exposition, Orlando, Florida, Jan. 4-7, 2011
[20] Thompson, M. O., & Peebles, C. "Flying without wings : NASA lifting bodies and the birth of the space shuttle", Washington : Smithsonian Institution Press, 1999.
[21] Pape, G. R., & Campbell, J. M. "Northrop flying wings : a history of Jack Northrop's visionary aircraft", Schiffer Publishing, 1995.
[22] Sears, W. W. "Flying-wing airplane : the XB-35/YB-49 program", AIAA, 1980.
[23] Venios, A. A., & Poll, D. A. "Comparison of range characteristics of conventional aircraft and flying wing configuration", A. Venios, 2000.
[24] Panagiotidis P, Poll D. "Flying Wing Performance Compared With Conventional Aircraft Configurations", 1999.
[25] Agte, J., Hadley, M., & Creviston, D. O. "Student evolution of an unconventional flying wing configuration", Washington, D.C : AIAA, 1997.
[26] Lv, X., & Smith, H. "Aerodynamic characteristics and flying qualities research of large aircraft with box-wing configuration", 2009.
[27] Reynaud, R. R., & Poll, D. I. "BWB, the future airliner : comparison between flying wing and conventional aircraft", 2005.
[28] Martins Pires, R. M., & Fielding, J. P. "BWB-01 : pressurized forward centre body vaulted design", 2002.
[29] Hume, T. S., & Fielding, J. P. "Integrated approach to a BWB aircraft family", 2003.
[30] Milsom, J. J., & Smith, H. H. "BWB-01 rear wing body design", 2002.
[31] Quenet, G. G., & Smith, H. H."BWB-01 inner wing design", 2002.
[32] Abdirahman, M. I., & Brown, J. C. "Comparison of different configuration for BWB pressure hulls with pillar tension bracing", 2002.
[33] Wiplier, A. A., & Smith, H. H. "BWB-01 cabin and cargo hold layout : evacuation issues", 2002.
[34] Sodzi, P. P., & Zhang, X. "Damage tolerant wing-fuselage integration structural design applicable to future BWB transport aircraft", 2009.

[35] Eelman, S., Schmitt, D., Becker, A., & Granzeier, W. “FUTURE REQUIREMENTS AND CONCEPTS FOR CABINS OF BLENDED WING BODY CONFIGURATIONS--A SCENARIO APPROACH”, Journal Of Air Transportation, 9(2), 4-22.
[36] Mialon, B. B., Fol, T. T., & Bonnaud, C. C. “Aerodynamic Optimization of Subsonic flying wing configurations”, AIAA, 2002.
[37] Martiénez-Val, R. R., Pérez, E. E., Alfaro, P. P., & Pérez, J. J. “Conceptual design of a medium size flying wing. Proceedings Of The Institution Of Mechanical Engineers -- Part G”, Journal Of Aerospace Engineering (Professional Engineering Publishing), 221(1), 57. doi:10.1243/09544100JAERO90
[38] Le Moigne, A. “A discrete Navier-Stokes adjoint method for aerodynamic optimisation of BlendedWing-Body configurations". Cranfield University, 2002.
[39] Xie, J. J., Yang, Z. C., & Guo, S. J. “Trim optimizations of an adaptive tailless aircraft with composite wing”, 2011.
[40] A, L., & Guo, S. S. “A composite wing structure with morphing control surface”, 2010.
[41] Phillips, B. J., Guo, S., Fielding, J., & Clark, G. “Multidisciplinary optimisation of a CFRP wing cover”, 2009.
[42] Dhanyamraju, R. R., & Guo, S. S. “Conceptual design of an unconventional wing box structure using composite materials”, 2007.
[43] Xiong, C. C., & Guo, S. J. “Conceptual design of aircraft thin-walled structure configuration”, 2008..
[44] Zhou, Z. Z., & Guo, S. S. “Optimal design of aircraft composite stiffened panels subject to weight and buckling constraints”, 2008.
[45] Sodzi, P. P., & Zhang, X. “Damage tolerant wing-fuselage integration structural design applicable to future BWB transport aircraft”, 2009.

APPENDICES

Appendix A Database

The database of certain basic items concerning the 150-250-seat existing aircraft as well as the Blue Bird is provided in Table A-1 and Table A-2. In order to make that clearer, certain items in relation to passengers are plotted in Figure A-1.

Table A-1 Database of certain items concerning the 150-250-seat aircraft

Items \ Aircraft	A321-320	B707-320B	B727-200	B737-900	B757-200
Passengers	150-180	185-220	147-202	189	200-234
Average passengers	165	202.5	174.5	189	217
Cargo capacity/ m^3	37.41	51.73	50.16	43	50.55
MTOW/tons	78	93.5	151	95	115.7
Range/km	5,900	5,600	10,650	4,400	7,222
Mach number	0.78	0.78	0.92	0.81	0.8
Total thrust/KN	231	280	337.6	232.2	326
Cost/million dollars	85	99.7	4.3		65
Engines	2 engines low wing	2 engines low wing	4 engines below wing	3 engines tail	2 engines low wing
Taking-off runway length	2180	2090	3,280	1585	2911
Doors	4+4e	8	6+4e	4+4e	8 or 6+4e

Table A-2 Database of certain items concerning the 150-250-seat aircraft

Items \ Aircraft	B767-200	B787-8	MD90-30ER	DC-8-63	T204SM	Blue Bird
Passengers	181-255	210-250	153-172	180-259	175-210	220-248
Average passengers	218	230	162.5	219.5	192.5	234
Cargo capacity/ m^3	81.4	137	36.8	70.8	44.5	44.4
MTOW/tons	142.9	228	76.2	161	105	176
Range/km	7,300	14700	4,023	3,445	4,000	13,890
Mach number	0.8	0.85	0.76	0.9	0.8	0.82
Total thrust/KN	444	560	249.1	338	314	2×196
Cost/million dollars	144.1	185.2	48.5		35	185
Engines	2 engines low wing	2 engines low wing	2 engines tail	4 engines below wing	2 engines below wing	2 engines over wing
Taking-off runway length	1710	2820	2270	3505	1800	1852
Doors	4+2e	8	3+4e	4+4e	8	4+6e

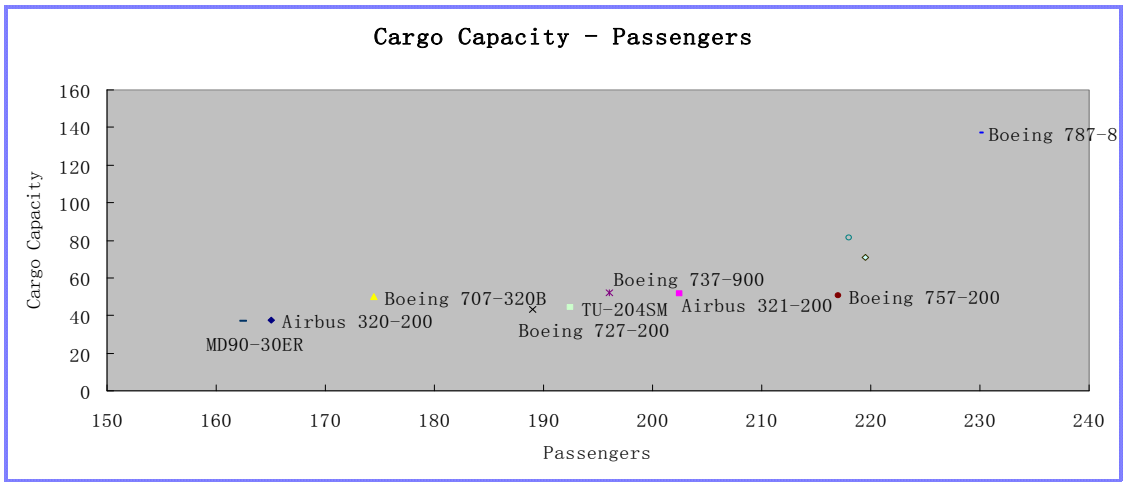
Cargo Capacity - Passengers
Cargo Capacity
Passengers
160
140
120
100
80
60
40
20
0
150
160
170
180
190
200
210
220
230
240
Boeing 787-8
Boeing 737-900
Boeing 707-320B
TU-204SM
Airbus 321-200
Boeing 757-200
Airbus 320-200
Boeing 727-200
MD90-30ER

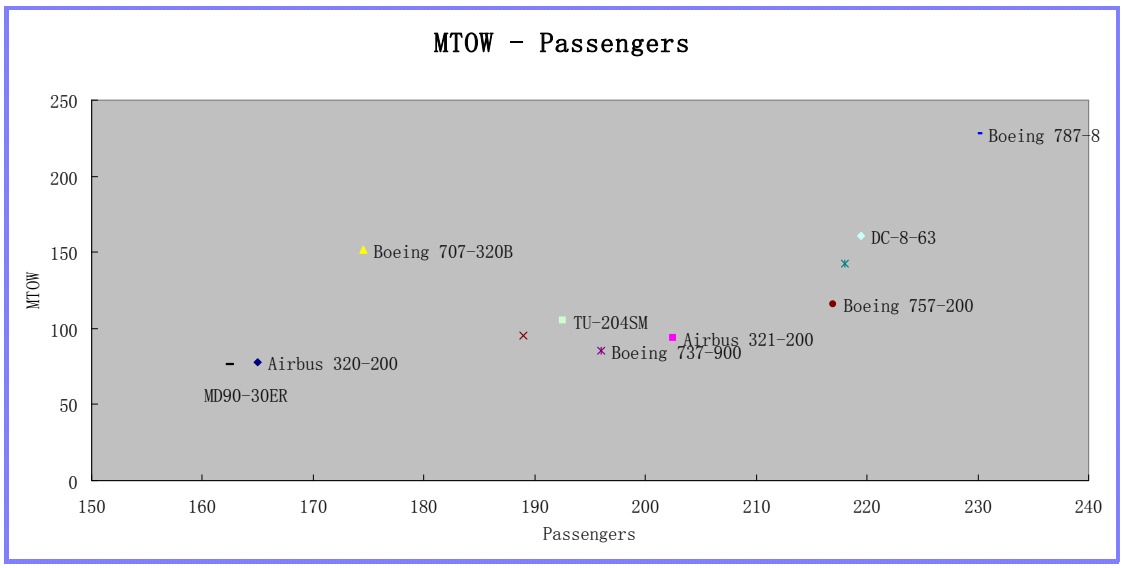
MTOW - Passengers
MTOW
Passengers
250
200
150
100
50
0
150
160
170
180
190
200
210
220
230
240
Boeing 787-8
DC-8-63
Boeing 707-320B
Boeing 757-200
TU-204SM
Airbus 321-200
Boeing 737-900
Airbus 320-200
MD90-30ER

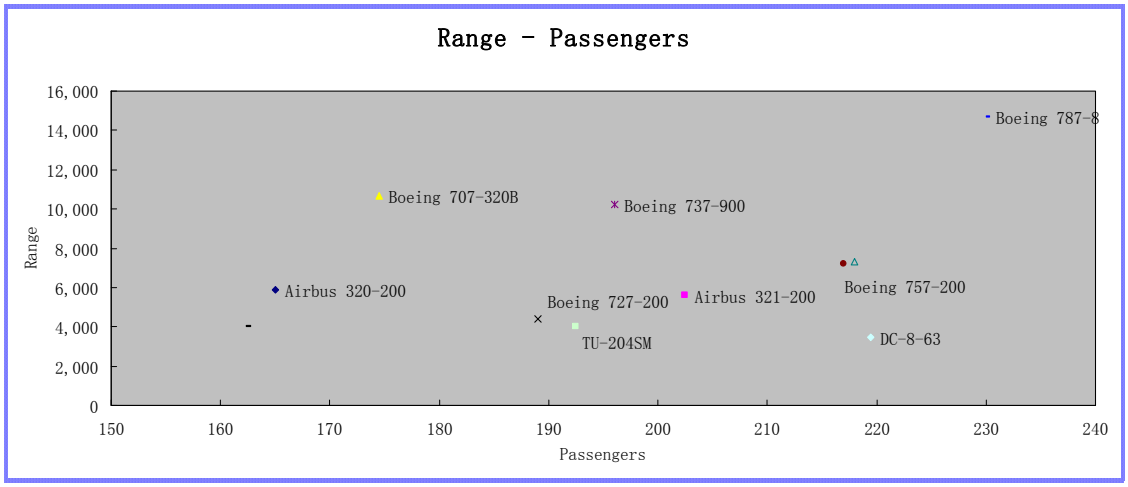
Range - Passengers
Range
Passengers
16,000
14,000
12,000
10,000
8,000
6,000
4,000
2,000
0
150
160
170
180
190
200
210
220
230
240
Boeing 787-8
Boeing 707-320B
Boeing 737-900
Boeing 757-200
Airbus 320-200
Boeing 727-200
Airbus 321-200
TU-204SM
DC-8-63

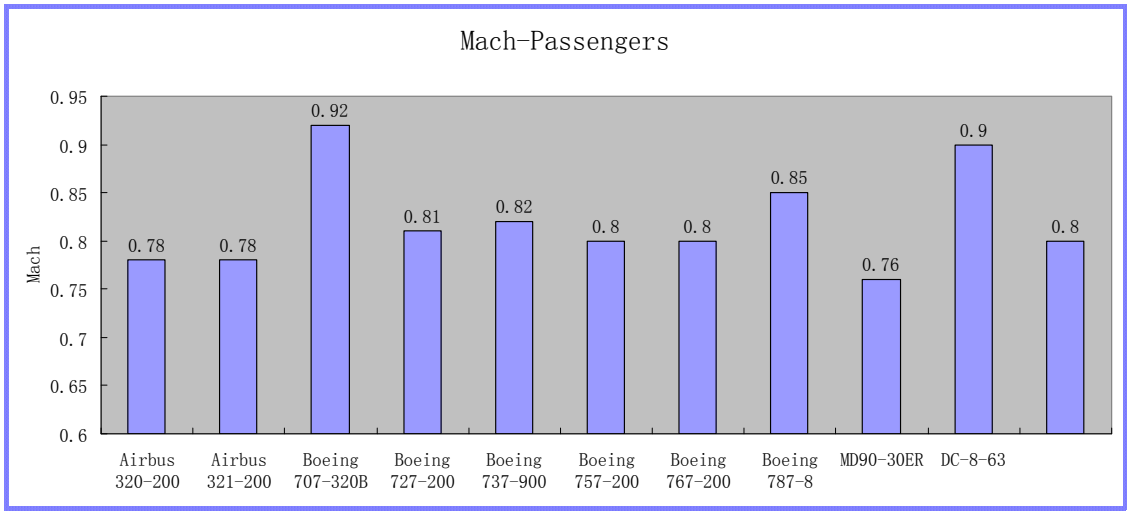

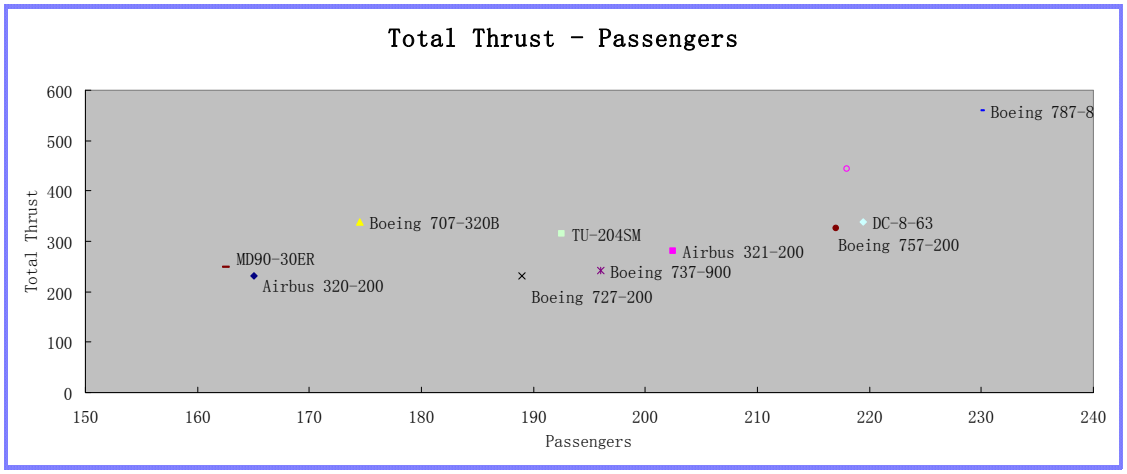

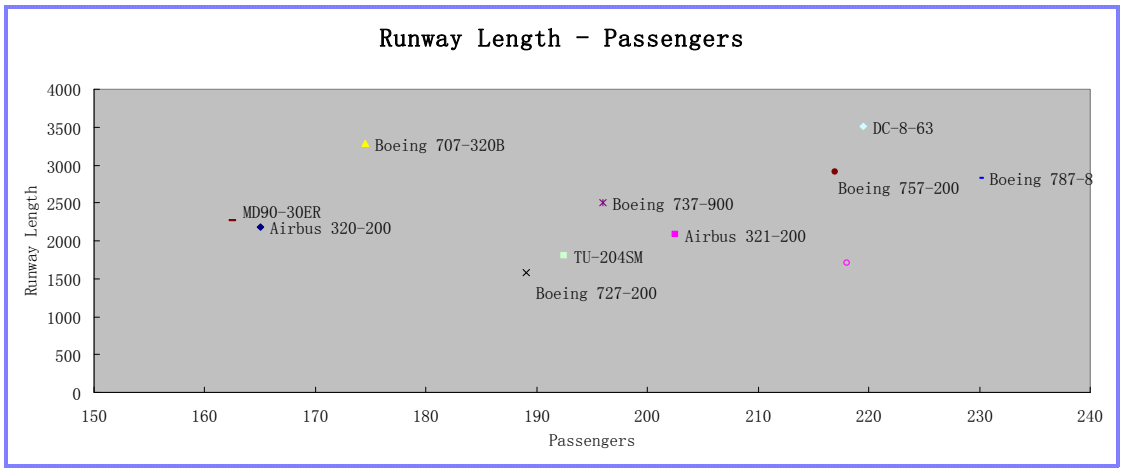

Figure A-1 Certain items in relation to passengers

Appendix B Optimal Curvature Calculation

In this appendix, two curves are intended to be plotted in one chart by using the commercial software of Matlab. One is to describe the relationship between the radius of the shell and the thickness of the shell, under the pressure load. The other one is to illustrate that how the thickness of the shell is related to the compression load.

The former curve is determined by the following equations.

$$\sigma_p = \frac{\Delta pR}{t}$$

The program to plot the curve in Matlab is:

σ_p=100; Δp=0.137;

t=(0:1:100);

R=(1450:100:30000);

$$\sigma_p = \frac{\Delta pR}{t};$$

plot(R,t)

The latter curve is defined by the following equations:

$$\sigma_b = \frac{M \cdot y}{I} = \frac{P\delta \cdot \frac{t}{2}}{\frac{1}{12}bt^3} = \frac{6P\delta}{bt^2}$$

$$e^2 + (R-\delta)^2 = R^2$$

The Matlab program to plot that curve is:

syms δ t R;

b=500;P=290000; σ_b=340;

f=solve('R^2-1450^2-(R-δ)^2','δ')

ff=σ_b-6*P*f(2)/b/t^2;

tt=solve(ff,'t')

R=1450:10:30000;

t=subs(tt(1),R)

plot(R,t)

Combine the two programmes together, they are:

σ_p=100; Δp=0.137;

t=(0:1:100);

R=(1450:100:30000);

$\sigma_p = \frac{\Delta pR}{t}$;

plot(R,t)

hold on

syms δ t R;

b=500;P=290000; σ_b=340;

f=solve('R^2-1450^2-(R-δ)^2','δ')

ff=σ_b-6*P*f(2)/b/t^2;

tt=solve(ff,'t')

R=1450:10:30000;

t=subs(tt(1),R)

plot(R,t)

Eventually the curves are plotted out as follows in the commercial software Matlab..

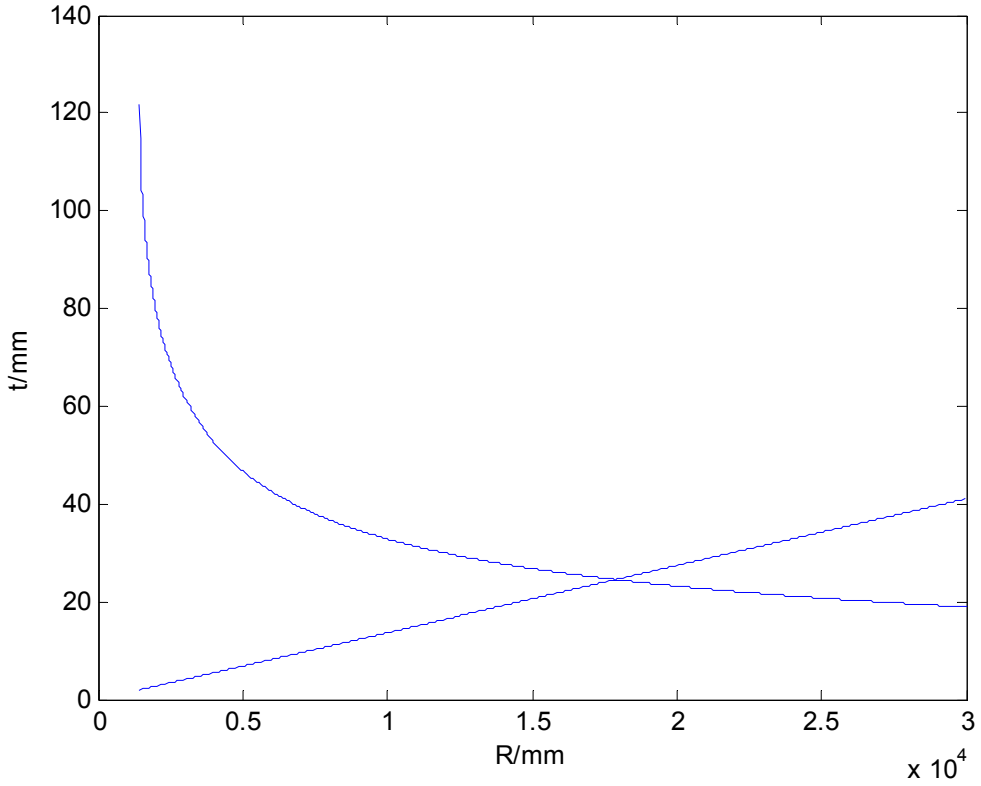

Figure B-1 w-R curve

Appendix C Initial Sizing

C.1 Loads

The critical shear force (SF), bending moment (BM) and torque moment (TM) are needed to conduct the initial sizing. These loads normally take quite a long time to be figured out somewhat accurately, as thousands of load cases should be considered. However, it is desirable to make a rough estimation of those loads at an earlier design stage, which could be used for initial structural sizing. A rude estimation of the loads are accomplished in C.1.1. The more accurate results based on the outcome of Mr Chao Tong' work at a later stage are also provided in C.1.2.

C.1.1 Rough Estimation

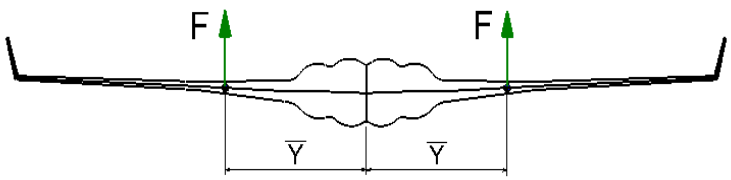

Figure C-1 Shear force and its arms

At the early stage, it is reasonable to assume that the maximum lift on the wing equals to the maximum taking-off weight M, which is 176 Tons according to Reference [12], multiplied by the maximum overload factor of 2.5, and it is located at the Aerodynamic Centre, so the total force on the wing might be 2.5Mg-1Mg=1.5Mg. Besides, a security factor of 1.5 should be incorporated. As a result, the ultimate load on the half wing, F, can be given as:

$$F = \frac{1}{2} Mg * 1.5 * 1.5 = 1.98 \times 10^6 N$$

The maximum force arm to the x axis is $\overline{Y} = 11700mm$ (Chapter 3.3.4), so the maximum bending moment to the x axis, M_y, is:

$$M_y = F \cdot \overline{Y}$$
$$= 1.98 \times 10^6 N \times 11340 mm$$
$$= 2.25 \times 10^{10} N \cdot mm$$

The dimensions shown in Figure C-2 are used to define the shear centre of the cross section, e_c.

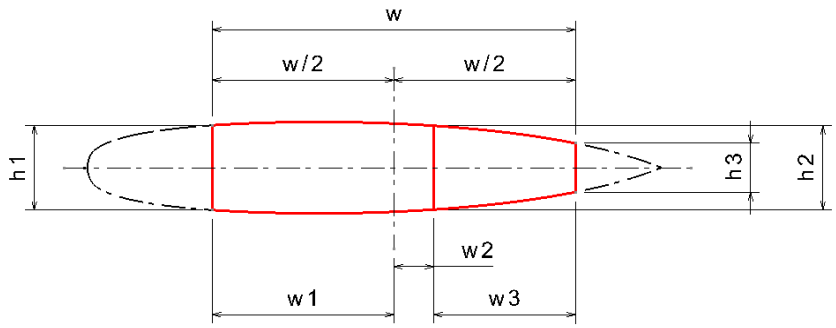

Figure C-2 Cross section

$$e_c = h_1^2 / (h_1^2 + h_3^2)$$

Where e_c is the position of the shear centre forward of the rear spar as a fraction of the width of the box, w.

For the centreline span station, $h_1^2 = 3751mm, h_2^2 = 3710mm, h_3^2 = 2161mm$, then:

$$e_c = 0.75$$

For the outboard cabin span station, $h_1^2 = 1735mm, h_2^2 = 1223mm, h_3^2 = 1993mm$, then:

$$e_c = 0.43$$

So the Flexural Axis can be obtained by making a line going through the two shear centres, as shown in Figure C-3.

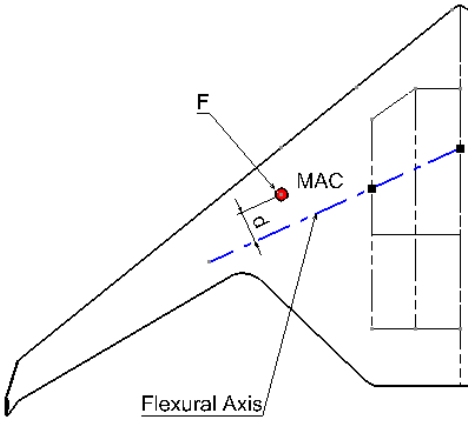

Figure C-3 The Flexural Axis

Therefore the torque moment can be approximately given as follows:

$$T = Fd$$
$$= 1.98 \times 10^6 N \times 2100 mm$$
$$= 4.2 \times 10^9 N \cdot mm$$

C.1.2 More Accurate Estimation

A more accurate estimation of the shear force, and bending moment were calculated by Chao Tong in Reference [10], in which the loads are obtained under 1g condition. Those loads can be transferred to the approximate critical design loads by multiplying two values of factors; one is 2.5, the overload factor, and another one is the security factor, 1.5. In conclusion, a combined load factor of "2.5×1.5" is incorporated. Eventually, the specific shear force and bending moment are figured out in Table C-1 along the span location, y. The distribution of the loads along the span is also plotted in diagrams in Figure C-4.

Table C-1 Shear Force, Bending Moment and Torque along the span

Location/m	Shear Force/N	Bending Moment/ $N \cdot m$
0.0	154678	24403879
0.2	200335	24380678
0.3	245363	24350628

0.5	289766	24313823
0.6	333541	24270358
0.8	376680	24220327
0.9	419185	24163825
1.1	461059	24100947
1.2	502307	24031789
1.2	502307	24031789
1.5	582934	23881097
1.8	661096	23706216
2.1	736828	23507888
2.4	810163	23286839
2.7	881134	23043790
2.9	927151	22867563
2.9	927151	22867563
3.2	942544	22589418
3.6	961252	22212400
3.8	969840	22020150
4.1	981785	21729198
4.3	989133	21532841
4.3	989133	21532841
4.5	995997	21335014
4.8	1005397	21036215

5.2	1016296	20634056
5.5	1023272	20329168
5.8	1029253	20022186
5.8	1200799	20022186
6.0	1190642	19782026
6.4	1169704	19305769
6.8	1147963	18837888
7.2	1125458	18378703
7.3	1119716	18266157
7.3	1119716	18266157
7.5	1111733	18042214
7.8	1098997	17708694
8.0	1089982	17488894
8.2	1080559	17270898
8.4	1070734	17054786
8.4	1070734	17054786
8.7	1113060	16768900
8.9	1149999	16479505
9.2	1182911	16180505
9.4	1211762	15872948
9.7	1236434	15557890
10.0	1257052	15236417

10.2	1273853	14909584
10.5	1287077	14578382
10.7	1296963	14243742
11.0	1303604	13915610
11.0	1303604	13915610
11.5	1289021	13278148
12.0	1267121	12647817
12.5	1239377	12028195
13.0	1207534	11422139
13.1	1195530	11212028
13.3	1183290	11004006
13.5	1170889	10798113
13.7	1158408	10594379
13.8	1145927	10392816
14.0	1133528	10193425
14.0	1133528	10193425
15.8	999365	8153073
17.6	861822	6354216
19.4	729704	4802937
21.2	603475	3489469
23.0	483590	2403213
24.8	370681	1532751

26.6	265678	865524
27.0	243520	759253
27.0	243520	759253
28.4	162489	418325
30.2	69914	125845
32.0	0	0

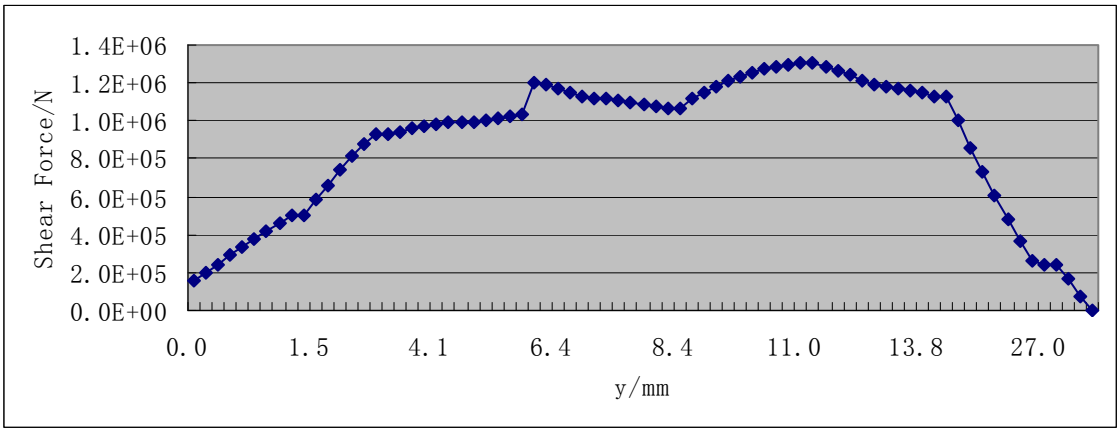

(a) Shear force

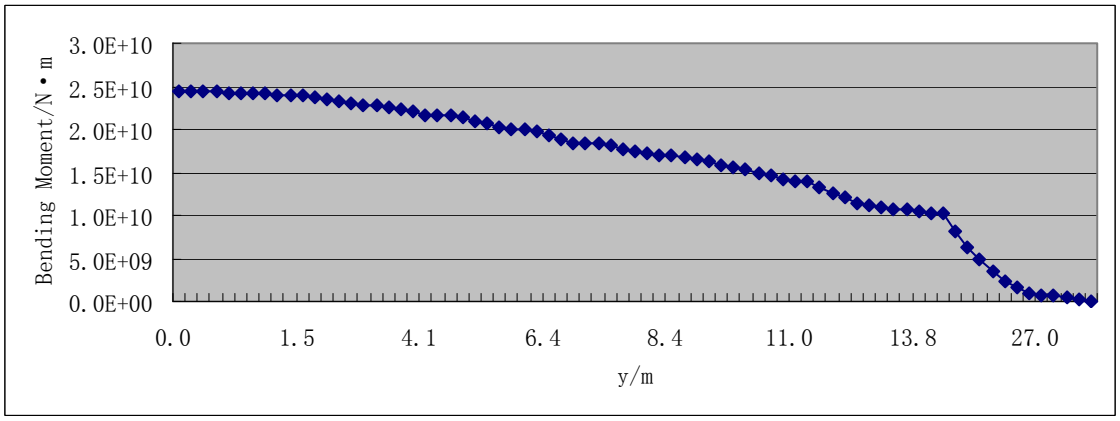

(b) Bending moment

Figure C-4 Load diagrams

C.1.3 Summarise

From the rude estimation in C.1.1, it can be known that the maximum shear force is $1.91\times10^{6}N$, and the maximum bending moment is $2.17\times10^{10}N\cdot mm$. While the results from the more accurate estimation in C.1.2 suggest that the shear force varies significantly along the span, ranging from zero at the tip to the maximum value at 11-metres span, $3.48\times10^{5}N$, and to about $4.12\times10^{4}N$ at the root; the maximum bending moment, $2.44\times10^{10}N\cdot mm$, is quite close to that obtained from the rough estimation. To conclude, the rough estimation method may be adequate to get an initial maximum bending moment, but is far from accurate to obtain the shear force. Therefore, the values in C.1.2 will be used to initially size the structural components in the following processes.

C.2 Initial Sizing for CWBC Inner Wing

In the initial design stage, aluminium alloy was used, the allowable stress $\sigma_b = 340MPa$, and the density $\rho = 2700kg/m^3$.

C.2.1 Overall Bending Moment

a) Evaluate the idealized depth of the inner box section, h:

$$\begin{aligned} h &= (h_1 + h_2 + h_3)/3 \\ &= (3461 + 3794 + 2215)/3 = 3157mm \end{aligned}$$

b) Calculate the effective direct loads, P, in the upper and lower surfaces needed to resist the bending moment, M:

$$\begin{aligned} P &= M/h \\ &= 2.44\times10^{10}N\cdot mm/3157mm = 7.72\times10^{6}N \end{aligned}$$

c) Evaluate the cross-section area required to react the bending moment at each side of the neutral axis of the wing box beam, A_b :

$$\begin{aligned} A_b &= \frac{P}{\sigma_b} \\ &= 7.72\times10^{6}N/340MPa = 2.27\times10^{4}mm^2 \end{aligned}$$

d) Assume a uniform equivalent thickness of the cover, t_e, across the width of the box, w, is:

$$t_e = \frac{A_b}{w} = \frac{M}{hw\sigma_b}$$
$$= 1.3mm$$

e) The idealized value, t_e, is derived from the area of the skin and stringers. As an initial estimate, it is desirable to suggest that the skin contributes 65 percent of the effective area, so the thickness of the skin, t_b is:

$$t_b = 0.65t_e = \frac{0.65M}{hw\sigma_b}$$
$$= 0.83mm$$

f) And therefore, the stringers take up 35 percent of the effective area.

g) Stringer pitch is often 1.5 to 5 times the stringer height, determined by practical considerations. For initial work a value of 3.5 can be assumed.

h) In terms of separate Zed-section stringers, the width of each of the shorter flanges is often approximately 40 percent of the stringer height, providing a total cross-section area of '$1.8h_st_s$' where h_s and t_s are respectively the stringer height and thickness. So the following equation can be derived based on the assumption that the total stringer area is 35 percent of the whole effective area:

$$0.35t_e \times 3.5h_s = 1.8h_st_s$$

so that t_s is approximately:

$$t_s = 0.68t_e$$
$$= 0.86mm$$

This suggests that the stringer thickness should be roughly equal to the skin thickness.

i) The width to thickness ratio of the free flange is typically about 16, due

to local and overall bucking considerations. Hence $0.4h_s$ equals $16t_s$, and therefore：

$$h_s = 40t_s = 35mm$$

The stringer area = $72(t_s)^2 = 70(t_b)^2 = 49mm^2$

C.2.2 Overall Torque Moment

The following method is to derive the thickness of outer surfaces and spar webs required to react the torque moment.

The following Equation (C-1) gives the approximate corresponding shear flow in the covers and webs:

$$\begin{aligned} Q_T &= T / 2A \\ &= \frac{6.69\times10^9 N\cdot mm}{2\times1.9\times10^7 mm^2} = 176N/mm \end{aligned} \qquad \textbf{(C-1)}$$

where

A is the enclosed area of the primary box cross-section at a given span wise, and T is the magnitude of the ultimate applied, distributed torsion.

Usually, the allowable shear stress is half of the allowable stress, so for aluminium alloy material, the allowable shear stress $\sigma_s = \frac{1}{2}\times\sigma_b = 170MPa$. The average material thickness required to react the torque moment can be given as:

$$\begin{aligned} t_q &= Q_T / A = T / 2A\sigma_s \\ &= \frac{6.69\times10^9 N}{2\times1.9\times10^7 mm^2\times170MPa} = 1.0mm \end{aligned}$$

C.2.3 Spar Webs

While an adequate initial estimate of the shear thickness needed in the upper and lower covers is given in the previous chapter, it is necessary to take account of the additional vertical shear loads to obtain the required thickness of the spar webs.

a) Evaluate the total effective depth of all the spars, h_T :

$$h_T = h_1 + h_2 + h_3$$
$$= 1713 + 1857 + 1345 = 4915mm$$

b) The shear flow in the webs due to the ultimate vertical shear force, V, is:

$$Q_V = V / h_T$$
$$= 1.3 \times 10^6 N / 4915mm = 265N / mm$$

c) The net shear flow in the webs is then approximately given by:

$$Q_w = Q_V + 2xQ_T / w$$

where

x is the chord-wise location of a particular web relative to the mid-point of the box.

Q_T was given by Equation (C-1).

For the front spar, x=7918, $Q_W = 441N / mm$

For the middle spar, x=1738, $Q_W = 303N / mm$

For the rear spar, x=6180, $Q_W = 402N / mm$

d) The web thickness can be got then:

$$t_w = Q_w / \sigma_s$$

For the front spar, $t_W = 2.6mm$

For the middle spar, $t_W = 1.8mm$

For the rear spar, $t_W = 2.4mm$

C.2.4 Plat Pressure Panels

According to the method provided by ESDU Data Sheet 71013, for a flat rectangular panel having isotropic material properties and simply supported edges under pressure load, the required thickness is approximately:

$$t = [0.71 \Delta p a^2 \{n^3 / (n^3 + 1.5)\} / \sigma_a]^{1/2} \quad \textbf{(C-2)}$$

where

σ_a is the allowable stress, =100MPa

Δp is the pressure differential, =0.137MPa

a is the length of the shortest side

n is the ration of the longer to shorter side

The skin is divided into grids by the stringers, with a longer side of 800mm and a shorter side of 170mm, so a=170mm, n=800/170=4.7. Therefore, the thickness can be calculated by Equation (C-2), t=5.3mm.

C.3 Initial Sizing for MBC Inner Wing

For the MBC Inner Wing, the pressure loads will be taken by the internal vessels, and outer covers will balance the bending moment, so the thickness of the internal vessels will be recalculated, and all other chapters, C.2.1-C.2.3, are still applicable.

As the internal shell to resist the pressure is cylindrical, the thickness required can be estimated by the following equation:

$$t = \frac{\Delta p R_c}{\sigma_p}$$
$$= \frac{0.137 MPa \times 1.9 m}{100 MPa} = 2.6 mm$$

C.4 Initial Sizing for WSC Inner Wing

C.4.1 Overall Bending Moment

For the WSC inner wing, in the flat part of the wing, the bending will be reacted by the covers, while in the curved section the bending will be reacted by the spars.

1. Curved spars

For the WSC inner wing, basically the whole bending and the shear force is reacted by the spars, so the initial sizes of the spars can be estimated by the bending moment and the shear force.

There are three spars in the inner wing configuration. Assuming each spar takes one third of the total bending moment and shear force. Spar flange thickness due to the maximum bending, which occurs at the root, can be calculated as follows (B is the flange width and h is the flange thickness):

$$P = \frac{M_x}{3 \cdot h} = \frac{2.44 \times 10^{10} N}{3 \times 2861 mm} = 2.84 MPa$$ (h is the mean depth at the root)

$$\sigma = \frac{P}{A} = \frac{P}{Bh}$$

$$h = \frac{P}{\sigma_b B} = \frac{2.84 \times 10^6 N}{340 MPa \cdot 200 mm} = 42 mm$$

Spar web thickness, b, due to the shear load could be computed from the following equation:

$$\sigma_s = \frac{F}{3A} = \frac{F}{3hb}$$

The maximum shear force occurs at the spanwise locaton of 5.8m, which is F=1.2×10^6 N(Table C-1, y=5.8m), at the idealised depth is h=1650mm. Given $\sigma_s = \sigma_b / 2 = 170 MPa$, then b=1.5mm.

2. Flat Covers

a) Evaluate the idealized depth of the outer box section, h:

$$h = (h_1 + h_2 + h_3)/3$$
$$= (902 + 912 + 530)/3 = 780mm$$

b) Calculate the effective direct loads, P, in the upper and lower surfaces needed to resist the bending moment, M:

$$P = M / h$$
$$= 1.39 \times 10^{10} N \cdot mm / 781mm = 1.78 \times 10^7 N$$

c) Evaluate the cross-section area required to react the bending moment at each side of the neutral axis of the wing box beam, A_b:

$$A_b = \frac{P}{\sigma_b}$$
$$= 1.78 \times 10^7 N / 340MPa = 5.24 \times 10^4 mm^2$$

d) Assume a uniform equivalent thickness of the cover, t_e, across the width of the box, w, is:

$$t_e = \frac{A_b}{w} = \frac{M}{hw\sigma_b}$$
$$= 4.4mm$$

e) The idealized value, t_e, is derived from the area of the skin and stringers. As an initial estimate, it is desirable to suggest that the skin contributes 65 percent to the effective area, so the thickness of the skin, t_b is:

$$t_b = 0.65t_e = \frac{0.65M}{hw\sigma_b}$$
$$= 2.9mm$$

f) And therefore, the stringers take up 35 percent of the effective area.

g) Stringer pitch is often 1.5 to 5 times the stringer height, determined by practical considerations. For initial work a value of 3.5 can be assumed.

h) In terms of separate Zed-section stringers, the width of each of the shorter flanges is often approximately 40 percent of the stringer height,

providing a total cross-section area of '$1.8h_s t_s$' where h_s and t_s are respectively the stringer height and thickness. So the following equation can be derived based on the assumption that the total stringer area is 35 percent of the whole effective area:

$$0.35t_e \times 3.5h_s = 1.8h_s t_s$$

so that t_s is approximately:

$$\begin{aligned} t_s &= 0.68t_e \\ &= 3.0mm \end{aligned}$$

This suggests that the stringer thickness should be roughly equal to the skin thickness.

i) The width to thickness ratio of the free flange is typically about 16, due to local and overall bucking considerations. Hence $0.4h_s$ equals $16t_s$, and therefore：

$$h_s = 40t_s = 35mm$$

The stringer area = $72(t_s)^2 = 70(t_b)^2 = 585mm^2$

C.4.2 Overall Torque moment

The following method is to derive the thickness of outer surfaces and spar webs required to react the torsion loading.

Equation (C-3) gives the approximate corresponding shear flow in the covers and webs:

$$\begin{aligned} Q_T &= T / 2A \\ &= \frac{6.69 \times 10^9 N \cdot mm}{2 \times 6.6 \times 10^6 mm^2} = 507N / mm \end{aligned} \qquad \textbf{(C-3)}$$

where

A is the enclosed area of the primary box cross-section at a given span wise, and T is the magnitude of the ultimate applied, distributed torsion.

Usually, the allowable shear stress is half of the allowable stress, so for aluminium alloy material, the allowable shear stress $\sigma_s = \frac{1}{2} \times \sigma_b = 170MPa$. The average material thickness required to react the torque moment can be given as:

$$t_q = Q_T / A = T / 2A\sigma_s$$
$$= \frac{6.69 \times 10^9 N}{2 \times 6.6 \times 10^6 mm^2 \times 170MPa} = 3mm$$

C.4.3 Spar Webs

While an adequate initial estimate of the shear thickness needed in the upper and lower covers is given in the previous chapter, it is necessary to take into account the additional vertical shear loads to obtain the required thickness of the spar webs. The critical position is the tip of the model, 11 meters in span.

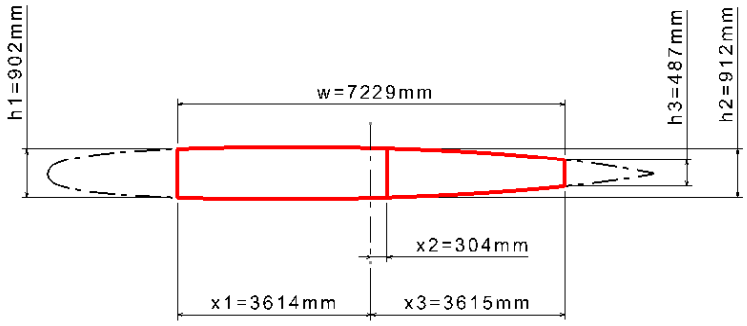

Figure C-5 The cross section

a) Evaluate the total effective depth of all the spars, h_T:

$$h_T = h_1 + h_2 + h_3$$
$$= 902 + 912 + 487 = 2301mm$$

b) The shear flow in the webs due to the ultimate vertical shear force, V, is:

$$Q_V = V / h_T$$
$$= 1.31 \times 10^6 N / 2301mm = 570N / mm$$

c) The net shear flow in the webs is then approximately given by:

$$Q_w = Q_V + 2xQ_T / w$$

where

x is the chord-wise location of a particular web relative to the mid-point of the box.

Q_T was given by Equation (C-3).

For the front spar, x=3614, $Q_W = 1681N/mm$

For the middle spar, x=304, $Q_W = 814N/mm$

For the rear spar, x=3615, $Q_W = 1437N/mm$

d) The web thickness can be got then:

$$t_w = Q_w / \sigma_s$$

For the front spar, $t_W = 9.9mm$

For the middle spar, $t_W = 4.8mm$

For the rear spar, $t_W = 8.5mm$

C.4.4 Pressure

As the internal shell resisting the pressure is cylindrical, the thickness required can be estimated by the following equation:

$$t = \frac{\Delta p R_c}{\sigma_p}$$
$$= \frac{0.137MPa \times 1.9m}{100MPa} = 2.6mm$$

Appendix D Loads Applied to the FE Models

The source of the loads used in this thesis is from that for the Blue Bird, on which the Conventional Wing-Box Configuration and Multi-Bubble Configuration are exactly based, so the loads should be suitable for FE analysis for both the Conventional Wing-Box Configuration and Multi-Bubble Configuration. With the Wave-Section Configuration, as it involves slight changes in the arrangement, there should be some differences in load distribution. However, in order to ensure the comparisons are carried out under the same circumstances, it might be reasonable to assume that the same shear load, compression load and tension load are also applied to the Wave-Section Configuration model as those applied onto the Conventional Wing-Box Configuration model and the Multi-Bubble Configuration model.

D.1 Pressure load

According to FAR 25.843 [11], pressurized cabins and compartments must provide a cabin pressure altitude of no more than 8,000 feet at the maximum operating altitude of the aircraft under normal operating conditions. The maximum designed altitude of the aircraft is 35,000 feet (Reference [12]), so a pressure differential of 27,000 feet (35,000-8,000) must be provided by the structural compartments, and a security load factor of 1.5 should be taken into account. Then a pressure differential, Δp, can be obtained:

$$\Delta p = \frac{27000 \times 0.3048m}{12m} \times 1.5 = 1030mmHg = 0.137MPa$$

D.2 Shear load

It can be seen from Table C-1 that the overall shear force is about $1.3 \times 10^6 N$ at the spanwise position of 11 metres. Because the model is about 60 percent of the box in cross section, the load applied to the model should be 60 percent of the total shear load accordingly, which is $1.31 \times 10^6 N \times 60\% = 7.88 \times 10^5 N$.

D.3 Compression and tension loads due to bending moment

From Table C-1 , it is known that the overall bending moment at 11-metres span is approximately $1.39\times10^{10} N\cdot m$. As the model is approximate 60 percent of the box in cross section, the load applied to the model should be 60 percent of the total bending moment accordingly, which is $1.39\times10^{10} N\cdot m\times 60\% = 8.35\times10^{9} N\cdot m$. This bending moment results in compression load in the top cover and tension load in the bottom cover, which are obtained by dividing the bending moment by the idealised depth of the box. The calculation process is as follows:

From Figure D-1, the idealised (mean) depth, h, can be obtained:

$$h = (h_1 + h_2 + h_3)/3 = 1638mm$$

Then the magnitude of the resulted compression/tension load, P, from bending moment, is:

$$P = \frac{M}{h} = \frac{8.35\times10^{9} N\cdot mm}{1638mm} = 6.08\times10^{6} N$$

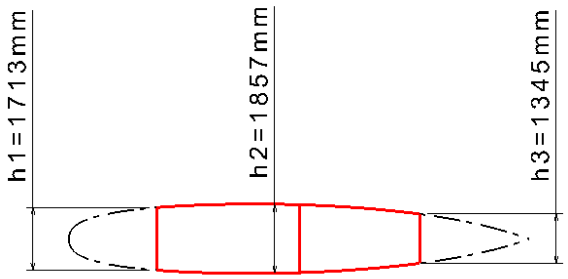

Figure D-1 Cross section for CWBC and MBC models